UC Berkeley
UC Berkeley Electronic Theses and Dissertations

Title

Generating Protein-Functionalized Nanomaterials via Rationally Designed Statistically Random Heteropolymers

Permalink

https://escholarship.org/uc/item/4dv872c8

Author

Panganiban, Brian

Publication Date

2016

Peer reviewed|Thesis/dissertation

Generating Protein-Functionalized Nanomaterials

via Rationally Designed Statistically Random Heteropolymers

By

Brian Matibag Panganiban

A dissertation submitted in partial satisfaction of the

requirements for the degree of

Doctor of Philosophy

in

Engineering – Materials Science and Engineering

in the

Graduate Division

of the

University of California, Berkeley

Committee in charge:

Professor Ting Xu, Chair

Professor Phillip Messersmith

Professor Niren Murthy

Fall 2016

Generating Protein-Functionalized Nanomaterials

via Rationally Designed Statistically Random Heteropolymers

Abstract

Generating Protein-Functionalized Nanomaterials
via Rationally Designed Statistically Random Heteropolymers

By

Brian Matibag Panganiban

Doctor of Philosophy in Materials Science and Engineering

University of California, Berkeley

Professor Ting Xu, Chair

The focus of this dissertation is on the development of a modular approach toward protein-based nanomaterials. Over the past billion years, nature has optimized proteins to sustain the complexities of life. The efficiency, reproducibility, and diversity of functions that proteins poses is unmatched by any biomimetic product. Successful integration of active proteins with synthetic polymers has the potential to combine the advantages of both the biological as well as the synthetic world. Proteins would provide materials with chemical heterogeneity, structural precision, catalytic activity, and system dynamics not offered by manmade materials, and polymers would provide a platform that is chemically diverse, processable, and robust. Protein-functionalized materials can clearly open a viable approach to improving current technologies and will positively impact the current paradigm of materials science and device engineering.

However, most proteins reside in aqueous media and the majority of their uses are for biomedical applications. Their insolubility and inability to remain functional in non-aqueous solvents as well as their susceptibility to high temperatures are major barriers preventing their general usage toward biofunctional hybrid materials. In order to make proteins viable building blocks in the materials community, proteins must be processable, their structure must remain stable during processing, and their function must be preserved post-fabrication. Reverse micelles have been shown to successfully encapsulate a variety of proteins and make them processable. Using common small molecules surfactants, protein-based materials can indeed be created without modification of the protein itself, but surfactants were observed to only meet the criteria for processability and lent itself to protein denaturation during and after processing.

Many non-covalent interactions of similar energy scales underlie protein folding, polymer chain conformation, protein-polymer interactions, polymer-solvent interactions,

and solvent-protein interactions. The delicate balance of the various energetic contributions must be understood in order to manipulate these interactions without interfering with a protein's structure and built-in functionality. Using a rational approach, statistically random heteropolymers were developed that provided increase stability of proteins in organic solvent and elevated temperatures without interfering with both protein folding as well as material fabrication. This rational approach limited the parameter workspace and provided boundaries in which polymers were synthesized. A mixture of structural characterization of protein-polymer complexes and spectroscopic analysis of protein-polymer interactions were used to identify polymers that optimized preservation of protein activity.

This development of statistically random heteropolymers provides a path toward protein-based materials. By mixing proteins, statistically random heteropolymers, and commercially available polymers, protein patterning and devices for catalysis were generated. This work demonstrates the potential of statistically random heteropolymers as a vehicle toward functional materials, opening up a wide range of possible applications, from sensors to catalysis to energy.

Generating Protein-Functionalized Nanomaterials via Rationally Designed Statistically Random Heteropolymers

Table of Contents

Chapter 2: Co-Assembly of Protein-Encapsulated Reverse Micelles and Block Copolymer-Based Supramolecules toward Functional Hybrid Materials

Chapter 3: Design and Optimization of Statistically Random Heteropolymers toward Enhanced Protein Stability and Processability

Chapter 4: Preserving Protein Hierarchical Structure in Organic Solvents via Rationally Designed Statistically Random Heteropolymers

Chapter 5: Enhanced Thermal Stability of Proteins in Aqueous Solutions using Rationally Designed Statistically Random Heteropolymers

Chapter 6: Generating Protein-Based Nanoassemblies via Rationally Designed Statistically Random Heteropolymers

References

Appendix

Acknowledgements

This dissertation would not have been possible if it weren't for my advisor, Professor Ting Xu. For 5 ½ years, she supported immensely – academically, financially, personally. She was a mentor who pushed me constantly to improve as both a researcher and a person, but she did it within reason, prioritizing physical and mental health over everything else. Looking back to when I first started, I am truly amazed by how much I've progressed because of your guidance. Thank you Ting.

I also appreciate all the undergraduate researchers who were by my side in the trenches: Haoming, Ashley, Kathryn, Jefferson, Mariane, and especially Izaac and Alisa. There were numerous 24 hour studies that had to be conducted and these undergrads were willing to put in those extra hours. This project progressed immensely because of them.

In addition, I would like to thank "The Amigos." Joo Chuan, Shawn, Jose, Isaac, Tim, and I all came into the program at the same time and we remained close throughout our years here in Berkeley. The research world can feel a bit isolated and depressing at times and having this close group of friends really made graduate school enjoyable.

I would like to give a special thanks to a particular lab member who made my last year of grad school miserable. This person reminded me, through their own actions, that the world of academia can be hostile. Although science is a community based on collaboration and support, my interactions with this particular person taught me that self-preservation, selfishness, and unwavering arrogance are traits I will also encounter in the research field. I am more resilient and mentally tough after this low point in my life.

Lastly, I would like to thank my parents, Edgar and Minda, and my brothers, Raymond and Justin. I was not the easiest person growing up with, but the four of them supported me unconditionally throughout my entire life. They emphasized happiness and did not place any unnecessary pressure on me. Because of this healthy environment, I was able to shape my life into what it is now. Thank you.

Chapter 1

Opportunities in Protein-Functionalized Nanomaterials

§ 1.1. Introduction

Proteins have evolutionarily been optimized to sustain and regulate the complexities of living. Whereas DNA encodes life, proteins allow life to happen. They are involved in catalyzing biological reactions, transporting molecules within cells, providing structural support for biological assemblies, and regulating cellular processes.[1] Translation of these biologically-derived functions into engineered materials would provide improvements in a variety of technological sectors. This may lead to immediate impacts in catalysis, sensing, medicine, energy, storage, stimuli responsive materials, and hierarchically structured nanomaterials.[2-15] Although large strides have been made to create synthetic biomimetics (e.g. molecularly imprinted polymers[16-18], artificial photosynthetic systems[19]), they have generally not been able to replicate the same level of performance proteins possess.

However, direct incorporation of proteins into current processing practices remains a challenge. Proteins primarily reside in aqueous media and are typically not amenable for usage beyond biomedical applications. Organic solvent-use generally remains a common necessity for the industrial-scale fabrication of various materials. A protein's insolubility and inability to remain functional in non-aqueous solutions are significant hurdles that need to be addressed. Although some proteins can natively tolerate low levels of organic solvent exposure, this trait is only reserved for a few special cases and this organic solvent is typically polar and miscible with water.[20-23] Nonpolar solvents would give rise to key issues pertaining to protein solubility, stability, and processability. Nevertheless, utilizing proteins in organic solvents opens up new possibilities in creating new hybrid materials.[24, 25]

There have been a variety of methods that address organic solvent incompatibility. Unfortunately, each technique has glaring limitations; there is no single, approach that can link any protein to any application. In order to understand and implement new modifications that stabilize protein structure, a basic understanding of protein folding and dynamics is required. In this chapter, I will briefly discuss the fundamental aspects of protein assembly, the origin of their inherent functionality, and the benefits of translating protein function into engineered systems. I will also outline protein stability from both a thermodynamic and kinetic viewpoint and review existing approaches toward protein stabilization. Finally, I will elaborate on the potential benefits of protein-functionalized nanomaterials and how the approach outlined in this dissertation will pave the way for a new generation of enhanced technology.

§ 1.2. Proteins

Proteins, the building block for all biotic matter, are special biological polymers that have adopted a variety of roles in organisms. Proteins can be found in compacted globular states that freely solubilize in biological serum, acting as biocatalyst.[26] They can

also be found in more complex arrangements, such as fibers for structural support[27] or embedded in membranes as receptor molecules.[28] No matter the assumed macroscopic state, all proteins hierarchically fold into a unique multi-order structure. Although this may not hold entirely true for intrinsically disordered proteins (IDPs), IDPs do adopt an ensemble of predictable structures that result in unique functions.[29]

From a one dimensional line of information, proteins spontaneously adopt a functional three dimensional configuration. The shape and chemistry of this conformation dictate a protein's recognition and interaction with ligands. Through billions of years of evolution and mutagenesis, fluctuations and irregularities of protein structures gave rise to a diverse set of functions and properties that have propagated the advancement of life. Understanding this structure-function relationship and being able to retain protein native structure is the key toward generating functional biomaterials.

1.2.1. Structure

Unlike the majority of synthetic polymers, proteins possess a precise monomeric sequence that induces a reproducible three dimensional fold. This three dimensional structure can be explained and predicted by the interactions that the monomers experience intramolecularly as well as intermolecularly. A concerted hierarchical assembly occurs as the protein finds its final conformation, from local assemblies made up of tens of monomers, to structural domains made up of tens to hundreds of monomers, and finally to overall structures made up of hundreds to thousands of monomers, as seen in Figure 1.1. Although there is an endless amount of configurations that a protein can mathematically adopt, restrictions stemming from monomeric and environmental interactions result in a single native structure.
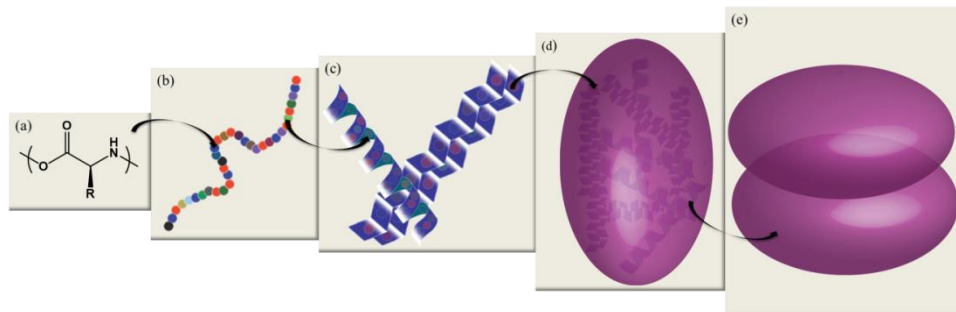
Figure 1.1. Hierarchical structure of proteins. (a) Amino acids are the basic building block for proteins. Each amino acid is composed of a carboxylic acid, an amine, a hydrogen atom, and a unique R-group. (b) The linear sequence of amino acids makes up a protein's primary structure. (c) The chain of amino acids folds into secondary structures, primarily found as α-helices and β-sheets. (d) Tertiary structure arises as multiple intramolecular secondary structures collapse into a dense structural domain. (e)

Multiple polypeptide chains can hybridize, resulting in the formation of a quaternary structure.

1.2.1.1. Primary Structure

Proteins, at the most fundamental level, are composed of an unbranched chain of conjugated monomers called amino acids, as seen in Figure 1.1(a-b). There are 20 canonical amino acids, each containing a basic amino group, an acidic carboxyl group, a hydrogen atom, and a sidechain. Each amino acid differs in the chemical moiety found on this sidechain. These chemical groups can vary, from something as simple as hydrogens or methyls, to something slightly more complex like alkanes, hydroxyls, and carboxamides, to something more unique such as thiols, guanidiniums, and indoles. These amino acids are typically grouped into four categories – positively charged polar, negatively charged polar, non-charged polar, nonpolar – each providing different driving forces for protein folding. For example, nonpolar sidechains are hydrophobic in nature and have the propensity to cluster in the presence of water. Contrastingly, polar sidechains are hydrophilic and prefer to remain hydrated.

Some amino acids offer special attributes. For instance, inclusion of glycine, which has a hydrogen side group, provides backbone flexibility. Proline is a pyrrolidine-containing amino acid that tethers α-carbon to the amine along the side group. This restricts the conformational flexibility of the backbone. Cysteine, an amino acid that contains a thiol, can form intramolecular, reversible disulfide bonds as a way to further increase protein stability.

Unlike the secondary, tertiary, and quaternary structure, the primary structure is held together by covalent bonds. Condensation reaction of the amine from one amino acid and the carboxylic acid of another amino acid produce a peptide bond linkage. This type of bond restricts the amount of thermodynamically viable configurations. The peptide bond hinders rotation around an amide plane, and each amino acid has a specific geometric shape that sterically restricts certain orientations. When this backbone rotates to find energetically favorable states, only a few angles are thermodynamically acceptable. This limits the available conformations that can actually be accessed by the protein.

1.2.1.2. Secondary Structure

Depending on the localized amino acid sequence, proteins hierarchically fold into secondary structures, composed primarily of α-helices, β-sheets, and unstructured loops (Figure 1.1c). α-helices are right-handed helical structures, typically ranging from 4 to 40 amino acids in length. β-sheets are planar structures formed when two or more β-strands come together. These β-strands are fully extended, typically ranging from 5 to 10 amino acids in length. The main driving force for secondary structure formation is the fulfillment of all intramolecular hydrogen bonds along the backbone, from the N-H

hydrogen bond donor of one amino acid to the C=O hydrogen bond acceptor of another amino acid. In α-helices, the N-H forms a hydrogen bond with a C=O four amino acids earlier in the protein sequence. In β-sheets, each β-strand is aligned adjacent to another β-strand to facilitate optimal geometric packing for hybridization.

Unstructured loops are found between α-helices and β-sheets. These loops are generally formed in the presence of glycines and prolines, amino acids that provide backbone flexibility and unique backbone kinks, respectively. Unlike α-helices and β-sheets, hydrogen bonds are not formed intramolecularly in loop structures. Hydrogen bond donors and acceptors are found within the aqueous solution. This results in loops favoring the exterior of the protein.

1.2.1.3. Tertiary Structure

The next level of hierarchical complexity arises from the packing of secondary structures into three dimensional units called structural domains. Domains range from 50 to 200 amino acids, where each domain has a well-defined hydrophobic core. Whereas the main driving force for secondary structure arises from the formation of hydrogen bonds, the main interaction that gives rise to structural domains is the hydrophobic effect. Hydrophobic residues pack and segregate to the core of these domains so as to minimize their interaction with water. One to several dozen of these structural domains then pack into a protein's tertiary structure (Figure 1.1d).

1.2.1.4. Quaternary Structure

Some proteins contain more complex arrangements, termed quaternary structure. Quaternary structures involve the association of different protein chains into a multi-component assembly (Figure 1.1e). These chains are not covalently linked, and quaternary structure can be composed of multiple copies of the same tertiary subunit as found in hemoglobin,[30] or different tertiary subunits as found in ribosome.[31] These tertiary subunits are often the fundamental unit of function; by having multiple tertiary subunits, proteins can possess more complex functions.

1.2.2. Forces Governing Protein Folding

From an entropic standpoint, protein structures are highly unfavorable. The large entropic penalty associated with restricting a protein with millions of conformations to a single native structure is fairly large. For example, the Boltzmann's principle states that the entropy of a system is proportional to the natural log of the amount of microstates available:

$$S = k_B \ln \Omega \qquad (1.1)$$

In this equation, S is entropy, k$_B$ is Boltzmann's constant, and Ω is the number of microstates. If we assume that a protein has one million conformations, the entropic penalty associated with the folding process is around 50 kJ/mol at room temperature. In order for a protein to remain stable, the folded state must overcome this entropic penalty.

Enthalpically, stable protein conformation is attributed to the process of minimizing the overall free energy of the system, resulting from the sum of intra- and intermolecular interactions for a given set of environmental influences. Noncovalent interactions drive protein folding, from pairwise interactions between transient or stable atomic charges, as seen in Figure 1.2. Depending on the type of interactions that are present, there is an optimal interaction distance where repulsion and attraction are at equilibrium, resulting in the formation of a protein's structure.

Van der Waals Forces	Electrostatic Interactions	Hydrogen Bonding	Hydrophobic Effect
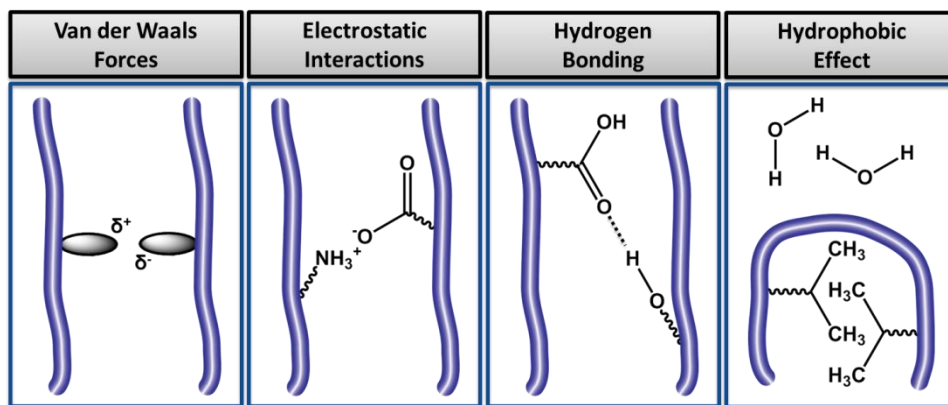
Figure 1.2. Native protein structure is stabilized by the sum of many non-covalent interactions. These interactions include van der Waals forces, electrostatic interactions, hydrogen bonding, and the hydrophobic effect.

The weakest of these noncovalent interactions are van der Waals' forces. This occurs when two neutral atoms are brought in close proximity to one another, causing an induced dipole. This induced dipole creates a transient separation in charge, leading to molecular attraction. For biological molecules, the optimal distance for van der Waals' forces occurs between 3 to 4 Å and becomes negligible after 5 Å.[32] At distances under 3 Å, the atoms behave like hard spheres and experience a repulsive force. This can be described by the Lennard-Jones Potential,

$$U(r) = -4\epsilon_{ij}\left[\left(\frac{\sigma_{ij}}{r}\right)^{12} - \left(\frac{\sigma_{ij}}{r}\right)^{6}\right] \tag{1.2}$$

where U is potential energy, ϵ_{ij} is a constant characteristic of the two atom types, σ_{ij} is the average diameter of the atoms, and r is the distance between the two atoms. These van der Waals' interaction result in energies of about 1 kJ/mol.[32]

The strongest type of interaction arises from permanent charges. Unlike van der Waals' forces, the optimal distance for each ion pair is around 3 Å, and the attraction falls off slowly with increasing distance. The strength of these interactions is fairly susceptible to changes in the local environment. In a vacuum, charges separated by 3 Å have an energetic strength of about 500 kJ/mol. At the same distance in water, ionic interactions result in an energetic strength of about 6 kJ/mol. This phenomenon can be described by Coulomb's Law,

$$U(r) = \frac{q_i q_j}{Dr} \tag{1.3}$$

where q_1 and q_2 are the charges of the atoms, D is the effective dielectric constant, and r is the distance between the two atoms. Water has a dielectric constant of 78.3 at room temperature while vacuum has a dielectric constant of 1.

Although the interior of the protein provides vacuum-like properties, fully charged atoms are rarely found in the interior of proteins. In order to bring a charged-atom into the interior of the protein, the strongly bound water molecules found near the charged moiety prior to protein folding must be separated. This would result in a large energetic penalty. Charged residues, consequently, are typically found on the protein surface, and depending on the extent to which the residue is exposed to water, the energy can range from 6-20 kJ/mol.[32]

The third type of interaction is hydrogen bonding. Hydrogen bonding is very common in biological molecules, where atoms are polarized due to differences in electronegativity. In biology, the most electronegative atoms are oxygen and nitrogen and the least electronegative are hydrogen and carbon. When an electronegative atom is covalent attached to hydrogen, atoms are pulled closer to the more electronegative atom, causing a partial positive charge on the hydrogen and a partial negative charge on the other.

Unlike the two previous interactions, hydrogen bonds are highly directional, like covalent bonds. Dipoles interact most favorably when dipoles are aligned. The hydrogen bonds found in secondary structure have an optimal energy when dipoles are co-linear and have a distance between 2.4 Å and 2.7 Å.[32] The rate at which the attraction falls off with respect to distance can be characterized as something between the interactions between transient charges in van der Waals' forces and interactions between stable charges in ion pairs. This can be described by a variation of the Lennard-Jones Potential,

$$U(r) = K_{ij}\left[\left(\frac{C_{ij}}{r}\right)^{12} - 2\left(\frac{D_{ij}}{r}\right)^{10}\right] \qquad (1.4)$$

where K_{ij}, C_{ij}, and D_{ij} are constants and r is the distance between the two atoms. Hydrogen bonding is weakened by the presence of water due to electrostatic shielding and competing hydrogen bond donors and acceptors. After accounting for the attenuation caused by water, hydrogen bonds are typically in the energetic range of around 5-20 kJ/mol.[32]

The largest contributor to protein folding arises from the hydrophobic effect. There is a relatively small population of charges found on proteins, and interactions caused by van der Waals' forces are far too weak to solely keep a protein together. Hydrogen bonding does not contribute significantly to the overall stability other than keeping secondary structures intact; the energy difference between intramolecular hydrogen bonding and hydrogen bonds formed with water is insignificant. The hydrophobic effect, however, is a large driving force for protein stabilization; there is a large increase in stability through the shielding of hydrophobic residues within the interior of the protein. The formation of a hydrophobic core reduces water ordering at the surface of the protein and increases the entropy of the system.

Although the hydrophobic effect is the main driving force for overall protein stability, hydrogen bonding that occurs at the secondary structure level is required. The backbone of proteins is polar and when hydrophobic residues pack into the interior of the protein, hydrogen bonding between the backbone and the water is disrupted. This is quite energetically unfavorable. In order to bring this backbone into the interior of the protein, hydrogen bonding must first be satisfied. This is achieved through secondary structure formation.

Kinetically, proteins constantly explore their conformational landscape, sampling the solvent and solutes that may be in their vicinity. Protein structure fluctuates rapidly between the different microstates, but these microstates do not deviate too far from the native conformation; this process is reversible. When a protein unfolds, there is a transition between the native and unfolded state, going through several intermediate conformations. Typically, these intermediate transition states are high in energy and require external stimuli to overcome the kinetic barrier. If proteins are kept in biological conditions, the rate of protein unfolding is minimized.

1.2.3. Function

As machines, proteins represent the pinnacle of efficiency and specificity. They have a fluid structure with atomically-precise conformational motion. This results in the ability to couple a mechanical action with a chemical event. At the core of all protein function, a physical interaction with another molecule occurs. For example, enzymes

interact with substrates, antibodies attach to viruses, and structural proteins assemble with one another to create macroscopic, load-bearing structures.

Proteins selectively bind to a ligand or set of ligands, such as ions, small molecules, or macromolecules. These events can be short- or long-lived, depending on the strength of binding. These interactions are non-covalent, and effective binding occurs only if protein-ligand complementarity occurs; the amount of interactions between the two molecules is maximized. The shape, contour, and size of the two molecules must match up and the placement of amino acids within the binding pocket must correlate well with the chemical moieties found on the surface of the ligand.

The conformation and chemical groups present at the binding site elucidate protein functionality. The alignment of the chemical moieties directs the intramolecular interactions that occur within the protein. There are two different mechanisms that can occur at the binding site. First, by changing the shape and local chemical environment of the binding site, proteins can restrict water molecules from interacting with the ligand. Water molecules can outcompete and attenuate protein-ligand interactions. Second, the pairing of polar amino acids can alter protein selectivity and reactivity. Changing the local charge environment can drastically promote or deter certain ligands from entering the binding site. Additionally, by controlling the orientation, spatial location, and chemical groups found in the binding pocket, protein reactivity can be enhanced. In the catalytic triad for example, a network of interactions between three residues results in the creation of a serine-based nucleophile.[33]

Enzymes, one particular subset of proteins, are an extremely desirable biological component for protein-functionalized materials.[34] Enzymes are macromolecules involved in the catalysis of biological reactions. They bind to one or more substrates and participate in the formation or breakage of covalent bonds. These reactions are very rapid, speeding up a reaction by a factor of a million or more. The binding that occurs between enzyme and substrate stabilizes the transition state and lowers the kinetic barrier of the reaction. Enzymes are associated with unrivaled substrate selectivity and the unparalleled ability to create products that are regio-, stereo-, and chemospecific.

Often, enzymes will sequester small molecules as a way to increase their chemical diversity – chemical elements that the canonical amino acids do not have – and acquire new functionality. One particular small molecule that will be discussed in future chapters is heme. Heme is an iron-containing porphyrin that can associate with a variety of proteins, such as horseradish peroxidase.[35] Heme provides an inorganic catalyst to decompose hydrogen peroxide into water. In cases where enzymes use a cofactor, a binding pocket that can coordinate well with the compound must be present. Once the pocket is disrupted, the cofactor no longer has an affinity to the protein and would result in dissociation.

§ 1.3. Current Limitations of Protein Processing

Translating these functions into engineered systems is not a trivial task. Making proteins soluble, stable, and processable in organic solvents is a large deterrent toward protein-functionalized materials. Water-soluble proteins are typically sold or stored in a lyophilized powder or an aqueous solution containing additives. These states do not readily lend themselves to protein solubilization in non-polar organic media. These powders remain undispersed after mixing, and aqueous solutions remain phase separated.

Preserving protein structure and function during and after fabrication is a more difficult challenge. As previously noted, protein function is highly correlated with protein structure. In nature, proteins are susceptible to conformational and activity change when their biological environment changes. For example, proteinases can act as chaperones at low temperatures and as proteinases at high temperatures.[36] In addition, phosphoglucose isomerase is a glycolytic enzyme in the cytoplasm and a nerve growth factor and cytokine out of the cell.[37] Changes in biological pH, temperature, or reducing environment can greatly influence native structure, which consequently induces a change in functionality. These biological influences are typically in the tolerable range of proteins. Outside of this tolerable range, a range that protein-functionalized materials may need, detrimental effects are highly expected.

Proteins adopt configurations that best balance both the favorable as well as the repulsive intramolecular interactions, typically only 20-60 kJ/mol more stable than the unfolded, non-functional conformation.[38] Each pair of weakly interacting amino acids can be readily strengthened or weakened via external stimuli. As previously mentioned, modifications in local conditions will result in protein conformational change and protein deactivation. These extrinsic influences may include changes in solvent polarity, pH, ionic concentration, or temperature. Even the thermal energy associated with room temperature (300 K) is around 2.5 kJ/mol, more than twice the energy of van der Waals' forces and on the same order of magnitude as ionic pairing, hydrogen bonding, and the desolvation of hydrophobic residues. Although the ability to respond to sensitive cues from the environment is the inherent origin to their function, protein structure is very fragile and generally less robust when compared to synthetic materials. Secondary, tertiary, and quaternary structures are all susceptible to these external stimuli and would result in protein unfolding, irreversible aggregation, and lost in protein function.

§ 1.4. Approaches toward Protein Stabilization

Although the energy landscape can be vast and complex, protein folding and unfolding can be simplified as an ensemble of three different macrostates: unfolded, transition, and folded. The unfolded macrostate encompasses protein conformations that sit at local minima and do not exhibit any sort of activity. The transition is an ensemble of unstable high energy states that segregates the folded and unfolded conformations. The

folded state is the lowest energy conformation, where this native structure results in protein activity. In order to stabilize proteins, there are three different approaches that can be taken, as seen in Figure 1.3. The unfolded state can be destabilized and made more energetically unfavorable. This will reduce the entropic penalty due to folding. The energetic level of the transition state can be increased, reducing the likelihood of conformational change. Lastly, the folded state can be stabilized enthalpically, making it more energetically favorable. All existing protein stabilization methods rely on these mechanisms, focusing on either altering the microenvironment, directly modifying the chemistry, or manipulating the dynamics of the protein.[39-41]
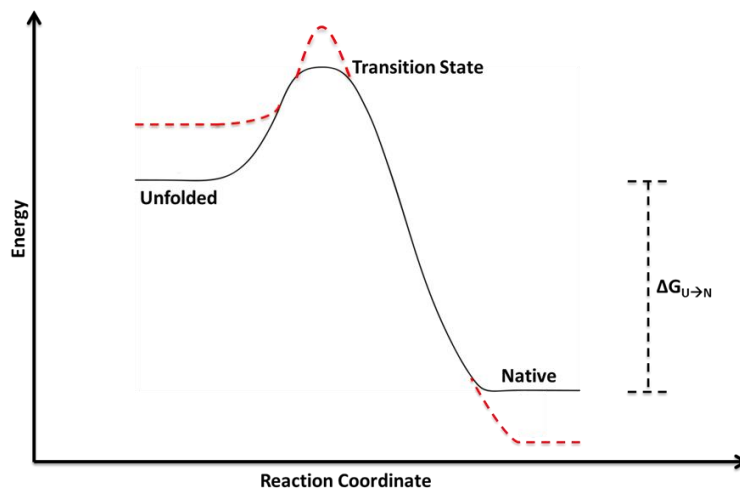
Figure 1.3. Simplified energy landscape of protein folding. Red dashed lines indicate ways to stabilize protein through modification of the unfolded, transition, and native state. Entropic, dynamic, and enthalpic contributions are considered, respectively.

1.4.1. Solution Modification

Dampening the motion of the protein's local environment would reduce the ability of the protein's backbone to rotate, translate, and vibrate. There is a direct link between the molecular motion of the protein and the molecular motion of its surroundings. When proteins are stored in solution, chemicals that stabilize protein structure are frequently added, such as polyols and sugars.[42-46] There have also been studies that indicate ionic liquids can stabilize protein structure.[47-49] A common feature of these chemical additives is their ability to modify protein structure and impede the motion of the water molecules in the immediate vicinity of the protein. Based on "water replacement hypothesis," stabilizing agents replace the local water molecules around the protein and stabilizes the three dimensional structure through hydrogen bonding, as seen in Figure 1.4a.[50] "Preferential exclusion hypothesis" is another theory stipulating that these agents are excluded from the macromolecule's surface and interact with the water instead. Water is excluded from the protein, making its structure more compact and less

susceptible to conformational change (Figure 1.4b).[43] Although there are substantial disputes on the correct mechanism toward protein stabilization, the two theories are well-received.
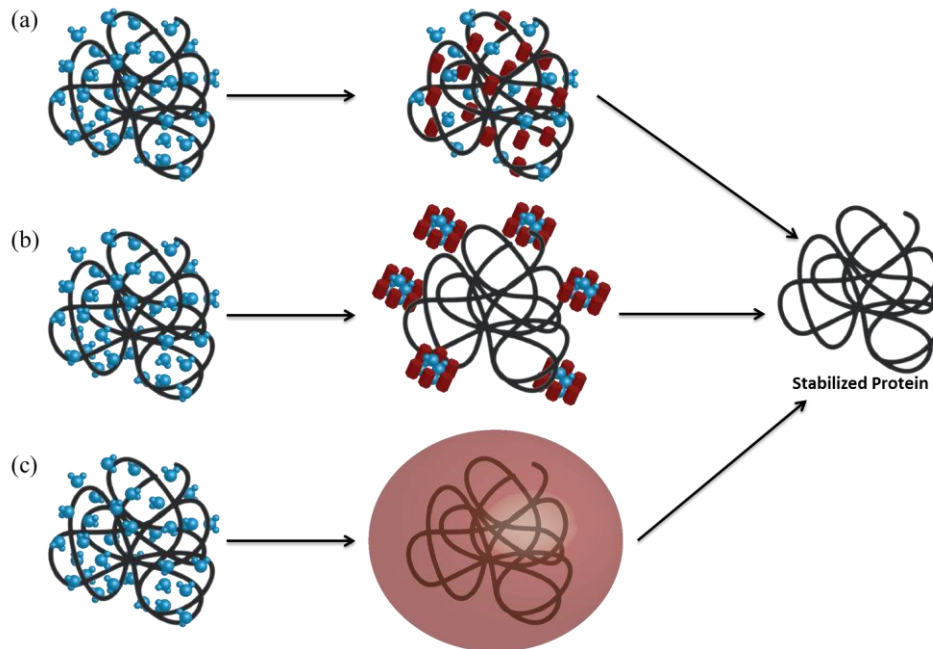
Figure 1.4. Various theories to explain protein stabilization through solution additives. (a) Water replacement theory involves the substitution of water molecules by protecting agents that can form hydrogen bonds with the protein. (b) Preferential exclusion theory proposes that there is no direct interaction between the protecting agent and protein. Instead, addition of the protecting agent sequesters water molecules away from the protein, decreasing its hydrated radius and increasing its compactness and stability. (c) Vitrification theory assumes that the protecting agent forms a glassy matrix that physically shields the protein from abiotic stress.

Protein stability can also be improved upon diluting proteins in a rigid, inert glassy solid matrix that slows down molecular motion (Figure 1.4c). This kinetic mechanism for protein stabilization is often referred to as "glass dynamic hypothesis" or vitrification.[51] This molecular crowding effect alters the molecular motion of water molecules, similar to that of osmolytes, and consequently modifies the localized environment of the protein. This method of entrapment results in molecular retardation and a reduction in conformational change. These approaches decrease the rate of molecular motion and provide a kinetic method toward protein stability.

Proteins can also be stored in solid form to prolong shelf lifetime. This is commonly achieved through freezing in solution or through lyophilization, also known as freeze-drying.[52] By storing proteins in the solid form, protein conformational change is

impeded. However, removal of a protein's hydration shell may shift the equilibrium between the native and unfolded state. Different types of interfaces, such as air/liquid, air/solid or solid/liquid, are introduced during the drying process. This local change in the protein environment can result in protein unfolding as a way to passivate the interfacial tension of this interface. In addition, the drying process may cause localized strain on the protein as the solvent expands or contracts during freezing.

1.4.2. Biological Modification

Another approach involves the modification of the protein itself. Protein primary structure can be altered to enhance the intramolecular interactions between residues, optimizing stability as a function of environmental conditions. A combinatorial protein library of macromolecular states provides a fast way to analyze a large group of permutations and to obtain a statistical evaluation on performance as a function of amino acid sequence. There are two biological techniques that are prevalent. One is through directed evolution[53, 54] (protein redesign) and the other is through de novo design[55] (protein design).

In protein redesign, an existing protein is evaluated in terms of thermodynamic stability and efficient functionality. Over multiple rounds of mutagenesis and screening, an accelerated version of divergent evolution is simulated. In several cases, changes to only a few amino acids is sufficient to offer higher orders of protein stability, tolerance to non-natural conditions, substrate specificity, and product selectivity.[56, 57] In de novo design, functional motifs are taken from an established collection of known sequences. Non-canonical proteins are constructed around these structural themes. A combinatorial library can then be made featuring this motif, creating new proteins with adequate performance for a desired set of environmental conditions.

These methods, though, are tedious, time consuming, and require extensive resources. Since directed evolution is performed in bacteria, using this technique to create proteins that solubilize and remain stable in non-polar organic solvents remains highly improbable. Using de novo design, on the other hand, can be used to generate proteins that fold in organic solvents. They can be used to predict and direct the synthesis of new proteins with new functions and new architectures.[58] However, the amount of computational time becomes a limiting factor; large protein assemblies are not appropriate for this technique. In addition, a predicted structure computationally does not guarantee a desired result experimentally.

1.4.3. Chemical Modification

Chemical modification has had great success in creating stable proteins in non-native environments. The chemistry is fairly straightforward and subsequent results have shown great promise. By targeting certain chemical moieties found on the protein, it is possible to create opportunities to make proteins more accessible in the engineering

sense. Something as simple as n-terminal acetylation can be used to stabilize helical protein structures.[59]

The most popular approach involves the covalent attachment of polymers onto the surface of proteins, i.e. protein-polymer conjugates.[3] Protein-polymer conjugates are a family of soft materials where polymers are either grown from or grafted to the surface of the protein, as seen in Figure 1.5.[60-65] The attachment of polymers with appropriate compositions could potentially mitigate the limitations of proteins by mediating the interactions between the proteins and the local medium.[62, 66, 67] One specific polymer, poly(ethylene glycol) (PEG), has unique chemical properties, such as high solubility, amphiphilicity, and inertness, which translates to stabilization of proteins in non-native environments. Unfortunately, PEGylation requires the protein to have a surface chemistry that is compatible with polymer attachment.
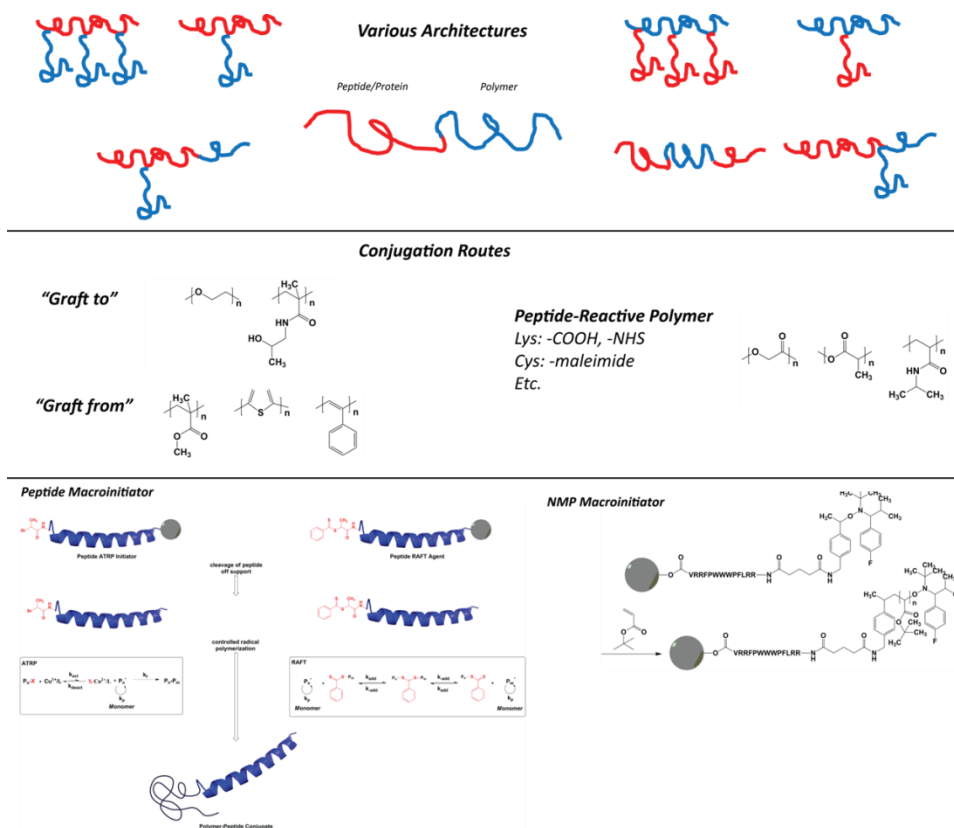
Figure 1.5. Overview of the various routes available for the conjugation of polymers onto proteins.

Alternatively, proteins can be intramolecularly crosslinked.[68] This reduces the amount of conformational states available to the protein and restricts unfolding. However, two limitations arise when employing this technique. First, as previously stated, chemical modification requires a certain chemical composition. Two amino acids

with chemical groups compatible with crosslinking must be in close proximity. Second, protein function is linked to a mechanical action. By crosslinking the interior of the protein, the fluidity that gives rise to protein response can be hindered and result in a loss of native protein activity.

1.4.4. Physical Modification

An approach that has less reliance on protein chemistry is through physical modification. This can be executed through adsorption onto a flat surface, ionic binding of proteins with protecting agents, physical entrapment in crosslinked matrices, sequestration of proteins in nanopores, or encapsulation of proteins in micellar constructions.[69-72] By confining the protein with a sterically hindering structure, the amount of microstates available to the protein is reduced.

Experimentally, nanoencapsulation has gained momentum as an emerging technique. Long-term room temperature storage of many proteins has been demonstrated in sol-gel matrices.[73] Confined enzymes not only remain reactive for extended periods of time but also show higher orders of activity retention than enzymes in suspension. In nature, chaperones enable protein folding and refolding.[74] They provide a nanoscopic environment that limits the energy landscape accessible to the protein. This approach toward protein stabilization can be replicated using synthetic nanometer-sized compartments as well as surface immobilization,[75] but the need for a solid support limits the number of viable applications.

Protein modification can also be achieved through the use of surfactants.[76-78] As an example, membrane proteins have notoriously poor stability and a high tendency to denature upon removal from their native environment. A class of random copolymer surfactants, amphipols (APols), has been developed to substitute small molecule surfactants for membrane protein reconstitution.[79-83] They are comprised of a hydrophilic polymer backbone with hydrophobic chains that act as anchoring points to the membrane protein, stabilizing the structure of the hydrophobic protein in the presence of water. APols also provide the extra benefit of thermostability and longer protein lifetimes. Micelles have been shown to successfully solubilize proteins, creating a colloidal dispersion in a variety of solvents, but the dynamic nature of micelles commonly results in loss of protein activity after extended storage.

§ 1.5. Heading toward the Nanoscale

Block copolymers (BCPs) provides a route toward protein assemblies at the nanoscale.[67, 84] BCPs can microphase separate into very distinct nanometer features[85] and have been shown to direct the assembly of proteins into a variety of nanometer-spaced hierarchical structures, such as lamellae, hexagonally-packed cylinders, closed-packed spheres, and gyroids.[67, 85] At the nanoscale, chemical processes are enhanced. The

frequency of particle-to-particle interactions is increased and substrate diffusion limitations are reduced. This can greatly improve a variety of technologies, including sensors and enzyme cascades.[86]

Through the use of different processing techniques, various macroscopic structures can be generated to fit a specific application. Co-assembly of block copolymers and proteins can generate bulk gel structures with a bicontinuous phase, generating materials ideal for gas transport with in built-in gas selectivity (Figure 1.6a). Block copolymer thin films can be used to arrange proteins into two dimensional arrays with high transparency, ideal for smart coatings, separation, and sensing devices (Figure 1.6b). Electrospun nanofibers can provide building blocks for the construction of macroscopic materials with high surface area, useful for catalysis (Figure 1.6c). Lastly, multilayered colloidal particles are useful for the controlled release of protein therapeutics (Figure 1.6d).
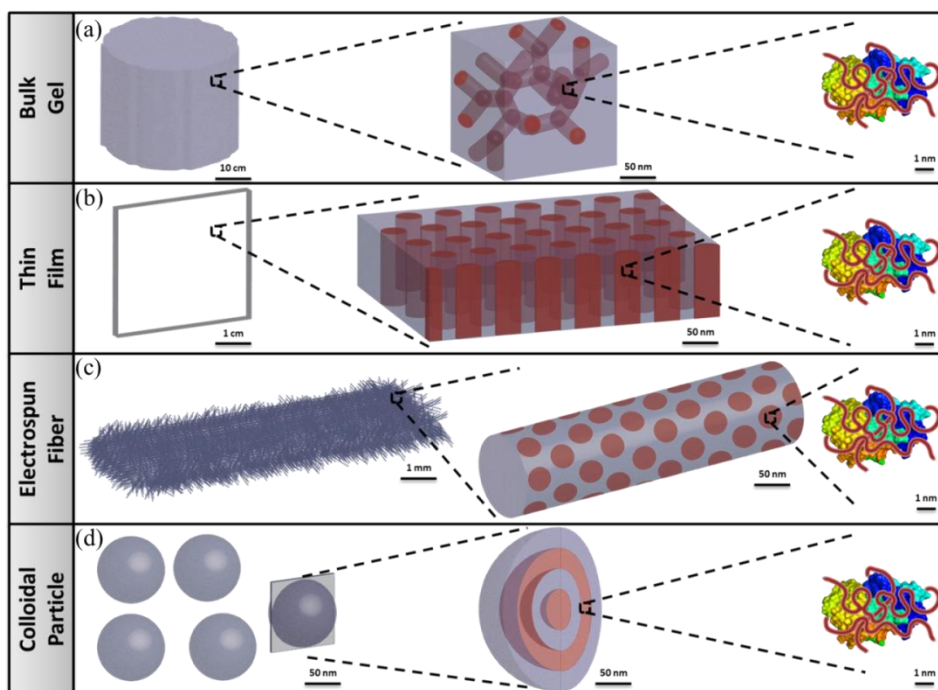
Figure 1.6. Co-assembly of proteins in block copolymer templates. Different macroscopic structures provide appropriate architectures for specific applications. Directed assembly of proteins in block copolymer (a) bulk gels, (b) thin films, (c) electrospun fibers, and (d) colloidal particles.

§ 1.6. Perspective and Outlook

The materials field needs an approach for the generation of protein-based materials. Proteins offer unprecedented performance that cannot be replicated solely

through synthetic reproductions. Areas of industrial scale catalysis, energy, purification, and even military weapons would see immediate impacts, areas typically not associated with proteins. The motivation of this work is to understand protein-macromolecule interaction at the fundamental level and use this knowledge to engineer new functional materials. It is only when we understand the relationship between chemistry, structure, and performance can we generate protein-functionalized materials. This success will translate into an enhanced quality of life.

For example, proteins can selectively modify complex molecules, creating products that are enantiomerically pure with precise stereospecificity and chemoselectivity. In the multitrillion dollar pharmaceutical industry, the Food and Drug Administration pushes for products that are monodispersed, homogenous, and pure. Batch to batch variation or deviations in stereochemistry can make drugs less reliable and less effective. Paclitaxel is a chemotherapeutic drug that suffers from poor water solubility and has a structure with multiple chemical handles. Through the use of specific enzymes, divinyl adipate and lipases, it is possible to selectively attach glucose to this hydrophobic therapeutic.[87-89] This results in an increase in hydrophilicity and pharmacokinetics. In a different industry that requires catalysts, the conversion of cellulosic materials into suitable biofuel products requires the initial breakdown of cellulose into its monomeric sugar units. Currently, the most effective way in breaking down cellulose is through the use of cellulase, a class of enzyme that hydrolyzes cellulose into glucose.[90-92]
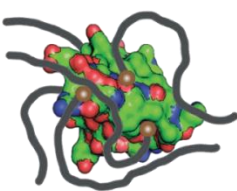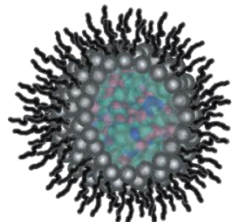
In the energy field, proteins can be used in a variety of novel applications. Photosystem I protein can be used to generate a current using sunlight.[93-96] There has been a recent push toward both artificial and synthetic photosynthesis. The incorporation of photosystem I proteins into next generation photovoltaics, a macromolecule that has efficiencies far exceeding synthetic reproductions, would cause a definitive resurgence in the solar energy field. Enzyme-based fuel cells, another approach toward alternative energy sources, involves the use of reductive and oxidative protein-pairs that can split and reform molecules.[97, 98] This results in the generation of a current with substrates and products that are environmentally safe.

In the military, proteins can be used to improve the lives of soldiers on the battlefield. Chemical warfare agents are problematic weapons with detrimental effects. The incorporation of organophosphorus hydrolase proteins into smart fabrics and filters would provide a device that can save lives.[70, 99-102] These proteins degrade organophosphates into inert molecules with high efficiency. In addition, the United States Airforce has experimented with the use of proteins in ammonium perchlorate-loaded apoferritin-Al hybrids. The combination of proteins with inorganic materials, oxidizing agents, and explosive materials have resulted in a new class of explosives, called biothermite, where reactivity is controlled by the amount of protein adsorbed onto the surface of the material.

No matter the application, there are always improvements needed for these protein-based systems. Paclitaxel and lignocellulose require organic media for solubilization and processing. In addition, proteins are expensive reagents and finding a way to recycle them in these processes would benefit the industry financially. Being able to have precise control over protein-synthetic material interactions is also needed. For example, enzyme-based fuel cells require proteins to interface properly with anodes and cathodes. Photosystem I proteins must be oriented properly in order to participate in efficient electron transport. By finding a way to stabilize proteins in organic solvents, it is possible to improve a lot of these cutting-age technologies.

§ 1.7. General Approach and Synopsis of Subsequent Chapters

Throughout subsequent chapters, I will present on a new route toward protein stabilization. Past members in our group have focused on the enhancement of protein structure and function through the use of covalently attached polymers, as seen in Figure 1.7.[3, 15, 62, 66, 67, 103-105] The protein-polymer conjugate field is well established, with bioconjugate synthetic protocols widely available. In addition, there are a variety of polymers with chemical handles that can be attached to proteins. However, the chemistry of the protein must be compatible to conjugation, and the chemistry of the polymer must not interfere with protein structure. In addition, purification of protein-polymer conjugates is difficult, time consuming and reduces product yield.

Figure 1.7. Advantages and limitations of protein-polymer conjugates and protein-encapsulated reverse micelles.

A different approach, which will be the topic of this dissertation, involves the use of surfactants to solubilize and stabilize proteins. Unlike protein-polymer conjugation, this technique is non-specific and can be easily done through emulsions. These structures, however, are fairly dynamic in nature and long-term protein stability is compromised. In order to make reverse micelle encapsulation a viable method, enhancement to the current approach must be explored.

In this dissertation, I will first show a method of developing hierarchically structured protein-based composites using an existing approach, specifically reverse micelle formation using small molecule surfactants. Next, I will show its limitations and the need for new polymer surfactants. I will go over the design process, the characterization of the polymer, and our analysis of its ability to stabilize proteins in both organic solvents and elevated temperatures. Lastly, I will demonstrate the viability of this approach to create new model protein-functionalized materials that can be used as a platform for future technologies.

Co-Assembly of Protein-Encapsulated Reverse Micelles and Block Copolymer-Based Supramolecules toward Functional Hybrid Materials

Hybrid materials with persistent nanoscale protein ordering have the potential to provide significant improvements for a variety of applications. Combining block copolymers and proteins would endow benefits from both the synthetic and natural world. Block copolymers provide a three-dimensional scaffold for protein patterning, and proteins provide a level of functionality unmatched by manmade materials. However, maintenance of protein structure and activity while permitting uninhibited block copolymer microphase separation are two self-assembly processes that require compatible processing techniques. In this chapter, I will discuss an approach toward simultaneous co-assembly of proteins and a block copolymer-based supramolecule in organic media. Proteins are first encapsulated in reverse micelles and then co-solubilized with the block copolymer prior to spin casting and electrospinning. This bottom-up approach toward protein nanoassemblies provides unimpeded microphase separation of the block copolymer-based supramolecule and demonstrates our ability to preserve protein activity and accessibility. Endowment of protein functionality to block copolymer-based supramolecules will lead to nanocomposites containing complex hierarchical structures with enhanced processability and potential scalability.

§ 2.1. Introduction

Nanostructured materials for display or delivery of proteins have the potential to alleviate many scientific shortcomings. Nanoscale protein arrays have been developed to improve diagnostic applications.[1] Multivalent ligand presentation on drug nanocarriers has proved to increase the efficacy of drug therapeutics through active targeting.[2] Cell-culture substrates with a controlled presentation of biological ligands have the ability to manipulate cellular differentiation, migration, and viability.[3] Furthermore, tethered proteins with nanometer spacing have aided in enzyme cascades.[4]

Block copolymers (BCPs) are an important class of nanostructured materials that have found diverse applications in lithography, electronics, and inorganic materials synthesis, and they have the potential to be exploited for protein-based nanomaterials. Their utility arises primarily from the well-defined nanoscale morphologies that result from the microphase separation of two or more chemically incompatible polymer blocks.[5] These blocks are covalently tethered along the polymer backbone, resulting in a unique set of accessible hierarchical structures when processed from solution. BCP assemblies have been studied in solution as well as in condensed phases, which include bulk preparations, thin films on surfaces, and fibers. Long-range ordering in these latter cases can be achieved through a variety of annealing techniques, and polymer functionality can be augmented through the addition of nanoparticles,[6] homopolymers,[7, 8] and small molecules.[9-11] Furthermore, BCPs have the ability to direct the assembly of these types of additives. Incorporation of proteins is very desirable as it would endow BCP nanostructures with a diverse set of functional and structural elements with angstrom-level resolution.[12]

Top-down assemblies are generally employed to pattern proteins at the nanoscale. Nano-patterned protein assemblies are prepared via stepwise adsorption of proteins onto a substrate. As discussed in the previous chapter, retention of protein activity during material processing is a large concern. A top-down approach provides a means to retaining protein function; it separates scaffold processing from the ability to keep proteins in a compatible environment. Techniques such as direct dip-pen and native protein nanolithography,[13-15] photolithographic patterning,[16] and microcontact printing[17] have seen great success in the scientific community.

Alternatively, BCPs can be used to pattern protein nanoassemblies via a bottom-up approach. Previously, our group had reported the co-assembly of peptides and proteins with amphiphilic BCPs in thin films.[18, 19] While the majority of protein/BCP assemblies have been prepared via stepwise anchoring of proteins from an aqueous solution onto prefabricated polymer surfaces,[20-22] our group demonstrates the ability to simultaneously co-assemble protein-polymer conjugates and BCPs from organic solution. This co-assembly strategy benefits from enhanced processability as well as increased biological activity. In addition, proteins are made an integral component of the material rather than just a discrete, appended layer on the surface. In many cases, however, target proteins cannot be sufficiently modified so as to maintain structure and function during assembly. Rather, proteins remain insoluble in the non-aqueous environment or are denatured.

In this chapter, I will report the use of surfactant-based reverse micelles as a way to expand the scope of proteins compatible with BCP co-assembly. Reverse micelles, comprised of a colloidal dispersion of surfactant-bound water droplets in a non-polar phase, have been used to solubilize a variety of polar molecules, including proteins and other biomolecules, in organic solvents.[23-29] In particular, sequestration of proteins in reverse micelles has allowed for protein purification via liquid-liquid extraction, led to enhanced protein stability, and expanded the scope of enzymatic chemistry that would otherwise be limited to aqueous media. I will demonstrate that reverse micelles can be assembled with BCPs and be used to incorporate enzymes in the resulting hybrid materials. Proteins remain active throughout the entire process and can be incorporated not only into block copolymer thin films but in block copolymer electrospun fibers. I anticipate that further development of this modular system will allow us to incorporate proteins in BCP materials that were previously considered bio-incompatible, leading to a new generation of materials.

§ 2.2. Results and Discussion

Previously, our group had reported the co-assembly of heme-binding coiled coil α-helix bundle peptides and horse heart myoglobin (Mb), a naturally occurring heme protein, with poly(styrene)-*block*-poly(ethylene oxide) (PS-*b*-PEO) in thin films.[18] Conjugation of PEO to these biomolecules resulted in stabilization of peptide structure in the case of the helix bundles and preservation of protein structure and function in the case

of Mb. Unmodified Mb, on the other hand, was incompatible with the organic solvents used in solution processing and thin film solvent annealing.

Polymer conjugation in this manner was employed to enhance compatibility with organic solvents, although this approach proved unsuitable for various proteins in conjunction with the PS-*b*-PEO and other amphiphilic BCPs. For example, co-assembly of BCPs with PEO-modified horseradish peroxidase (HRP), a heme protein widely used for detection in biological assays, resulted in precipitation of proteins from organic solution prior to film processing. When this strategy was employed for the co-assembly of BCPs with glucose oxidase (GOx), a flavin-dependent enzyme used for glucose determination and other sensing applications, GOx was dissolved in solution. However, no activity was observed after incorporation of GOx-PEO conjugates with BCPs. PEO conjugation was verified using gel electrophoresis (Appendix A.1.1), but as shown in Appendix A.1.2, introduction of methanol decreased the activity of the protein and incorporation of GOx-PEO in a 2:1 mixture of benzene and methanol caused complete protein denaturation.

Limited compatibility of HRP and GOx is presumably related to the low levels of PEO that can be appended to the protein surfaces using conventional conjugation chemistry. Therefore, a strategy that obviates the need for covalent modification of proteins was investigated. Surfactant reverse micelles were used to incorporate proteins into BCP samples in organic solution. Sodium 2-bis(hexylethyl) sulfosuccinate (AOT) was chosen for the formation of protein-containing reverse micelles. AOT has been widely studied and is known to solubilize relatively large volumes of water in nonpolar solvent. The surfactant facilitates formation of thermodynamically stable, spherical reverse micelles with nanometer dimensions.[30] This provides a good vessel for protein processability in organic solvents; proteins remain in the aqueous reverse micelle core and the reverse micelle shell allows enhanced organic solvent solubility.

In order to form reverse micelles, an aqueous protein solution was injected into an AOT-containing, non-polar toluene solution. After sonication and brief mixing under a stream of nitrogen, the reverse micelle solutions were optically clear. This indicated that AOT reverse micelles accommodated HRP and GOx, as seen in Figure 2.1a and Figure 2.1b respectively. Without AOT, the aqueous protein solution remained insoluble in toluene and was unable to be further processed (Figure 2.1c). The $[H_2O]:[AOT]$ molar ratio was kept at w~13, which led to an AOT-protein particle size of around 4 nm,[31] small enough to be incorporated into the block copolymer microdomains. AOT-protein particle size was verified by dynamic light scattering (DLS) (Figure 2.1d). Colorimetric assays were used to evaluate the activity retention of HRP in AOT/HRP reverse micelles and of GOx in AOT/GOx reverse micelles after incorporation into toluene. Over 24 h, aliquots of AOT/protein reverse micelles were dispersed in aqueous buffer. This allowed us to disrupt the reverse micelle, free the protein, and evaluate protein functionality exclusively. As shown in Figure 2.1e, about 20% of HRP activity and 90% of GOx activity was maintained after 24 h. These times can be considered extreme cases for

block copolymer co-assembly; co-processing would occur within the first hour, which would provide enough protein activity to produce a viable functional hybrid material.
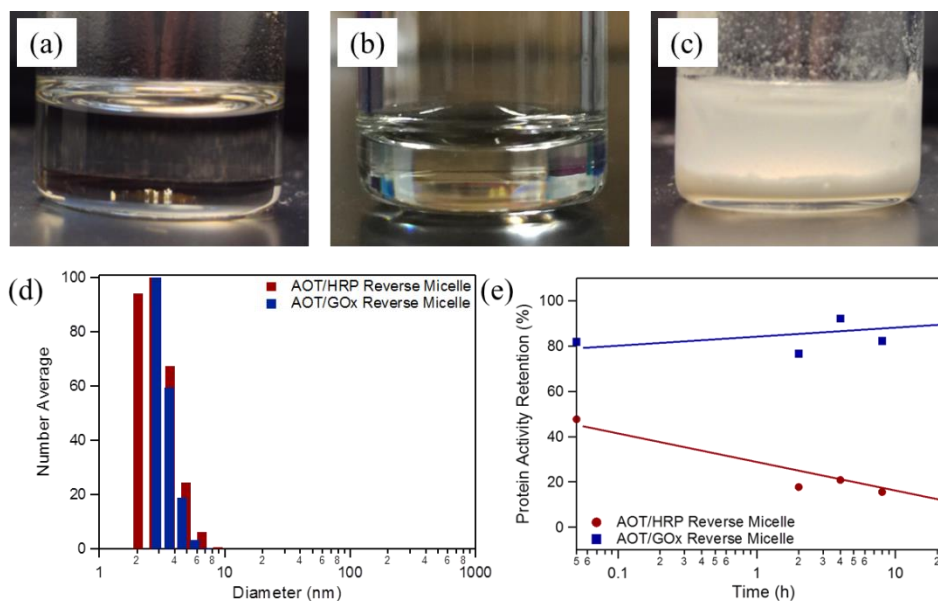
Figure 2.1. Encapsulation of proteins in AOT-mediated reverse micelles. Photos after AOT-mediated encapsulation of (a) HRP and (b) GOx in toluene. (c) Photo of aqueous HRP processing attempt in toluene without AOT. (d) Number average DLS distribution of AOT/HRP reverse micelles and AOT/GOx reverse micelles. (e) Activity of HRP and GOx after storage in organic media and subsequent dispersion in aqueous buffer.

The reverse micelles were blended with chloroform solutions containing (24 kDa)poly(styrene)-*block*-(9.5 kDa)poly(4-vinyl pyridine) (PS-*b*-P4VP) and 3-pentadecylphenol (PDP), and the resulting mixtures appeared homogenous with no protein precipitation. In this manner, the reverse micelle-based strategy proved much more versatile with respect to protein incorporation than the previously reported polymer conjugation approach. The selection of this comb-coil block supramolecule is three-fold. First, directed assembly of alkyl-functionalized nanoparticles has been well-studied in this PS-*b*-P4VP(PDP) system.[32, 33] AOT's alkane moieties are chemically similar to the PDP that is hydrogen bonded to the P4VP pyridyl sidechains, as shown in Scheme 2.1. Therefore, AOT reverse micelles are expected to segregate within the PV4P(PDP) microdomain in the block copolymer-based supramolecule. Second, solvent annealing has been shown to provide sufficient mobility in this system to achieve long-range ordering without the need for elevated temperatures.[34] Heat, consequently, would provide an additional extrinsic source that may lead to protein denaturation. Third, adjustment of PDP loading alters the volume ratio of the supramolecule block, providing another method for controlled organization of proteins within thin films.[9]
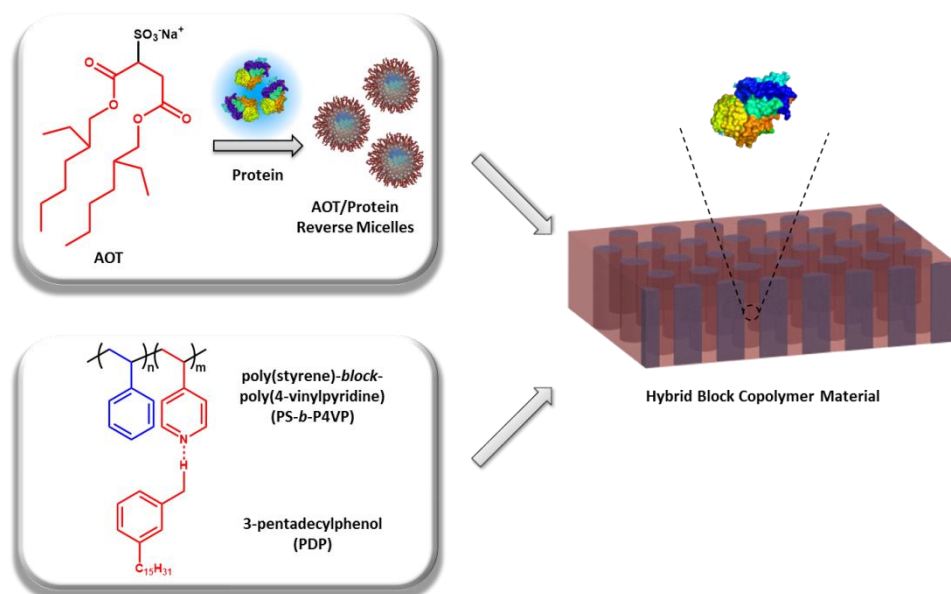
Scheme 2.1. Co-assembly process of protein-encapsulated AOT reverse micelles and PS-*b*-P4VP(PDP). The AOT alkyl tail, shown in red, is chemically compatible with the PDP alkyl chain, also shown in red.

Thin films were prepared by spin-casting the blended solutions onto silicon substrates, resulting in films with thicknesses of ~100 nm. The protein loading ranged from 0.005-5% (w/w). Following spin casting, the films were solvent-annealed with chloroform vapor to provide polymer mobility and promote microdomain ordering. Chloroform is both a good solvent for polystyrene and 4-vinyl pyridine, compatible with PDP, and miscible with the toluene used during protein encapsulation. The thin film morphology was found to depend on the level of AOT loading. Thin films containing a [4VP]:[PDP] molar ratio of 1:1 exhibited a lamellar film morphology. Addition of up to 0.2 molar equivalents of [AOT] per [4VP] and 0.5% GOx also resulted in thin film lamellae, as observed by atomic force microscopy (AFM) with a sample containing 1:0.14 [4VP] to [AOT] (Figure 2.2).
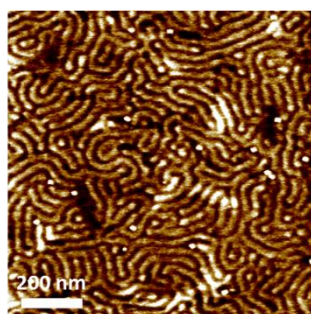
Figure 2.2. AFM phase image of PS-*b*-P4VP(PDP) containing GOx. Film was fabricated with a [4VP]:[AOT] ratio of less than 0.2 molar equivalents.

25

When more than 0.2 equivalents of AOT was added, films exhibited a hexagonally-packed cylindrical morphology. Addition of AOT/protein reverse micelles with a [4VP]:[AOT] molar ratio of 1:0.7 resulted in a BCP thin film with hexagonally-packed cylinders for HRP-containing (Figure 2.3a), GOx-containing (Figure 2.3b), and HRP/GOx-containing films (Figure 2.3c). The cylinders presumably consist of polystyrene, while the matrix is comprised of P4VP/PDP/AOT. With the addition of AOT/protein reverse micelles, the volume fraction of the P4VP(PDP) microdomain increases through sequestration of the AOT and protein, providing an explanation for this shift from lamella to cylinders. The composite thin films were studied by grazing-incidence small angle x-ray scattering to characterize macroscopic ordering and morphology beneath the film surface. Although hierarchical ordering on multiple length scales has been demonstrated for this PS-*b*-P4VP/PDP system, reverse micelle incorporation was found to interfere with angstrom-scale ordering within the P4VP/PDP comb-blocks as well as the nanometer-scale ordering of the BCP microdomains below the surface (Appendix A.1.3). Further optimization of annealing conditions will be required for preparation of well-ordered materials.
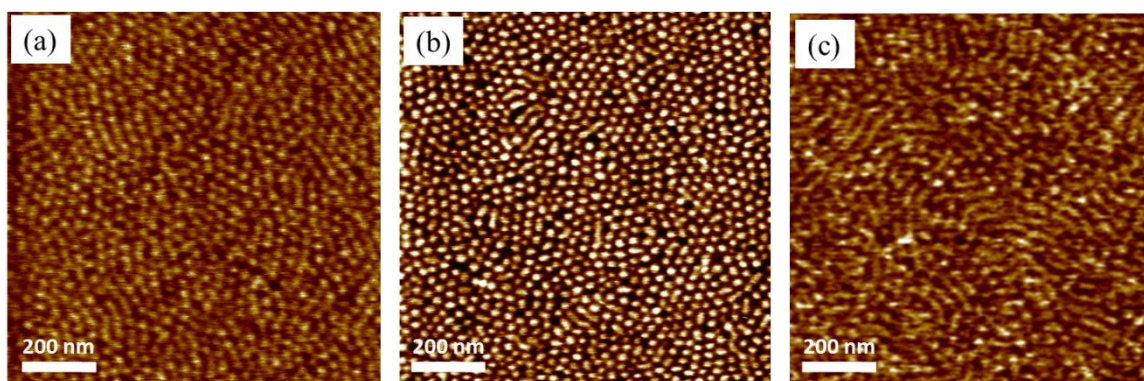
Figure 2.3. AFM phase image for PS-*b*-P4VP(PDP) containing a [4VP]:[AOT] ratio of more than 0.2 molar equivalents. Films were loaded with (a) 0.5% (w/w) GOx, (b) 0.5% (w/w) HRP, and (c) 0.25% (w/w) GOx and 0.25% (w/w) HRP.

Enzymatic activity in thin films was assessed using colorimetric assays. Retention of activity was observed for HRP and GOx, as well as two serine-based proteases, chymotrypsin and subtilisin. Figure 2.4a depicts the detection of HRP decomposition; reduction of hydrogen peroxide was monitored using a colorimetric electron donor, 3,3',5,5'-tetramethylbenzidine (TMB). When TMB is converted into its diimine version, the reaction can be verified visually by the appearance of a blue chromophore. Figure 2.4b depicts the detection of GOx-generated hydrogen peroxide upon glucose oxidation. As 4-aminoantipyine is converted to 4-N-(p-nitrobenzquinone)-antipyrine during this multistep assay, the activity of GOx can be verified visually by the

appearance of a red chromophore. This result is in marked contrast to previous assembly attempts with GOx-PEO conjugates.
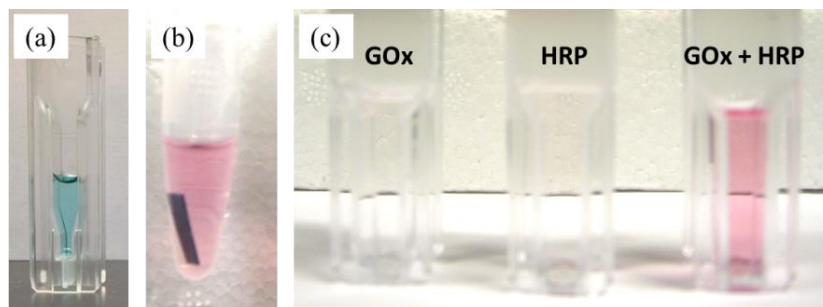
Figure 2.4. Assessment of protein activity after thin film processing. Changes in solution color for (a) HRP, (b) GOx, and (c) HRP/GOx mixed films indicate functional enzymes.

Product formation was also observed when both enzymes were loaded in thin films via reverse micelles (Figure 2.4c). The combination of multiple proteins proved to be a potential route for hybrid materials that require specific functionality, enhanced sensing capabilities, and increased reaction rates. Enzyme cascades, for instance, would benefit from this co-assembly approach.[35, 36] Combining multiple enzymes into block copolymers would increase protein density in localized areas of the material. This would result in a subsequent decrease in complementary enzyme spacing. Substrate diffusion between the two enzymes would be greatly reduced, thus enhancing the kinetics of the multistep catalytic conversion.

Protein storage within these polymer thin film hybrids was also evaluated. For example, HRP and GOx were both only able to retain ~25% of their initial activity in the PS-*b*-P4VP(PDP) thin films after 20 h under ambient conditions, as shown in Figure 2.5a and Figure 2.5b respectively. Chymotrypsin (CT), contrastingly, was able to retain ~60% of protein activity after storage in BCP thin films at ambient conditions for 20 h and ~40% after 50 h, as shown in Figure 2.5c. These results suggest that by tuning the interactions between the different components, it is possible to tailor the required storage time for a given application.
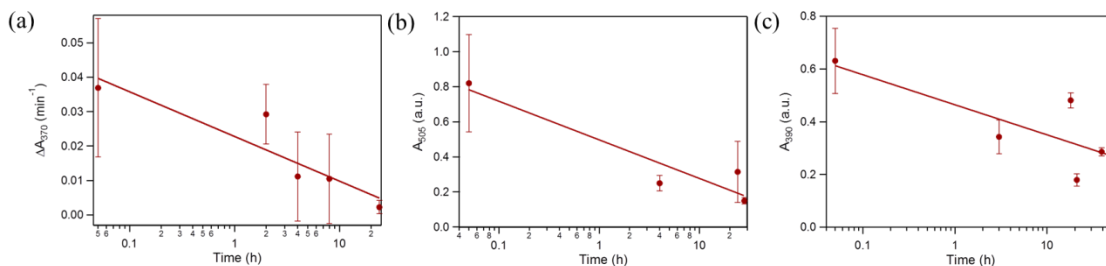
Figure 2.5. Storage assessment of protein-containing thin films. (a) HRP-, (b) GOx-, and (c) CT-containing thin films were stored under ambient conditions until tested in buffer.

Similarly, tuning the interactions between protein, surfactant, and block copolymer will allow us to tailor protein delivery. Upon exposure to aqueous solutions, proteins are expelled out of the films at different rates. HRP was observed to leach out of BCP thin films immediately. Assays verified that all of the detected activity was observed in the buffer bath – about 90% – and very little was observed in the films after 30 min (Figure 2.6a). This was also observed for films containing AOT/GOx reverse micelles. In fact, nearly complete leaching of HRP and GOx was observed during bath times in as short as 10 min. Contrastingly, ~90% of the CT remained in BCP thin films after exposure to an aqueous buffer for 30 min. Very little activity was found in the bath (Figure 2.6b).
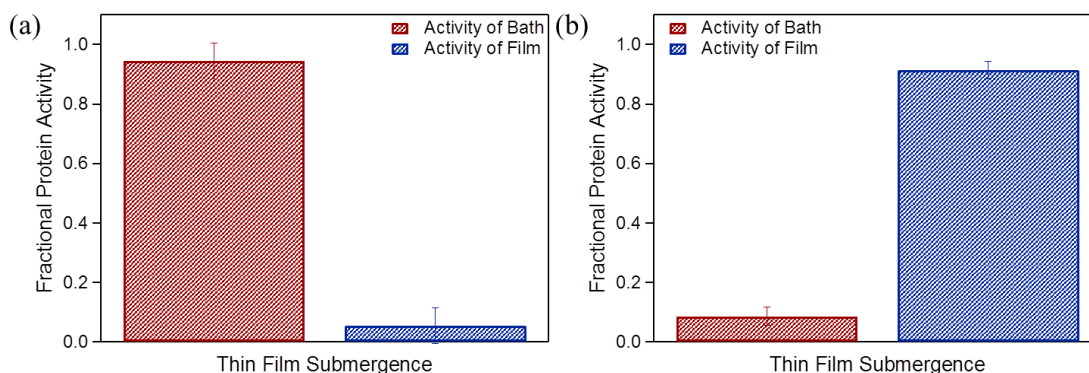
Figure 2.6. Leaching assessment of protein-containing thin films. (a) HRP- and (b) CT-containing thin films were submerged in their respective buffers for 30 min. These baths were analyzed using colorimetric assays.

It was not immediately clear, however, why CT should be retained in the BCP thin films while the HRP and GOx leached into solution within several minutes. Two variables, molecular weight and isoelectric point, are obvious differences between the three proteins. These two attributes may affect thin film assembly characteristics. In particular, the relatively high pI of CT (9.4) results in a positively-charged protein under assay conditions which may interact with anionic AOT. This may explain the increased retention time for CT in block copolymer thin films. HRP and GOx, meanwhile, are not positively-charged under assay conditions and would not be subjected to electrostatic-based retention.

In an attempt to increase the protein residence time in thin films, formation of protein-surfactant ion-pair complexes was investigated. We speculated that hydrophobic protein-surfactant complexes formed via pairing of positively-charged amino acid residues with negatively-charged surfactant head groups would be less likely to leach into the aqueous solution. The relatively low levels of surfactant required to form the ion-pair complexes might also be an advantage, possibly leading to minimal perturbation of BCP

morphologies after thin film processing. AOT did not form active complexes with HRP or GOx in our hands, but the detergent was suitable for formation of active CT complexes, as reported in literature.[37] Contrary to our expectations, however, chymotrypsin loaded as ion-paired complexes leached from thin films to a greater extent than chymotrypsin loaded as reverse micelles. As shown in Appendix A.1.4, the majority of chymotrypsin leached from thin films prepared with ion-paired complexes within 10 minutes after exposure to aqueous solution. As previously stated, ~90% of chymotrypsin loaded in reverse micelles was retained in the PS-*b*-P4VP(PDP) thin films after 30 min in a buffer bath. This result suggests that particles or surface coatings composed of the BCP/reverse micelle hybrids may be an effective vehicle for protein storage or delivery, but further analysis must be used to evaluate why ion-paired complexes leached out of films to a much greater extent.

AOT reverse micelles were prepared with HRP in buffers with pH values below the protein's pI. This ensured positively-charged protein and promoted interaction with the negatively-charged surfactant. Small increases in retention were observed when the pH of the reverse micelle buffer and the reaction buffer was reduced (Appendix A.1.5). Highest retention levels (~40%) were observed when the reverse micelle buffer pH was reduced to 4.6 and the reaction buffer pH was reduced to 6. Further decreases in pH led to an observed drop in protein retention. As an alternative to protein charge tailoring via pH adjustment, the use of cationic cetyltrimethylammonium bromide (CTAB) for pairing with negatively-charged proteins was explored. CTAB proved too crystalline for effective incorporation into the PS-*b*-P4VP(PDP) thin films, however, as seen in Appendix A.1.6.

HRP, GOx, and CT span a relatively large range of molecular weight, isoelectric points, and structural motifs. Because chymotrypsin remained active and resident within the PS-*b*-P4VP(PDP) thin films, co-assembly of the block copolymer and other serine-based proteins with similar physical and chemical characteristics were explored. Reverse micelles comprised of AOT and trypsin or subtilisin were prepared. Although chymotrypsin and trypsin are close analogues, reverse micelles containing trypsin capable of cleaving p-nitroanilide substrates were unable to be prepared. Several reports describe the preparation of reverse micelles containing active trypsin, so additional studies are needed to optimize AOT/trypsin reverse micelles in our hands. Active subtilisin, conversely, was readily incorporated into AOT reverse micelles. Despite similarities in molecular weight and isoelectric point for chymotrypsin and subtilisin, subtilisin was observed to leach from the films into aqueous solution within 30 min (Figure 2.7), no matter what buffer was used: a buffer optimized for chymotrypsin or a buffer optimized for subtilisin. This may indicate that chymotrypsin's extended residence time in thin films may not be a function of solely size or isoelectric point. Further investigation must be conducted.
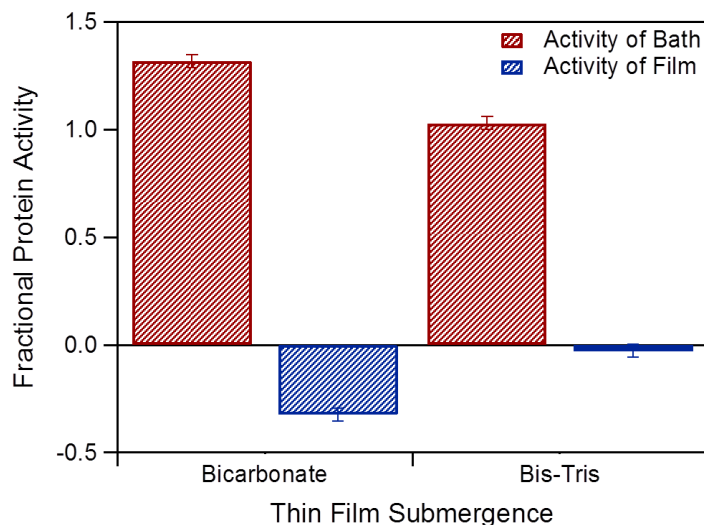
Figure 2.7. Analysis of subtilisin activity in thin films. Activity is assayed based on proteolysis of N-succinyl-Ala-Ala-Pro-Phe-p-nitroanilide at pH = 8.0. Activity was measured in (a) bicarbonate buffer optimized for subtilisin and (b) bis-tris buffer optimized for chymotrypsin. Films were incubated in the bath for 30 min.

Electrospun fibers are useful building blocks to construct macroscopic materials with high surface area, useful for catalysis.[38-42] Electrospinning is a technique that takes advantage of an electric potential to drive the creation of thin fibers from a polymer solution or melt. The application of a sufficiently high voltage uniaxially stretches the viscoelastic liquid out from a narrow outlet. For electrospun BCP fibers, BCPs self-assemble and form nanostructures mainly governed by the BCP phase behavior.[43, 44] The creation of protein-loaded electrospun fibers often involves the dissolution of protein in a biocompatible polymer fluid and electrospinning from water. Proteins are embedded within the interior of the fiber and are shielded from the environment.[45] Proteins provide a functional aspect to the fiber and the BCP provides an internal structure that could play a vital role in tailoring these fibers to achieve desirable attributes.

Upon electrospinning of a solution containing AOT/HRP reverse micelles and PS-*b*-P4VP(PDP) from chloroform, successful formation of a fibrous mat was observed optically (Figure 2.8a), cylindrical fibers were observed using scanning electron microscopy (Figure 2.8b), and microphase separation of BCP domains within the interior of the fiber was observed using cross-sectional transmission electron microscopy (Figure 2.8c). Incorporation of HRP-encapsulated reverse micelles shows little interference with electrospun fiber formation, and the fibers exhibited the ability to microphase separate into two unique domains. Furthermore, the application of an electric potential and an increase in solution viscosity, needed for electrospinning, produced minimal disturbance of reverse micelle complexes, as verified by active HRP.
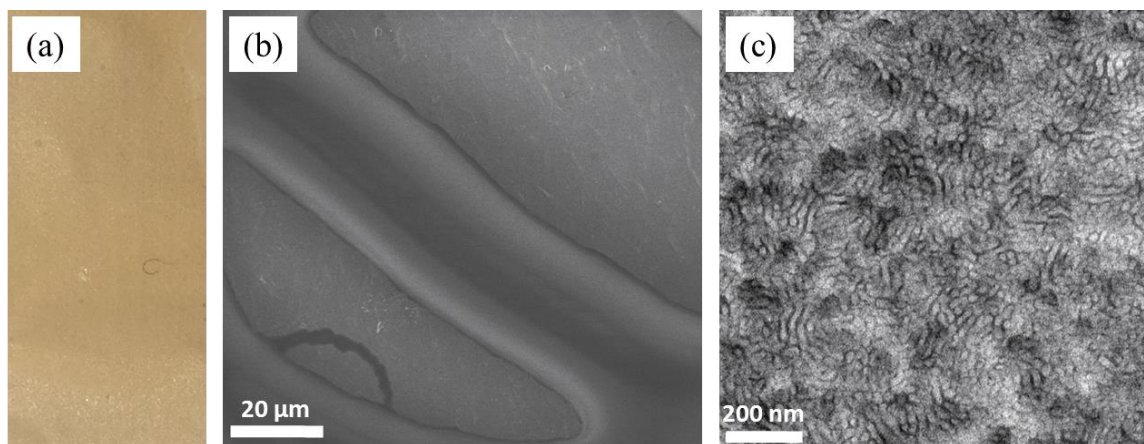
Figure 2.8. HRP-containing electrospun fibers. (a) Optical image of electrospun fiber mat containing AOT/HRP reverse micelles. (b) SEM and (c) cross-sectional TEM of BCP fiber mat.

§ 2.3. Conclusion

In conclusion, we have demonstrated the co-assembly of protein-containing surfactant reverse micelles and BCP-based supramolecules in both thin films and electrospun fibers. This strategy greatly expands the scope of proteins that could be incorporated into protein-based hybrid materials. Protein activity was retained for various classes of proteins, and proteins remained functional during storage in thin films, more so for chymotrypsin. Proteins were observed to leach from the thin films upon exposure to aqueous solution, although chymotrypsin was a notable exception. Upon further investigation of this co-assembly process and a better understanding of the interactions between protein, surfactant, and block copolymer is obtained, it would be possible to optimize the behavior of these protein-based materials to elucidate a specified protein elution rate and protein storage timeline. The system may be useful for applications that include protein delivery, catalysis, and transport.

§ 2.4. Experimental Section

2.4.1. Materials

Horseradish peroxidase type II (HRP), glucose oxidase type X-S (GOx), α-chymotrypsin type II (CT), subtilisin type VIII, sodium 2-bis(hexylethyl) sulfosuccinate (AOT), α-D-glucose, phenol, 4-aminoantipyrine, and N-Succinyl-Ala-Ala-Pro-Phe p-nitroanilide were obtained from Sigma Aldrich. TMB Peroxidase EIA Substrate Kit was obtained from Bio-Rad Laboratories. (24 kDa) poly(styrene)-*block*-(9.5 kDa) poly(4-vinyl pyridine) (PS-*b*-P4VP) was obtained from Polymer Source with a PDI of 1.10. 3-n-pentadecylphenol (PDP) was obtained from Acros. Toluene and chloroform were

obtained from Fisher Scientific, and Milli-Q water was obtained from EMD Millipore. Silicon wafers were obtained from International Wafer Service. All materials were used as received.

2.4.2. Assembly of Protein-Encapsulated Reverse Micelles

AOT was dissolved in toluene at a concentration of 200 mM. HRP and GOx were individually dissolved in DI water to a concentration of 2 w/v %. α-CT was dissolved in 10 mM Bis Tris, 2 mM $CaCl_2$ at pH 8.4 to a concentration of 1 w/v %. Injection emulsion was used to create AOT-protein reverse micelles. The suspension was sonicated, mixed, and partially evaporated using a constant stream of N_2 gas until optically clear. Additional toluene was added to compensate for evaporated solvent in order to reestablish the original concentration.

2.4.3. Dynamic Light Scattering

Size of AOT-HRP reverse micelles and AOT-GOx reverse micelles were measured using a Brookhaven Instruments BI-200SM Research Goniometer and Laser Light Scattering System. The refractive index of the particle was taken as the refractive index of H_2O, n = 1.33. Temperature was controlled and set at 25°C. Measurements were sorted by number average and a NNLS fit was used to analyze the correlation curves.

2.4.4. Assay of Protein Activity in Aqueous Buffer

HRP activity was assessed using 3,3',5,5'-tetramethylbenzidine and hydrogen peroxide. Baseline HRP activity was determined by preparing a stock protein solution in 100 mM KH_2PO_4/K_2HPO_4 phosphate buffer at pH 6 and applying a prepared TMB assay solution, as outlined by the manufacturer. Solution was thoroughly mixed and UV-visible spectroscopy was performed on a Hewlett-Packard 8453 Spectrophotometer. A 1-cm path length cuvette was used and absorbance at 370 nm was monitored.

$$(2.1)$$

GOx activity was assessed using an assay containing glucose, phenol, 4-aminoantipyrine, and HRP. Baseline GOx activity was determined by preparing a stock protein solution in 100 mM KH_2PO_4/K_2HPO_4 phosphate buffer at pH 6 and applying the colorimetric assay. Absorbance at 505 nm was monitored.

(2.2)

CT and subtilisin activity were assessed using an assay containing N-Succinyl-Ala-Ala-Pro-Phe p-nitroanilide. Baseline CT and subtilisin activity were determined by preparing a stock protein solution in 10 mM Bis-Tris with 2 mM $CaCl_2$, pH 8.4 for CT and in 25 mM sodium bicarbonate, pH 8.5 for subtilisin and then applying the colorimetric assay. Absorbance at 390 nm was monitored.

(2.3)
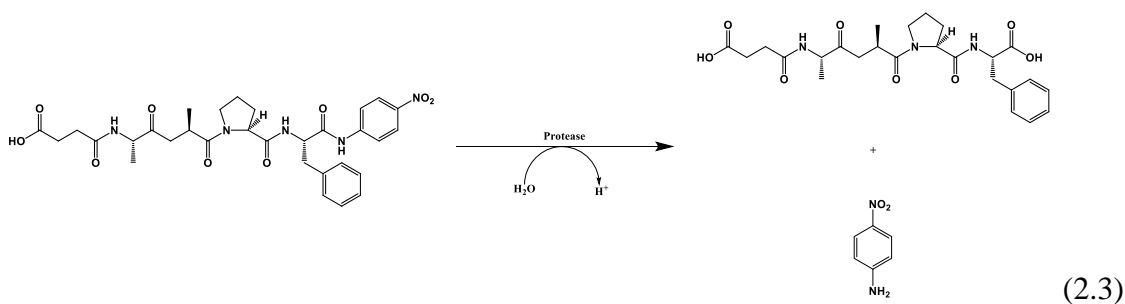
AOT-protein reverse micelles were left in ambient room temperature conditions for 0, 2, 4, 8, and 24 h in toluene. After specified times, aliquots were taken and diluted in the protein's respective buffers. After thorough mixing, the assay solution is applied. Activity was quantified using UV-visible spectroscopy by monitoring the conversion rate of the colorimetric assay for 5 min for HRP. For the other proteins, activity was quantified by monitoring absolute absorbance after a specified time.

2.4.5. Assembly of PS-*b*-P4VP(PDP) Supramolecule

PS-*b*-P4VP and PDP were dissolved separately in chloroform. Both solutions were combined at a mole ratio corresponding to 1:1 [PDP]:[4VP] in chloroform and

stirred overnight to promote hydrogen bonding. The final concentration of the solution was 1 w/v % PS-*b*-P4VP(PDP).

2.4.6. Fabrication of Protein-Containing Thin Films

Prior to spin casting, four spinning solutions were created: 0.5 w/w % HRP, 0.5 w/w % GOx, 0.25 w/w % HRP + 0.25 w/w % GOx, 0.25 w/w % CT, 0.25 w/w % subtilisin. Solutions were created by mixing AOT-protein reverse micelle solution and PS-*b*-P4VP(PDP) solution. Thin films were prepared on silicon wafers. Solutions were prepared by spin-casting the blended protein-supramolecule solution for 20 s at 3000 RPM. Film thickness was assessed using a Filmetrics F20 interferometer. Samples were solvent annealed in a sealed 250 mL jar containing 500 µL of chloroform for 20 min.

2.4.7. Atomic Force Microscopy

Thin films were imaged using atomic force microscopy. AFM was performed on a Molecular Imaging PicoSPM II with a PicoScan 2500 controller. A scan rate of 2 Hz and a resonant frequency ranging between 300-400 kHz were used.

2.4.8. Colorimetric Analysis of Protein in Thin Films

Thin films were submerged for 30 min in buffer and evaluated with their respective colorimetric assays.

2.4.9. Leaching of Protein from Thin Film

Protein-containing thin films were placed in 400 µL of their respective buffers. Protein-containing thin films were incubated at room temperature for 30 min and then removed. Films were subsequently placed in another 400 µL bath of the same buffer solution. Their colorimetric assay solution is applied to each bath. Activity was quantified using UV-visible spectroscopy by monitoring the conversion rate of the colorimetic assay.

2.4.10. Protein Activity Retention in Thin Film

Protein-containing thin films were left at ambient room temperature conditions for a prolonged time period post fabrication and solvent annealing. After specified times, protein-containing films were placed in buffer containing an assay solution. UV-visible spectroscopy monitored the protein activity by looking at the rate of conversion of the colorimetric assay.

2.4.11. Fabrication of Protein-Containing Electrospun Fibers

Prior to electrospinning, a 1 w/v % HRP solution was created containing HRP encapsulated in AOT reverse micelles in toluene and a 17 w/v % PS-*b*-P4VP(PDP) in chloroform. The final spinning solution contained 13 v/v % toluene. Electrospun fibers were created with a solution feed rate of 5 mL/h and a voltage of 10 kV. A tip-to-plate distance of 15-20 cm was manually set. 30 min was sufficient in fabricating fibers for characterization and testing.

2.4.12. Scanning Electron Microscopy

Electrospun fibers were mounted on an SEM holder using conductive carbon tape. SEM images were collected on a JEOL FE-SEM at an accelerating voltage of 5 kV.

2.4.13. Transmission Electron Microscopy

Electrospun fibers were embedded and cured in resin for 4 h at 60°C. Samples were then microtomed and exposed to iodine vapor for 10 min which selectively stains the P4VP(PDP) domain. TEM images were collected on a FEI Tecnai 12 TEM at an accelerating voltage of 120 kV.

Chapter 3

Design and Optimization of Statistically Random Heteropolymers toward Enhanced Protein Stability and Processability

Preserving protein function in non-native conditions have benefitted greatly from the development of statistically random heteropolymers. The chemical and architectural complexities of statistically random heteropolymers provide a modular platform for tunable protein-polymer-solvent interactions. This provides expansive opportunities not offered by small molecule surfactants or amphiphilic polymers. By understanding the relationship between statistically random heteropolymer composition, encapsulation route, and protein function retention, a set of parameters can be established for future iterations. In this chapter, I will report the synthesis of six rationally designed random heteropolymers whose physical and chemical properties were varied. Small changes in both chemistry and architecture resulted in clear behavioral differences in polar and non-polar solubility and aggregation. These differences in solution behavior result in clear differences in protein-polymer interactions. Furthermore, unlike traditional surfactants, the path taken to induce protein-amphiphile hybridization can be tuned to optimize activity preservation.

§ 3.1. Introduction

Random heteropolymers with a statistical distribution of monomers offer an approach toward protein stabilization. The chemical heterogeneity of the protein surface matches well with the chemical complexity offered by random heteropolymers.[1] Monomers can be chosen to interact favorably with amino acids on the protein surface.[2-4] Changes in polymer composition and backbone can be used to manipulate amphiphilicity.[5] Furthermore, tuning of monomer feed ratios can be used to direct the lateral correlation between a polymer and protein surface.[6]

Current approaches toward protein processability and stability are not as flexible. In solution, surfactant encapsulation and polymer conjugation are two popular approaches. Small molecule surfactants[7-10] and amphiphilic polymers[11, 12] can emulsify protein solutions in media, while end-functionalized polymers can be covalently attached to protein surfaces, mediating their interaction with the environment.[13] Yet, both techniques have their own drawbacks. Surfactants are greatly limited by the chemistry and architecture that are available; their ability to pack into micelles is bound by the geometry and strength of its hydrophobic and hydrophilic sections.[14] In addition, this micelle structure is fairly dynamic and participates in subunit exchange in solution, which can encourage solvent penetration and cargo leakage.[15-18]

Polymer conjugation uses accessible functional handles on the protein surface.[19] An insufficient amount of conjugation sites for polymers has been shown to provide little enhancement in terms of protein stability and processability, as seen in Chapter 2. The hydrophobicity of the polymer used is also limited, as the polymer will disrupt intramolecular interactions that hold the protein together if the hydrophobicity is too great.[20, 21] In addition, local distortion at the site of conjugation does occur, arising from the steric hindrance incurred by the protein.[22]

Statistically random heteropolymers (SRHPs) offer an alternative vehicle to solubilize, stabilize, and make processable a variety of nonspecific proteins. They combine the generality of surfactants and the stability of polymer conjugation. Similar to small molecule surfactants, the interactions they participate in are non-covalent; however, the polymer architecture provides multiple sites for the surfactant to bind. The sum of many non-covalent interactions can be comparable to the strength of a covalent bond. Sequence-controlled polymers could provide accurate control over chemical composition and architecture, but these macromolecules are plagued with scalability and synthetic scheme limitations, difficulties in high molecular weight polymerization, and a reduced library of applicable monomers.[23] The appeal of a defined monomer sequence can be simulated in SRHPs through controlled radical polymerization and proper monomer feeding ratios. The statistical randomness of the polymerization process will dictate the spacing between the different monomers that are introduced, with the caveat that the monomers have the same reactivity.[6]

Hydrophobically modified polymers (HMPs) are a class of synthetic macromolecules composed of a hydrophilic backbone and a statistical distribution of hydrophobic side groups.[24, 25] In aqueous solutions, these hydrophobic moieties self-associate, forming microdomains of hydrophobic pockets.[26-29] One specific type of HMP, amphipols (APols), has been shown to solubilize and stabilize hydrophobic transmembrane proteins in water.[5, 30-32] Their chemical complexity provides tunability of both solvent amphiphilicity and protein interactions. However, this technique requires initial solubilization of transmembrane proteins with small molecule surfactant micelles. In addition, this approach is limited to aqueous systems and has not been adapted to non-polar media.

SRHPs have greatly expanded the scope of functionalities and properties accessible to materials science and engineering. However, to design and use SRHPs effectively requires a deep understanding of how proteins, SRHPs, and solvents interact. Hereafter, I will report on a set of rationally designed SRHPs to investigate the interplay between SRHP composition, encapsulation technique, and protein preservation. This preliminary set of experiments will help dictate future designs and approaches.

§ 3.2. Results and Discussion

The protein surface is highly heterogeneous and chemically complex; however, the interactions that occur at the surface are predictable. A protein's surface can be simplified into a binary map of polarity (hydrophobic vs. hydrophilic) and a ternary map of charge (neutral vs. positive vs. negative). Magnitude of polarity and charge were ignored for this initial undertaking as it will complicate the initial SRHP design process. Taking horseradish peroxidase (HRP) as an example, its crystal structure was used as a model protein.[33] HPR was conceptualized as a patchy particle with clusters of

hydrophobic, cationic, and anionic patches (Appendix A.2.1). These patches can be measured to obtain a distribution of sizes and distances (Figure 3.1). When mapping out the surface based on these parameters, proteins can be simplified as spheres with patch diameters in the range of ~0-1 nm and average patch-to-patch distances of ~1-2 nm (Table 3.1).
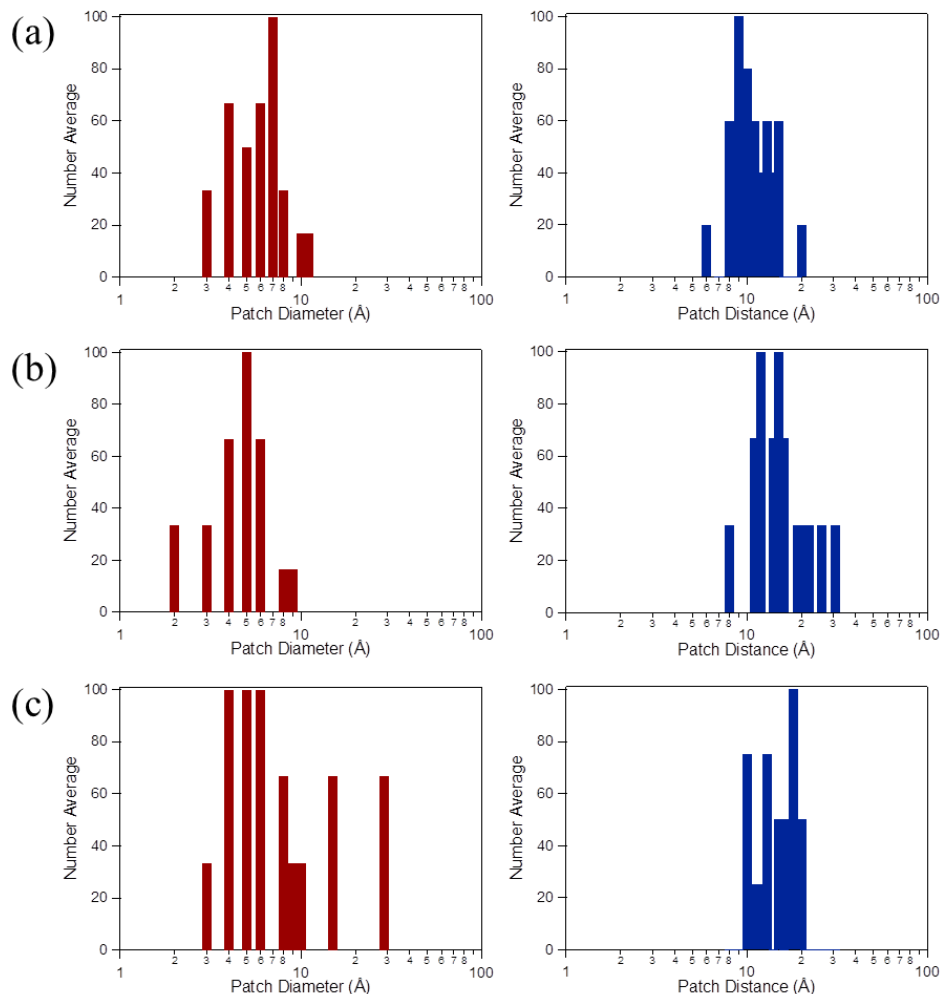
Figure 3.1. Surface analysis of HRP (1H55). The histograms of the patch diameters (left) and patch-to-patch distances (right) of (a) hydrophobic patches, (b) cationic patches, and (c) anionic patches.

Table 3.1. Surface Measurements of Horseradish Peroxidase

Patch	Average Diameter (Å)	Average Distance (Å)
Hydrophobic	6.1	11.3
Positive	4.9	16.1
Negative	9.5	15.1

The chain-based structure of SRHPs is expected to interact with proteins multivalently, increasing the binding affinity per surfactant. Monomer chemistry is tuned to interact favorably with patches on the surface. Interactions should stay below the energy threshold that would cause the polymer to outcompete protein intramolecular interactions. The spacing between interacting monomers is essential for protein-polymer complex stability; complimentary monomer distances that resonate well with the distances and sizes of protein patches would optimize binding. Tuning monomer spacing with respect to protein patch distances lowers polymer stretching and compression required to accommodate for hybridization. The enthalpic gain resulting from this protein-polymer interaction would compensate for the entropic penalty associated with encapsulation.

Upon hybridization with the protein, it is assumed that the polymer will adjust and correct for any deviation from this patch-to-patch average distance and maximize the number of favorable interactions. In addition, the presence of both a hydration layer around the protein and organic solvent will pin the polymer surfactant at the interface.[34] The SRHP will arrange itself to position the majority of hydrophobic monomers into the organic solvent and the majority of polar monomers into the water. Monomers in the water will anchor to the protein surface multivalently. The additive interactions of multiple weak interaction between SRHP and protein is critical to ensure that overall protein-polymer interactions is sufficiently strong to form a polymer shell yet weak enough to prevent localized protein denaturation. This design process is summarized by Scheme 3.1.
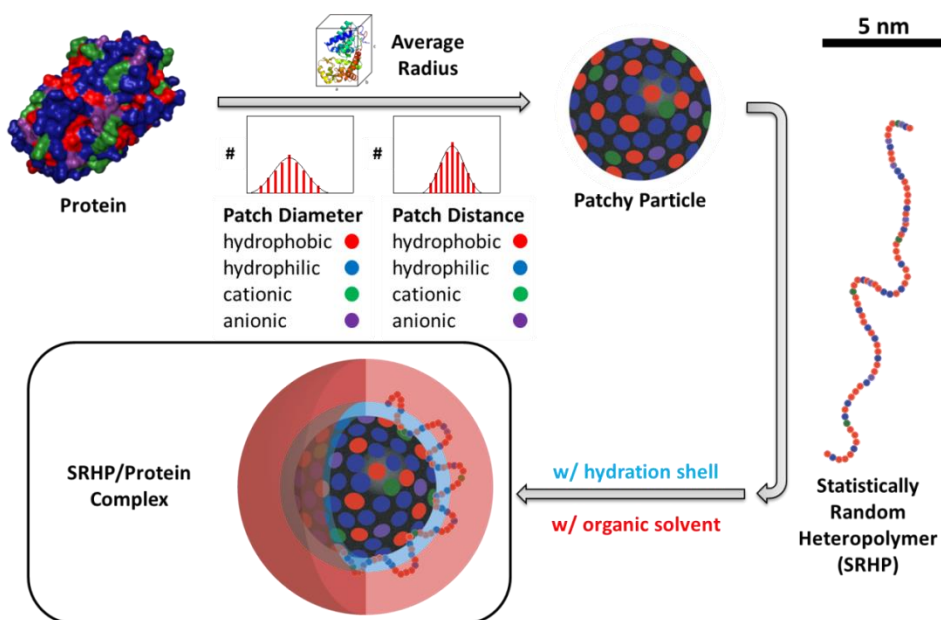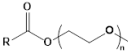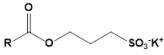
Scheme 3.1. Tailoring SRHPs for a protein's surface.

SRHPs were synthesized using reversible addition-fragmentation chain transfer (RAFT) polymerization. A controlled free radical polymerization system that is robust allows us to utilize a wide range of commercially available monomers and reaction conditions. RAFT is also sensitive enough to provide precise tuning over both the molecular weight and polydispersity.[35] Four monomers were chosen to provide SRHPs with enough chemical complexity to act as both an effective agent for protein attachment and a proper amphiphilic surfactant.

A methacrylate-based polymer was chosen as the foundation for SRHPs. There is a variety of functional groups offered in methacrylate-based polymer chemistry, and the backbone provides ample flexibility for protein wrapping. The majority of the polymer is composed o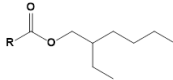f methyl methacrylate (MMA). MMA provides hydrophobicity to the polymer, allowing it to remain soluble in non-polar media. It also acts as a spacer between functional monomers that interact with the protein surface. Oligo(ethylene glycol) methacrylate (OEGMA) is expected to locally stabilize the protein because of poly(ethylene glycol)'s (PEG's) established phenomenon in stabilizing proteins.[36] In addition, PEG provides hydrophilicity to the polymer, making it soluble in aqueous solutions, and it is known to retain a hydration shell. This will be essential in providing proteins with an appropriate environment. 2-ethylhexyl methacrylate (2-EHMA) is expected to interact with the hydrophobic patches on the protein surface. It also increases the hydrophobicity of the polymer, balancing the effects of OEGMA. 3-sulfopropyl methacrylate (3-SPMA) is a hydrophilic anionic species that is expected to form salt bridges with the positive charges found on the surface of HRP. The monomer selection was guided by Hildebrand solubility parameters found in literature for the four monomers and the two solvents in the system (Appendix A.2.2).[37-39] A cationic monomer was excluded to prevent strong intramolecular interactions within the polymer that may hinder hybridization between SRHP and protein.
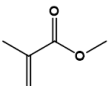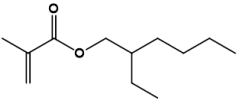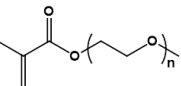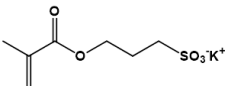
By varying the feeding ratios of the four monomers and varying the lengths of OEGMA and the polymer backbone, six different SRHPs were synthesized (Table 3.2). SRHP-1 was developed to match the lateral correlation found on the protein surface. SRHP-2 and SRHP-3 exchanged 2-EHMA with OEGMA, making the polymer exhibit a more hydrophilic characteristic. SRHP-4 and SRHP-6 were created to be analogues of SRHP-1, where the ratios remained the same but OEGMA length was increased. These two routes in increasing OEG (increasing OEGMA monomer vs. increasing OEGMA length) would provide direction for future iteration. Increasing OEG content would benefit the protein greatly due to the aforementioned ability of PEG to stabilize proteins. Lastly, SRHP-5 was synthesized to evaluate the effects of increasing molecular weight. As molecular weight is increased, the amount of anchoring moieties per polymer is increased; however, as the case for higher molecular weight polymers, the entropic penalty associated with polymer ordering during encapsulation also becomes greater and may hinder proper protein-polymer interactions.

Table 3.2. Theoretical Monomer Composition of SRHPs

Sample	(methyl ester structure)	(2-ethylhexyl ester structure)	(OEG ester structure)	n	(sulfonate ester structure)
SRHP-1 (OEG$_{3-4}$ 25%)	50%	20%	25%	3-4	5%
SRHP-2 (OEG$_{3-4}$ 30 %)	50%	15%	30%	3-4	5%
SRHP-3 (OEG$_{3-4}$ 35%)	50%	10%	35%	3-4	5%
SRHP-4 (OEG$_9$ 25%)	50%	20%	25%	9	5%
SRHP-5 (OEG$_9$ 25% 3x MW)	50%	20%	25%	9	5%
SRHP-6 (OEG$_{22}$ 25%)	50%	20%	25%	20	5%

Although these changes in monomer ratio and OEGMA length are small in magnitude, the resulting effects are drastic in terms of SRHP solubility and aggregation. Group contribution theory was used to evaluate the hydrophilic-lipophilic balance (HLB) of each individual monomer (Table 3.3).[40] These HLB values provide an indicator of monomer hydrophobicity. Lower HLB numbers indicate higher hydrophobicity and higher HLB numbers indicate higher hydrophilicity. For instance, alkanes are hydrophobic and contribute negatively to HLB. Charged moieties, such as sulfonates on the other hand, are highly polar and contribute significantly to increasing HLB.

Table 3.3. HLB Values using Group Contribution Theory

Functionality	Amount	Group #	Amount	Group #	Amount	Group #	Amount	Group #
-CH$_x$-	4	-0.475	11	-0.475	4	-0.475	6	-0.475
-CO$_2$R-	1	2.4	1	2.4	1	2.4	1	2.4
-CH$_2$CH$_2$O-	—	—	—	—	3-20	0.33	—	—
-OSO$_3^-$-	—	—	—	—	—	—	1	38.7
HLB	7.5		4.175		8.49-14.1		45.25	

By treating these SRHPs as a mixture of surfactants tethered along a polymer backbone, an HLB_{mix} value can be calculated (Table 3.4). HLB_{mix} values between the six SRHPs indicate little difference in solution properties. These values, though, straddle the boundary where surfactants prefer to create aggregates with a hydrophilic shell and hydrophobic core and where surfactants prefer the inverse.[41] HLB values between 1 and 10 prefer inverted structures where non-polar components face outwards and polar parts point inwards. HLB values between 10 and 40 prefer the opposite. As SRHP values fall between 9 and 11, all polymers are expected to solubilize in both non-polar organic solvents and water.

Table 3.4. HLB Mixture Values for SRHPs

	SRHP-1	SRHP-2	SRHP-3	SRHP-4	SRHP-5	SRHP-6
HLB_{mix}	8.97-9.05	9.19-9.28	9.40-9.52	9.47	9.47	10.37

In water, only SRHP-1, -4, and -6 were dissolvable. The remaining SRHPs appear as a transparent gel-like substance in solution. The increase in OEGMA monomer in SRHP-2 and -3 would lead us to believe that its increased hydrophilicity would make it more readily soluble; however, this is not the case. It is speculated that OEGMA monomers along the backbone become physically entangled due to the high density of OEGMA. It is possible heat can be used to provide the energy needed for entanglement disruption and assist in solubilization, but additional studies must be conducted. SRHP-6, with its long OEGMA chain, does not behave in this manner. OEG subunits are localized further away from the backbone and have more room, preventing entanglement. As seen in literature, hydrophobicity of an amphiphilic polymer is not dependent on solely chemistry but also on how well the sidechains pack.[42]

Increasing the molecular weight also results in a similar gel-like macrostructure as observed in SRHP-5. As previously speculated, increasing the molecular weight of SRHPs may hinder proper solubilization. The entropic penalty for polymer ordering increases as molecular weight increases. This phenomenon occurs due to the increase in the amount of available microstates. More microstates result in higher entropic penalty during the packing of hydrophobic monomers into the core. Again, heat may help during the dissolution of the macromolecule, but additional studies must be conducted. For this initial set of observations, it can be concluded that 3x molecular weight hinders polymer performance. Aggregation indicates an increase in intramolecular interactions which may impede protein-polymer interactions during processing.

Dynamic light scattering was used to monitor water-soluble SRHP behavior. In water, the three SRHPs behaved similarly, with hydrodynamic diameters ranging from 4-8 nm (Figure 3.2). An increase in diameter was observed as the length of OEGMA was

increased. Water is a good solvent for OEG and an increase in the amount of OEG subunit should result in an increase in the degree of swelling, which was observed.
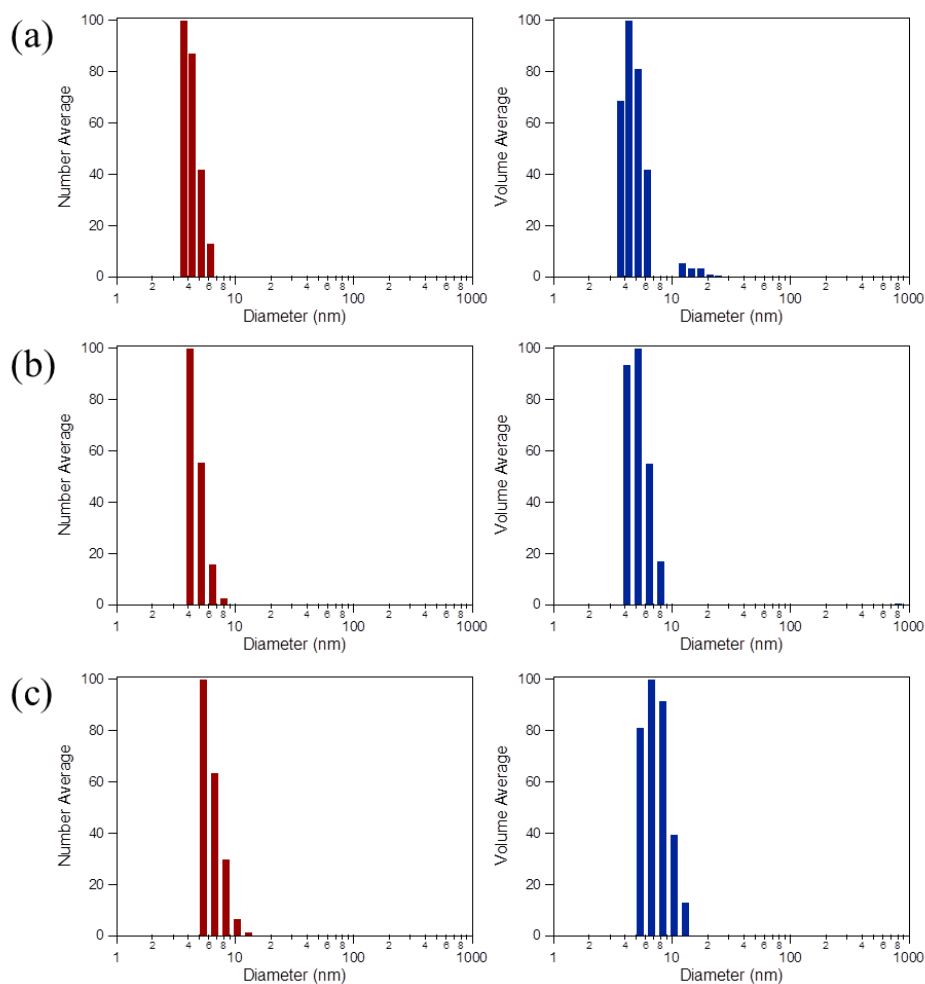
Figure 3.2. DLS histograms of SRHPs in water. Left column shows diameter distribution based off of number average values and right column shows diameter distribution based off of volume average values for (a) SRHP-1, (b) SRHP-4, and (c) SRHP-6.

Small angle x-ray scattering (SAXS) was used to provide further insight in SRHP morphology. The length scale of x-rays allows us to probe the internal structure of SRHPs. Figure 3.3 shows scattering profiles of SRHP-1, -4, and -6 fitted to a polydispersed core-constant shell model. In order to decouple structure factor and form factor, scattering profiles were fitted from 0.07 Å^{-1} to 0.2 Å^{-1}. Interestingly, with small OEGMA lengths, SRHP-1 adopts a core-shell cylindrical morphology in water, while SRHP-4 and -6, which have longer OEGMA lengths, adopt a spherical morphology. The reduction in OEGMA volume fraction in SRHP-1 forces a cylindrical morphology in order to maximize packing and shielding of hydrophobic MMA and 2-EHMA.

44
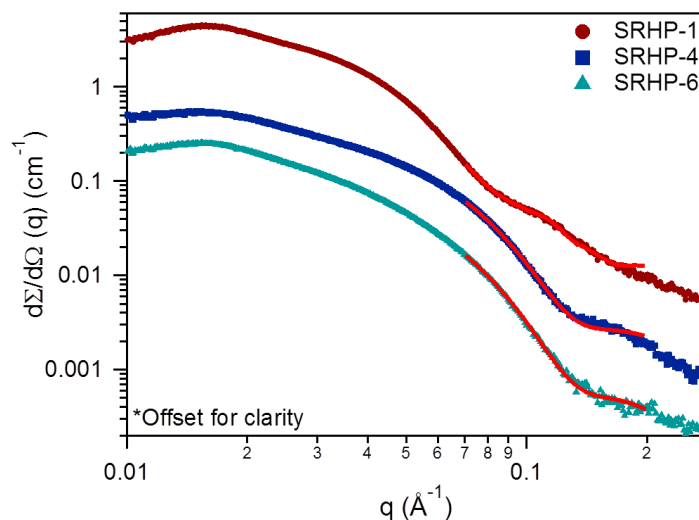
Figure 3.3. SAXS scattering profiles of SRHPs in water. Red solid lines represent PolyCore fits.

Table 3.5 summarizes information obtained from SAXS and DLS. Results from the two techniques are in good agreement. The radius of gyration of SRHP-4 and -6 cores are the same and there is only a slight increase in shell thickness. This indicates that the center of mass of this OEGMA shell remains close to the hydrophobic core-hydrophilic shell interface. It is speculated that this occurs as a way to passivate the interactions between the hydrophobic monomers and the water. Lastly, looking at the low q structure factor peak, little deviation from the three SRHPs was observed. The SRHPs seem well dispersed in solution, with polymer-to-polymer distances of 40 nm.

Table 3.5. Summary of SAXS and DLS Measurements of SRHPs

Sample	Shape	Small Angle X-Ray Scattering					Dynamic Light Scattering	
		r_{core} (nm)	t_{shell} (nm)	l_{core} (nm)	t_{face} (nm)	Autocorrelation Peak (nm)	r_{number} (nm)	r_{volume} (nm)
SRHP-1	Cylinder	1.6	0.6	6.6	0.9	39.9	2.2	2.6
SRHP-4	Sphere	0.7	2.6	—	—	40.5	2.4	2.6
SRHP-6	Sphere	0.7	2.7	—	—	40.5	3.2	3.8

When SRHPs were dissolved in non-polar media, the small changes in monomer ratio produced large difference in size. SAXS was used to evaluate polymer properties in toluene (Figure 3.4). Scattering profiles indicate that increases in OEGMA ratio and SRHP length caused large aggregation. Although dissolvable in toluene, the increasing slope at low q for SRHP-2, -3, and -5 revealed particles much larger than the observable range of our sample-to-detector distance. SRHP-6, although calculated to contain a stochastically higher number of OEG subunits than SRHP-2 and -3, shows better

45

solubilization behavior in toluene. This would suggest that chemical hydrophobicity is not sufficient to characterize these polymers and that future experiments must be designed to evaluate architecture role in SRHP solubility. Our speculation is that by placing this extra OEG away from the backbone, SRHP has more degrees of freedom to efficiently pack the hydrophilic portions of the polymer, similar to what was observed in water. For SRHP-5, it is still unclear on its inability to dissociate into smaller particles, but the large entropic penalty for ordering long polymers may be a potential explanation for this phenomenon.
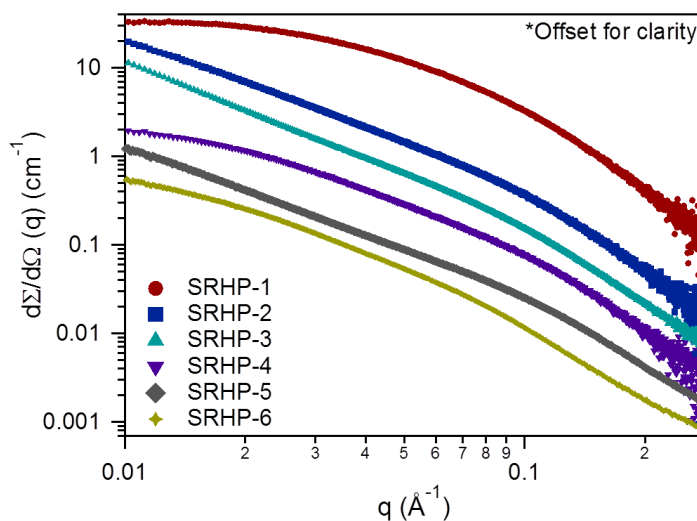
Figure 3.4. SAXS scattering profiles of SRHPs in toluene.

The Guinier approximation was used to calculate the radius of gyration of toluene-soluble SRHPs (Table 3.6). With the observed sizes, it is highly likely that these polymers exist as an aggregate of SRHPs rather than individual SRHPs floating in solution. In addition, the relationship between SRHP size and OEGMA length can be extracted from this data (Figure 3.5). Increasing the length of OEGMA causes an increase in overall aggregate size. Larger aggregates reduce the total amount of surface area and increase the total amount of volume. It is speculated that this would allow for better shielding of OEG from the toluene. It is also observed that this increase in SRHP size begins to plateau as OEGMA length increases. Further studies must be conducted to evaluate this phenomenon, but there may a critical OEGMA length where the system reaches equilibrium.

Table 3.6. Guinier approximation of SRHPs

Guinier Approx.	SRHP-1	SRHP-2	SRHP-3	SRHP-4	SRHP-5	SRHP-6
r (nm)	4.4	—	—	8.6	—	10.6
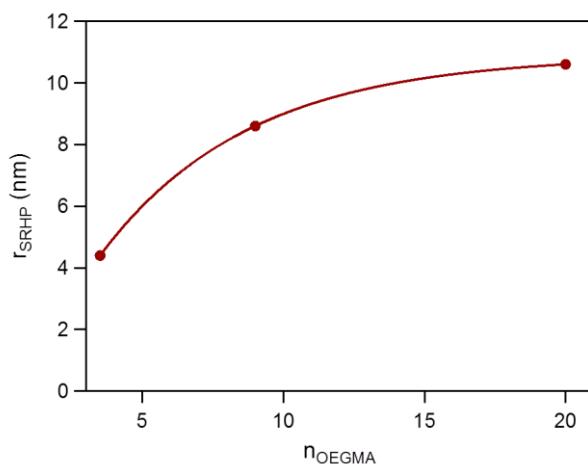
Figure 3.5. Relationship between OEGMA degree of polymerization and SRHP radius.

Three SRHPs were chosen to assess SRHPs' ability to stabilize proteins stored in organic media. Injection emulsion of an aqueous protein solution into toluene containing SRHP-1, SRHP-3, or SRHP-4 was used to create HRP-encapsulated reverse micelles. Over 24 h, aliquots of SRHP/HRP reverse micelles were dispersed in buffer. This allows us to disrupt SRHP/HRP hybridization and extrapolate the sole effects of protein denaturation. As seen in Figure 3.6a, both SRHP-1 and SRHP-4 showed great ability to initially encapsulate and stabilize the protein. Over a 24 h time period, the increase in OEGMA length correlates to enhanced activity retention in organic solvent. SRHP-3, which tends to cluster into large aggregates in toluene solution, showed inconsistent protein processing behavior (Figure 3.6b). During activity testing over a 24 h time period, large standard deviations were observed. Its strong interaction with itself most likely hinders its ability to interact with the protein. Further investigation must be done to evaluate the stabilizing effects of increasing OEGMA length.
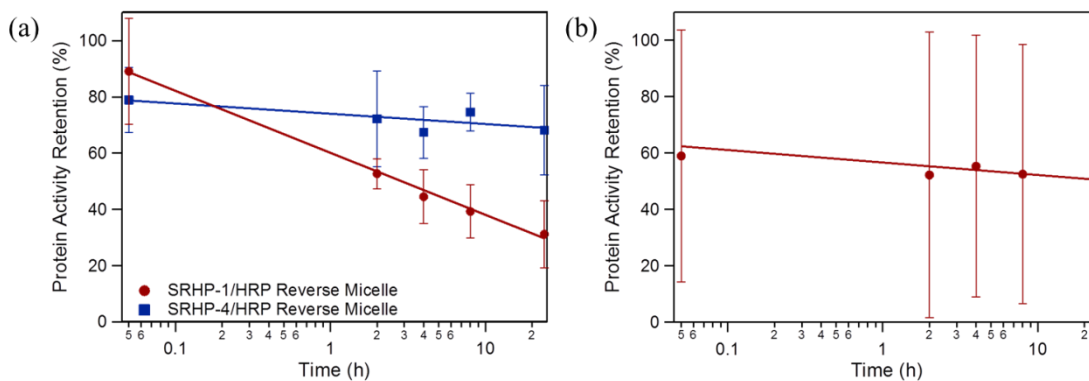
Figure 3.6. Activity of HRP after storage in organic solvent and dispersed in aqueous buffer in (a) SRHP-1 and SRHP-4 and (b) SRHP-3 reverse micelles.

Previous data was all obtained by encapsulating HRP in reverse micelles. Reverse micelle complexes are ideal in stabilizing proteins. An aqueous environment is maintained around the protein; however, obtaining high concentration solutions of SRHP-4/HRP reverse micelles is difficult. This has led us to investigate other encapsulation techniques, such as adsorption-evaporation-resuspension and adsorption-lyophilization-resuspension. SRHPs' ability to dissolve in both water and toluene offers multiple avenues for SRHP/HRP hybridization. By solubilizing both SRHPs and HRP in water first, it is possible to bring SRHPs in close proximity to proteins prior to exposure to organic solvent. In addition, we can control the amount of toluene that the complexes are resuspended in. This technique is similar to the ion pairing approach discussed in Chapter 2. Scheme 3.2 summarizes the differences in procedure.
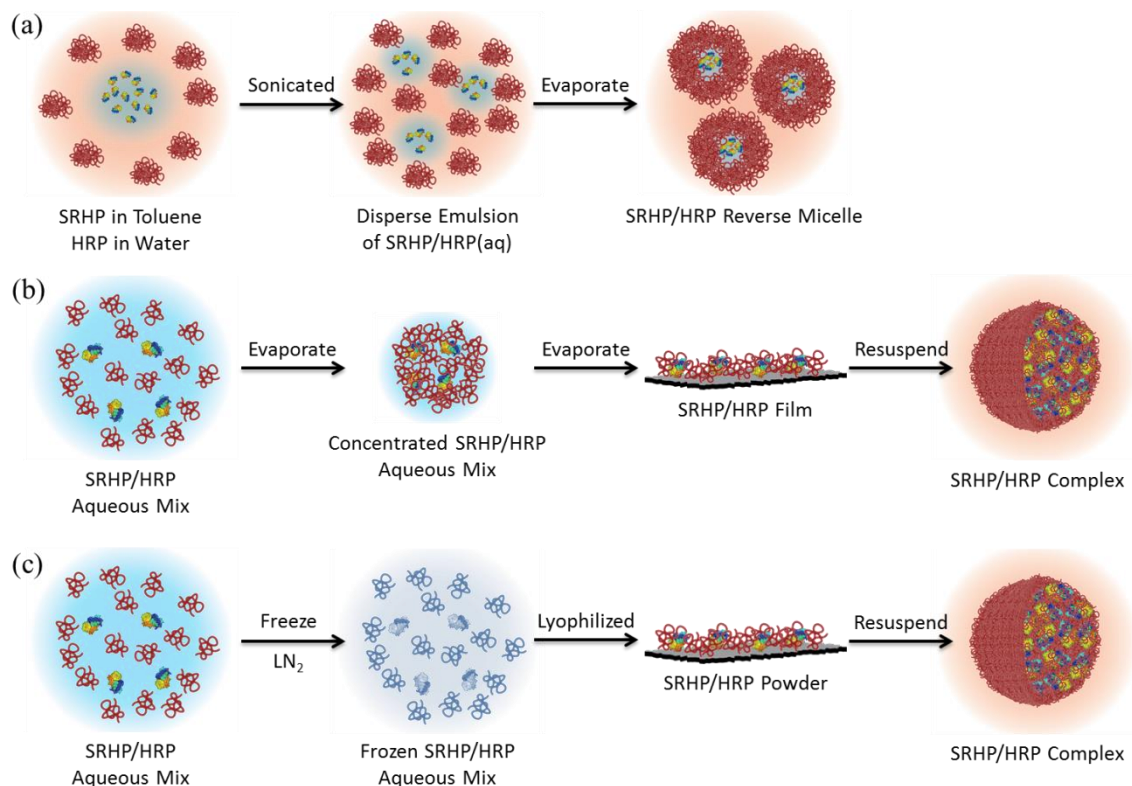
Scheme 3.2. Encapsulation method of HRP in toluene via SRHPs. (a) Injection emulsion technique. (b) Solvent evaporation technique. (c) Lyophilization technique.

Each encapsulation route resulted in different morphologies. In Figure 3.7, transmission electron microscopy (TEM) images are shown for free polymer (Figure 3.7a) and complexes formed through ejection emulsion (Figure 3.7b), solvent evaporation (Figure 3.7c), and lyophilization (Figure 3.7d). In the case of injection emulsion and

lyophilization, a bimodal distribution was observed, where one species corresponds to the diameter of free polymer (~20 nm), and the other species corresponds to the SRHP-4/HRP complex (~70 nm for ejection emulsion and ~50 nm for lyophilization). For evaporation, a more monodisperse solution was found with a diameter of ~30 nm (Figure 3.7(e-h)). The drastic reduction in particle size in evaporation-assisted complexes is speculated to result from the increased concentration of protein and polymer during water evaporation. Interactions between protein and polymer are enhanced and may result in a reduction of protein amount per complex. Further investigation must be conducted to verify this.
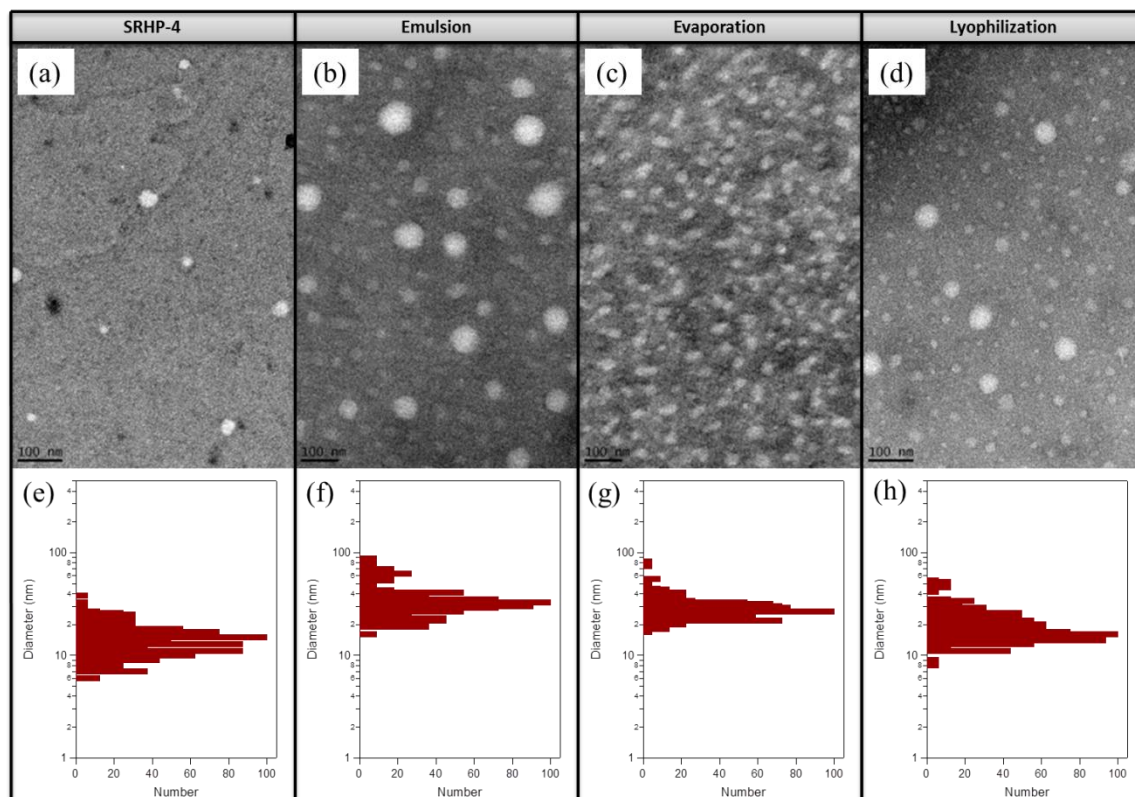
Figure 3.7. TEM of (a) SRHP-4 and SRHP-4/HRP complexes formed through (b) emulsion, (c) solvent evaporation, and (d) lyophilization. Image analysis was used to measure the diameters of (e) free SRHP-4, (f) reverse micelles, (g) evaporation-assisted complexes, and (h) lyophilization-assisted complexes.

SAXS was used to determine the internal structuring of these complexes. In order to fit our scattering profiles, we summed a spherical polydisperse core-shell model with a polydisperse Gaussian coil model to provide scattering contributions from both the SRHP-4/HRP complex and SRHP-4 aggregates respectively. Deconvolution of the individual scattering contributions was done by fitting the scattering profile of just SRHP-4 in toluene and modeling the SRHP-4/HRP complex at low q, where

49

contributions of the SRHP-4 aggregates are minimized. For SRHP-4/HRP reverse micelles, a core-shell structure was observed, with a radius of 10 nm and a shell thickness of 24 nm (Figure 3.8a). For SRHP-4/HRP complexes formed through evaporation (Figurer 3.8b) and lyophilization (Figure 3.8c), we observed no distinct core shell structure but rather a spherical particle with a mixture of protein, polymer, and water. The core for the evaporated-mediated complex was much smaller however, at 10 nm, while the core for the lyophilized-mediated complex was much larger, at 26 nm. These results are summarized in Table 3.7. The SAXS models agree well TEM results.
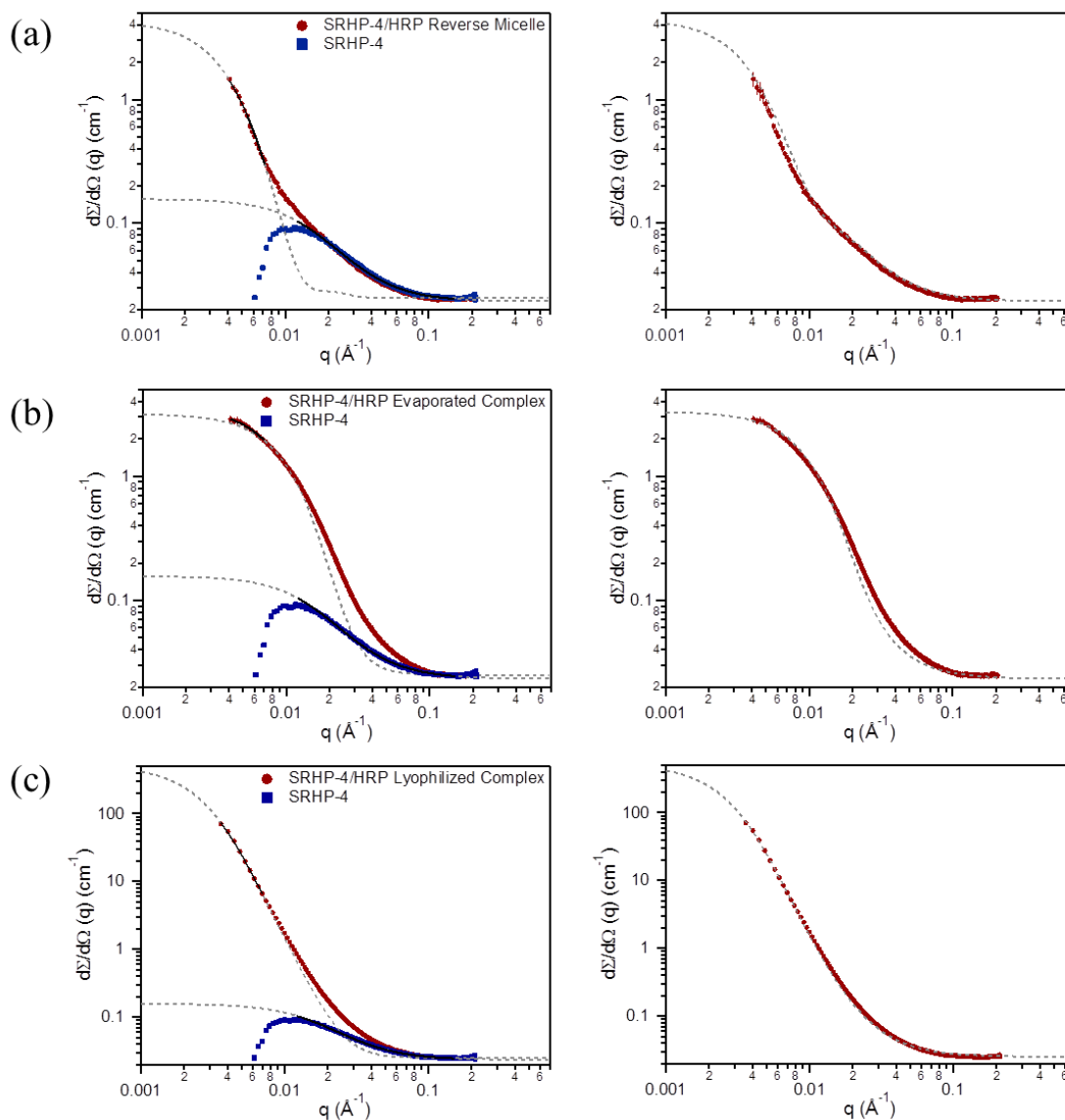
Figure 3.8. SAXS scattering profiles of SRHP-4/HRP complexes using various encapsulation techniques. (a) SRHP-4/HRP reverse micelle. (b) SRHP-4/HRP evaporated

complex. (c) SRHP-4/HRP lyophilized complex. The left shows individual fits of SRHP-4/HRP complex and SRHP-4 aggregates. The right shows a combined summed fit.

Table 3.7. Core-Shell Measurements from SAXS.

Approach	r_{core} (nm)	t_{shell} (nm)
Emulsion	10.1	23.8
Evaporation	10.1	0.6
Lyophilization	26	0.7

Comparing the three different encapsulation techniques and their ability to stabilize proteins stored in organic media, it was observed that evaporated and lyophilized complexes provided better initial activity retention (Figure 3.9). It is postulated that there is a reduction in solvent exposure experienced by the protein as the surfactant is already in close proximity prior to toluene resuspension. This increase in protein activity preservation is governed by short range diffusion of SRHP and protein. In emulsion-assisted encapsulation, the polymer must find the aqueous protein solution first. This long range diffusion results in increased organic solvent exposure. For evaporated complexes however, the activity diminishes at a much more drastic rate than the activity of HRP in reverse micelles. Further investigation must be conducted, but the reduced particle size may make it easier for solvent to penetrate and denature the protein. Complexes that are lyophilized preserved protein activity to the highest extent. In addition, complex formation was more reducible in the lyophilized system in comparison to evaporated complexes and reverse micelles.
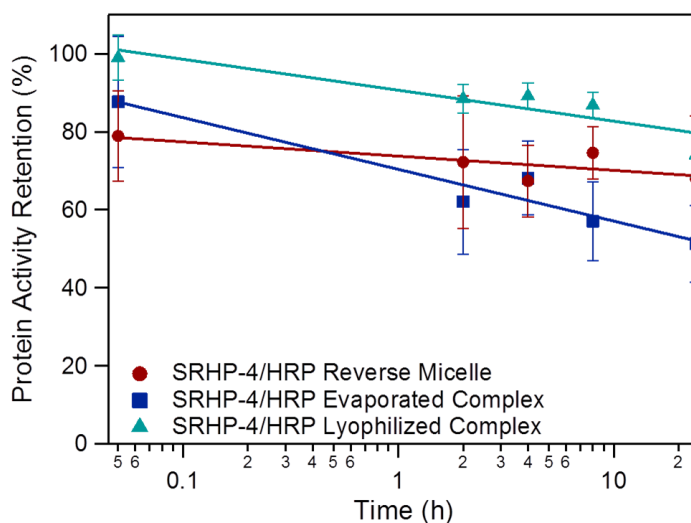
Figure 3.9. Activity of HRP after storage in organic solvent and dispersed in aqueous buffer for various SRHP-4 complexes.

§ 3.3. Conclusion

SRHPs are modular surfactants for protein stabilization in organic solvent. Its tailorability in monomer ratios, monomer chemistry, and polymer size provide opportunities to manipulate the interactions between protein and its environment. As revealed in this chapter, slight variations in polymer chemistry and architecture leads to changes in polymer solvent behavior, morphology, and protein interaction. In this study, we were able to optimize the polymer chemistry to achieve optimal performance. Lastly, since SRHPs are amphiphilic, it allows us to explore different avenues in protein-polymer hybridization. We observed different core-shell structures generated, based on processing procedure. SRHPs provide a solution to making proteins more soluble, stable, and processable in organic solvents.

§ 3.4. Experimental Section

3.4.1. Materials

Horseradish peroxidase type II (HRP), phosphotungstic acid, methyl methacrylate (MMA), ethylene glycol methyl ether methacrylate (OEGMA, M_n = 300 g/mol, 500 g/mol, and 1100 g/mol), 2-ethylhexyl methacrylate (2-EHMA), 3-sulfopropyl methacrylate potassium salt (3-SPMA), N,N-dimethylformamide, N,N-dimethylformamide-d7, dichloromethane, tetrahydrofuran, and diethyl ether were obtained from Sigma Aldrich. TMB Peroxidase EIA Substrate Kit was obtained from Bio-Rad Laboratories. Toluene was obtained from Fisher Scientific, and Milli-Q water was obtained from EMD Millipore. S-methoxycarbonylphenylmethyl dithiobenzoate RAFT transfer agent was synthesized as described by Perrier et al.[43] Dialysis membranes with a molecular weight cutoff of 6000-8000 g/mol were obtained from Spectrum Laboratories. TEM carbon grids were obtained from Ted Pella. All monomers were passed through a short column of neutral alumina to remove the inhibitor before use. All other materials were used as received.

3.4.2. Synthesis of SRHPs by RAFT Polymerization

A solution of MMA, OEGMA, 2-EHMA, 3-SPMA, and S-methoxycarbonylphenylmethyl dithiobenzoate in N,N-dimethylformamide was degassed by three freeze-pump-thaw cycles before being sealed off under vacuum. Reversible addition-fragmentation chain transfer polymerization was employed, as depicted by Scheme 3.2, and after 20 h at 60°C, the polymerization media was diluted in dichloromethane, precipitated in diethyl ether, and dried under vacuum. The resulting polymer was dissolved in tetrahydrofuran and dialyzed against a 1:1 mixture of

tetrahydrofuran and water for 3 days and against pure water for 2 days. The dialysis solutions were renewed every day. Finally, the water solution remaining in the dialysis membrane was freeze dried.
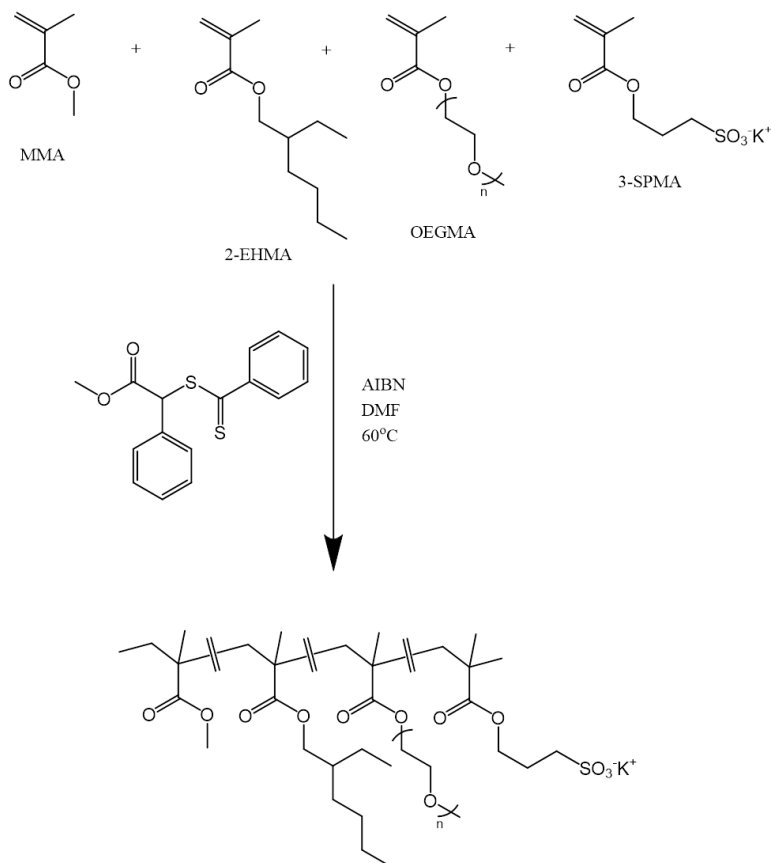
Scheme 3.3. Synthesis of SRHP by RAFT polymerization.

3.4.3. Characterization of SRHP

^{1}H NMR and ^{1}H-^{13}C heteronuclear single quantum coherence (HSQC) 2D NMR spectra were carried out at 363 K with a Bruker Avance III 400 spectrometer (400 MHz for 1H and 100 MHz for 13C) using a 5 mm BBFO+ probe. Quantitative 13C NMR distortionless enhancement by polarization transfer (DEPT135) spectra was carried out at 363 K and 100 MHz with a Bruker Avance II 400 spectrometer using a 10 mm selective 13C SEX probe. Polymer samples were examined as ca. 15% (w/v) solutions in N,N-dimethylformamide-d$_7$ (DMF-d$_7$). Chemical shift values (δ) are given in ppm in reference to residual hydrogenated solvent. Number average (M_n) and weight average (M_w) molar mass and polydispersity (PDI = M_w/M_n) of SRHPs were obtained from size exclusion chromatography (SEC) analyses using a Waters 717 Plus autosampler, a 515 HPLC pump, a 2410 differential refractometer, a 2487 UV−vis detector, a MiniDawn multiangle laser light scattering (MALLS) detector (measurement angles are 44.7°, 90.0°, and

135.4°) from Wyatt Technology Inc., a ViscoStar viscosity detector from Wyatt, and five Styragel HR columns connected in the following order: 500, 103, 104, 105, and 100 Å. Tetrahydrofuran was used as the eluent at a flow rate of 1.0 mL/min at room temperature. The results were processed using the Astra 5.4 software from Wyatt Technology Inc.

3.4.4. Analysis of SRHPs

^{1}H NMR spectra of SRHPs were used to verify that neither organic solvents nor monomer residuals were present in the final samples. The attribution of NMR signals was performed by comparing the 1H NMR, quantitative ^{13}C NMR and DEPT ^{13}C NMR, and ^{1}H-^{13}C HSQC 2D NMR spectra with those of monomers MMA, 2-EHMA, OEGMA, 3-SPMA and SRHP monomers (MMA+2-EHMA), (MMA+OEGMA) and (MMA+3-SPMA) with 80 mol% of MMA. Example spectra of SRHP-4 can be found in Appendix A.2.3-A.2.5.

Calculating experimental monomer ratios was performed by comparing the quantitative 13C NMR spectra integrations of MMA at 51.86 ppm (I_1), 2-EHMA at 68.74 ppm (I_2), OEGMA at 58.43 ppm (I_3), and 3-SPMA at 48.77 ppm (I_4). Molar ratios of monomers MMA (i), 2-EHMA (j), OEGMA (k) and 3-SPMA (l) were calculated using Equations 3.1-3.4.

$$i = I_1 / (I_1 + I_2 + I_3 + I_4) \qquad (3.1)$$

$$j = I_2 / (I_1 + I_2 + I_3 + I_4) \qquad (3.2)$$

$$k = I_3 / (I_1 + I_2 + I_3 + I_4) \qquad (3.3)$$

$$l = I_4 / (I_1 + I_2 + I_3 + I_4) \qquad (3.4)$$

3.4.5. Assembly of Protein-Containing Complexes

SRHPs were dissolved separately in toluene or water at a concentration of 0.1 w/v % and HRP was dissolved in DI water to a concentration of 1 w/v %. For reverse micelles, injection emulsion was used, where the resultant solution contained a volumetric ratio of 50:1 SRHP toluene solution to HRP solution. The suspension was sonicated, mixed, and partially evaporated using a constant stream of N_2 gas until optically clear. Additional toluene was added to compensate for evaporated solvent in order to reestablish the original concentration. For complexes formed through solvent evaporation, a solution that contained a volumetric ratio of 50:1 SRHP water solution to HRP solution was sonicated and blown with N2 gas for 1 h. After all water was evaporated, solid films were resuspended with toluene to the original concentration and sonicated. For complexes formed through lyophilization, aqueous SRHP solution was combined and sonicated with HRP solution at a volumetric ratio of 50:1. SRHP/HRP mixtures were lyophilized overnight, resuspended with toluene to the original concentration, and subsequently sonicated.

3.4.6. Small Angle X-Ray Scattering

SAXS experiments were carried out at the Advanced Light Source (ALS) at the Lawrence Berkeley National Lab (LBNL), Berkeley, California at the SAXS/WAXS/GISAXS beamline 7.3.3. The instrument was operated using an x-ray energy of 10 keV. For measurements of 0.5 w/v % SRHPs 1-6 in water, a sample-to-detector distance of 2.3 m was used. For measurements of 0.5 w/v % SRHPs 1-6 in toluene, a sample-to-detector distance of 1.8 m or 2.3 m was used. For measurements of SRHP-4/HRP complexes, a sample-to-detector distance of 3.8 m was used. A 2 M Pilatus detector was used to obtain scattering profiles. Samples were contained in standard boron-quartz capillaries situated in a customized sample holder which permitted the sample to be filled and removed using a syringe. This setup allowed for quantitative background subtraction. Absolute intensity calibration was performed using toluene. The capillary thickness was 1.6 mm. Scattering length densities were taken to be the following: $\rho = 8.0 \times 10^{-6}$ Å^{-2} for toluene, $\rho = 9.5 \times 10^{-6}$ Å^{-2} for H$_2$O, $\rho = 12.3 \times 10^{-6}$ Å^{-2} for HRP, $\rho \sim 9.2 \times 10^{-6}$ Å^{-2} for SRHP.

Guinier approximations were used to determine SRHP size in toluene.[44] Polydisperse Core with Constant Shell Thickness[45] or Core-Shell Cylinder with Polydisperse Radius[46] model was used to determine SRHP morphology in water. A sum two model function was used to fit the scattering profile associated with SRHP4/HRP complexes in solution. Polydisperse Gaussian Coil[47] was used to model aggregated SRHP-4 and Polydisperse Core with Constant Shell Thickness was used to model SRHP-4/HRP complexes.

3.4.7. Dynamic Light Scattering

Size distributions of 0.1 w/v % aqueous SRHP solutions were measured using a Brookhaven Instruments BI-200SM Research Goniometer and Laser Light Scattering System. Temperature was controlled and set at 25°C. Measurements were sorted by both number and volume average and a NNLS function was used to analyze the correlation curves.

3.4.8. Transmission Electron Microscopy

SRHP and SRHP/HRP complexes were drop cast on TEM carbon grids and dried for 5 minutes. Subsequently, several drops of water were used to wash off excess free polymer. Samples were stained using a 2 w/v% solution of phosphotungstic acid in water for 2 minutes. TEM images were taken on a JEOL 1200EX TEM at an accelerating voltage of 80 kV.

3.4.9. Assay of Protein Activity in Aqueous Buffer

HRP activity was assessed using a TMB Peroxidase EIA Substrate Kit (Bio-Rad). Baseline HRP activity was determined by preparing a stock protein solution in 100 mM KH_2PO_4/K_2HPO_4 phosphate buffer at pH 6 and applying a prepared TMB assay solution, as outlined by the manufacturer. Solution was thoroughly mixed and UV-visible spectroscopy was performed on a Hewlett-Packard 8453 Spectrophotometer. A 1-cm path length cuvette was used and absorbance at 370 nm was monitored.

$$(3.5)$$
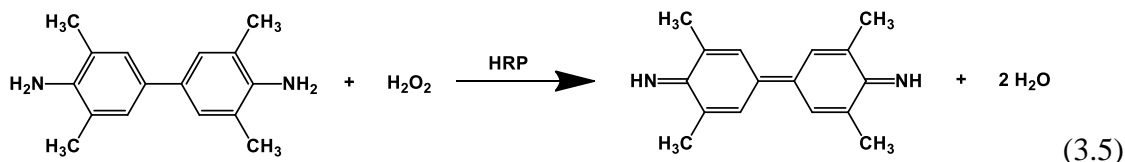
SRHP/HRP solutions were left in ambient room temperature conditions for 0, 2, 4, 8, and 24 hours in toluene. After specified times, aliquots were taken and diluted in 100 mM KH_2PO_4/K_2HPO_4 phosphate buffer, pH 6, to disperse the protein and SRHP. After thorough mixing, the assay solution is applied. Activity was quantified using UV-visible spectroscopy by monitoring the conversion of the colorimetric assay.

<div align="right">**Chapter 4**</div>

Preserving Protein Hierarchical Structure in Organic Solvents via Rationally Designed Statistically Random Heteropolymers

Protein-functionalized materials have the potential to change the current paradigm of materials science. However, it still remains a challenge to preserve protein hierarchical structure and function while making them readily processable. Protein structure is inherently fluid, and it is this property that contributes to their fragility outside of their native environment. In this chapter, I will show that through the use of rationally designed statistically random heteropolymers, it is possible to stabilize proteins at each hierarchical level and process them in organic solvents, a common need for materials fabrication. Through evaluation of horseradish peroxidase and green fluorescent protein structure, we show that statistically random heteropolymers can stabilize enzymes, allowing for activity retention when stored in organic solvent. Furthermore, we demonstrate that proteins (horseradish peroxidase and chymotrypsin), when encapsulated in statistically random heteropolymers, are still accessible to their substrates while remaining inaccessible to the denaturing organic solvent.

§ 4.1. Introduction

Proteins have been optimized by nature for the past billion years and have many attributes that are unmatched by any manmade counterpart. Successful integration of functional proteins into synthetic systems can greatly improve our ability to meet demands within the various technological sectors. This may lead to immediate impacts in catalysis,[1] sensing,[2] medicine,[3] energy,[4] molecular transport,[5] and nanostructured materials.[6] For example, combining proteins and synthetic polymers would provide materials with enhanced chemical heterogeneity, structural precision, catalytic activity, and controlled system dynamics.[7] However, most proteins reside in aqueous media and the majority of their uses are for biomedical applications. Their insolubility and inability to remain functional in non-aqueous solutions are major barriers toward the development of protein-functionalized materials.

The incompatibility between proteins and organic solvents hinders processability. Water-soluble proteins cannot be readily dissolved in organic media and cannot be directly incorporated into water-insoluble, synthetic materials. Polymer conjugation has had success in this regard; however, as discussed in Chapter 2, the protein[7] and polymer[8, 9] must have compatible chemistries. Reverse micelles have been shown to successfully encapsulate proteins, creating a colloidal dispersion in organic solvents,[10-13] but the dynamic nature of micelles could lead to loss of protein activity.[14-16]

In order to stabilize proteins in non-native media, it is required to separate proteins from extrinsic stimuli and to conformationally confine proteins to entropically impede the unfolding process. A class of hydrophobically modified polymers, amphipols, has successfully stabilized transmembrane proteins in water using these two stabilizing mechanisms.[17-20] However, as a two-step process, it requires small molecule surfactants

for initial solubilization. Amphipols also cannot be applied to water-soluble proteins nor organic solvents.

As shown in the previous chapter, statistically random heteropolymers (SRHPs) provide an enhanced route toward protein stabilization and processability. It has previously been shown that by using two monomers, it is possible to tailor a random copolymer's interfacial activity precisely.[21] SRHPs' chemical diversity thus will match well with the heterogeneity of protein surfaces. Its chain-based structure can interact with proteins multivalently. Although the protein surface is fairly intricate with its diversity in chemical functionality, the interactions that these amino acid residues participate in can be simplified into four categories: hydrophobic, hydrophilic, cationic, anionic. Stellacci et al. have shown that the spatial periodicity of AuNP is critical to modulate their interaction with proteins, where these interactions reside within the subnanometer regime.[22] SRHPs may interact with proteins and act as a chaperone to stabilize, mediate, and potentially create nanoreactors in non-native environments.

In this chapter, I will provide further analysis of an optimized SRHP variant (SRHP-4). This SRHP acts as synthetic chaperones and effectively disperses proteins in organic solvents without compromising protein structure and enzymatic activity. Using SRHP-4, we have been able to retain about 80% enzymatic activity in horseradish peroxidase (HRP) and close to 100% fluorescence in green fluorescent protein (GFP) when solubilized in toluene for 24 h. Furthermore, nanoreactors with encapsulated proteins can enzymatically interact with substrates in organic media as well as substrates encapsulated in reverse micelles. SRHPs clearly open a viable approach toward protein-functionalized materials and will positively impact the current paradigm of materials science and device engineering.

§ 4.2. Results and Discussion

Maintaining protein structure during encapsulation requires a fairly delicate balance among numerous energetic contributions, including protein folding, polymer chain conformation, macromolecular hybridization, and environmental influences. Molecular dynamics (MD) simulations of SRHP-4/HRP complexes were performed at the all-atom resolution. Multiple chains of SRHP-4 were first built by growing polymers from random seeds. The polymerization conditions for each seed were kept as close to the experimental values as possible. These polymers were then brought in close proximity to HRP and the interactions were evaluated. Simulations would provide insight into the individual SRHP-4/HRP interactions found within each nanoclustered complex. Figure 4.1a and Figure 4.1b show the final snapshots of the atomistic simulation of the SRHP-4/HRP complex in toluene and in water, respectively. In aqueous solutions, SRHP-4 and HRP were loosely complexed together and only ~40% of the HRP surface was covered by SRHP-4 whereas in toluene, the HRP surface was fully covered by

SRHP-4 and the complex was stable over the simulation duration of 200 ns. This suggests that the encapsulation process requires a water/organic solvent interface and that the multivalent protein-polymer interaction is not strong enough to counteract the resistance to encapsulation. This has led to our hypothesis that a water/toluene interface is present within the interior of the SRHP-4/HRP complex.

To further understand the mechanism of the SRHP-4/HRP assembly, the radial distribution of polymers around the protein's center of mass was calculated. The obtained results are presented in Figure 4.1(c-e). The majority of the hydrophilic components (i.e., monomers C and D, OEGMA and 3-SPMA respectively) were found to point inward toward the protein, while the majority of the hydrophobic components (i.e., monomers A and B, MMA and 2-EHMA respectively) were distributed outwards, in contact with the toluene environment. These results suggest that once anchored at the polar/nonpolar interface, SRHP-4 can adjust its local chain conformation to maximize protein-polymer and polymer-solvent interactions. With this arrangement, SRHP-4 forms a nanoscopic polymeric shell around HRP, effectively improving protein solubility and stability in organic solvent.
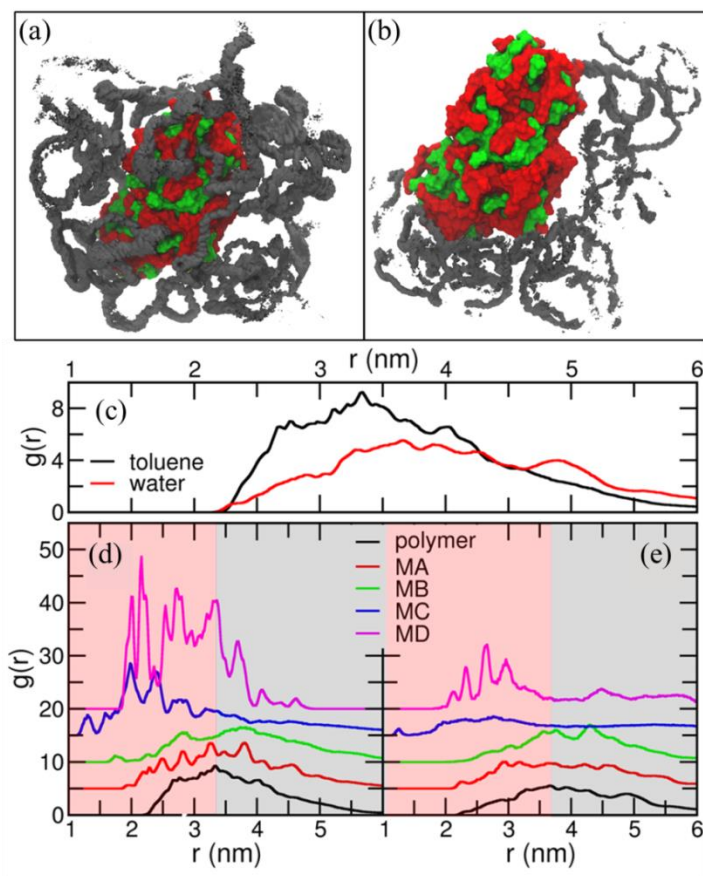
Figure 4.1. MD simulation snapshots of SRHP-4/HRP in (a) water and (b) toluene. (c) Radial distribution functions of the polymer backbone around HRP in toluene and water.

(d) Radial distribution functions of the monomers in toluene. (e) The corresponding radial distribution functions in water.

In these simulations, it was assumed that water was retained within the interior of the complex. Small angle x-ray scattering (SAXS) was performed on SRHP-4 after lyophilization from water and resuspension in toluene. This will allow us to verify this assumption. Similar to SRHP-4/HRP lyophilized complexes, a spherical polydisperse core-shell model and a polydisperse Gaussian coil model were summed to provide scattering contributions from both SRHP-4/H$_2$O lyophilized complexes and free SRHP-4 aggregates respectively, as shown in Figure 4.2(a-b). Deconvolution of the individual scattering contributions is done by fitting the scattering profile of just SRHP-4 in toluene and modeling the SRHP-4/HRP lyophilized complex at low q, where contributions of the SRHP-4 aggregates are minimized. For SRHP-4/H$_2$O lyophilized complexes formed through lyophilization, we observed a small increase in size. From the electron density of the complex, water was retained within its interior. The radius of the core is ~11.2 nm and the shell thickness is ~1.2 nm. The change in the scattering length density of the SRHP-4/H$_2$O lyophilized complex indicates that the complex is about 48.8% SRHP-4 and 51.2% H$_2$O by volume. It is speculated that this OEG monomer is able to hold water during the lyophilization process. This will provide proteins with a favorable environment within the interior of the complex.
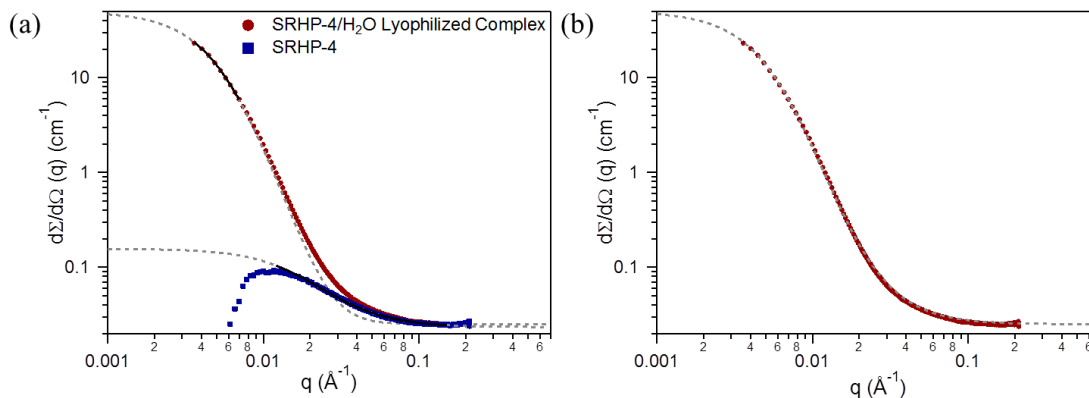
Figure 4.2. SAXS scattering profiles of SRHP-4/H$_2$O lyophilized complexes. (a) Individual fits of SRHP-4/H$_2$O complex and SRHP-4. (b) Combined summed fit.

In addition to water content, two additional parameters were explored: SRHP-4 concentration dependence and [SRHP-4]:[HRP] ratio dependence. SAXS was performed on SRHP-4 dissolved in toluene at concentrations of 5 mg/mL and 1 mg/mL. A polydisperse Gaussian coil model was used to fit each curve, as shown in Figure 4.3. As tabulated on Table 4.1, we observed no distinguishable change in size between the two concentrations. To self-validate our individual fits, scaling factors were obtained. The

relative scaling factor values between the two fits agree well with the change in solution concentration.

Figure 4.3. SAXS scattering profiles of SRHP-4 dissolved at different concentrations in toluene. Red line indicates fitted Polydisperse Gaussian Coil Model.

Table 4.1. Concentration Dependence on SRHP-4 Size in Toluene

Concentration (mg/mL)	r (nm)	Scaling Factor
5	9.5	4.69
1	9.2	1

In Chapter 3, a [SRHP-4]:[HRP] ratio of 11:1 was used. Morphology is a large factor in the protein stability performance. To optimize size, three different (SRHP-4)-to-HRP ratios were evaluated: 6-to-1, 11-to-1, and 110-to-1. Using dynamic light scattering (DLS), we observed that at 11:1, the hydrodynamic diameter of the SRHP-4/HRP lyophilized complex is around 60 to 70 nm (Figure 4.4). When the ratio was reduced two-fold, complex size increased to 250 nm and a significant amount of 1000 nm aggregates was present. This is not ideal as processing larger complexes into nanostructured materials may not be compatible. Furthermore, complexes with larger diameters may cause diffusion limitations for substrates to enter these nanoreactor complexes, which will discussed later in this chapter.

When the ratio of (SRHP-4)-to-HRP was increased 10-fold, no change in hydrodynamic diameter is observed. We believe that our original molar ratio used in Chapter 3 lies above a critical value. Molar ratios below this critical value would result in

larger particles. Once the critical value is reached, complex size does not change with molar ratio. The thermodynamic driving force for self-assembly is at an equilibrium.
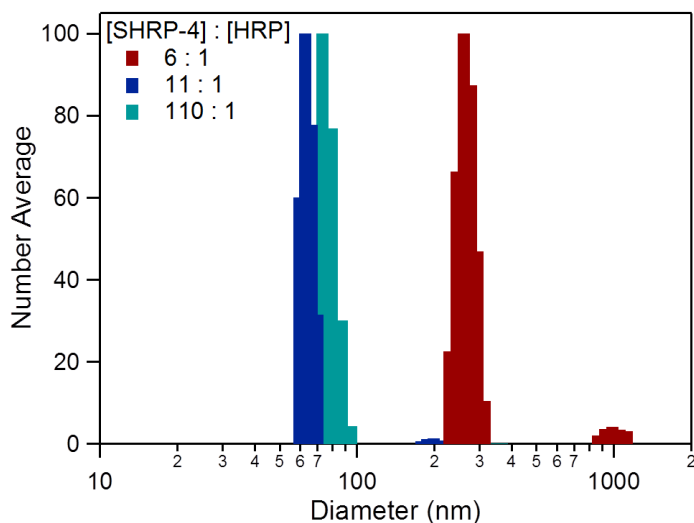
Figure 4.4. DLS (SRHP-4)-to-HRP study on SRHP-4/HRP lyophilized complex size. Number average was used to determine diameter distribution.

Fourier transform-infrared (FT-IR) spectra of SRHP-4/HRP lyophilized complexes were obtained over 24 h and are shown in Figure 4.5a. Monitoring the amide I band (1700 cm^{-1} to 1600 cm^{-1}) allows for secondary structure analysis. The amide I band indicates the presence of C=O carbonyl stretching. In the case for proteins, a band is present rather than an individual peak; the carbonyl moiety on the protein backbone stretches differently depending on the geometry of hydrogen bonding. Depending on the adopted secondary structure (α-helix, β-sheet, or β-turn), hydrogen bond angles and distances will result in slight fluctuations in wavenumber. These spectra can then be deconvoluted using the negative second derivative (Figure 4.5b).[23] From the FT-IR spectra, we observed little change in protein secondary structure over 24 h in toluene; less than a 20% change in intensity was observed for the α-helix (1656 cm^{-1}), β-sheet (1633 cm^{-1}), and β-turn (1685 cm^{-1}) peaks.

To compare SRHP-4 with currently available surfactants, small molecule Aerosol OT (AOT) and amphiphilic block copolymer, poly(styrene)-*block*-poly(ethylene oxide) (PS-*b*-PEO), were used to create HRP-encapsulated reverse micelles. HRP secondary structure in these reverse micelles could not be measured. In order to obtain a decent signal-to-noise ratio in FT-IR, solutions must be concentrated. Fortunately for the SRHP-4 lyophilization technique, this was not a problem. For reverse micelle injection emulsion technique, this was not possible. By concentrating the solution, gelation occured as molecules interact, thus rendering solution FT-IR inappropriate for these samples.
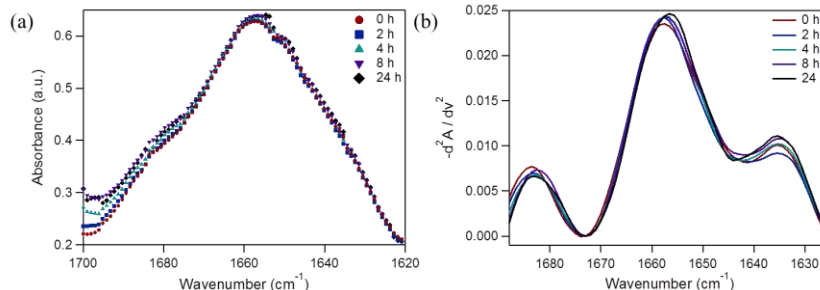
Figure 4.5. Spectroscopic analysis of HRP 2° using FT-IR. (a) FT-IR spectra of amide I band in SRHP-4/HRP lyophilized complex over 24 h. (b) Negative second derivative of FT-IR spectra.

HRP was exchanged with green fluorescent protein (GFP) in order to monitor tertiary structure in situ. The fluorescence intensity of GFP as well as the emission peak maxima is highly dependent on its tertiary structure. A decrease in tertiary structure will result in a decrease in fluorescent intensity. In addition, protein unfolding would result in solvent interactions with the fluorescent moiety, changing the emission peak position.

Upon encapsulation of GFP with SRHP-4, GFP can be effectively solubilized in organic solvents as well. Due to sample limitations, the concentration of GFP is kept low in comparison to HRP. In order to see the effects of this change in SRHP-to-GFP molar ratio, SAXS was used to evaluate the structure of the SRHP-4/GFP lyophilized complex. Again, a spherical polydisperse core-shell model and a polydisperse Gaussian coil model were summed to provide scattering contributions from both the SRHP-4/GFP lyophilized complex and free SRHP-4 aggregates respectively, as shown in Figure 4.6(a-b). It was determined that the radius of the core is ~8.9 nm and the shell thickness is ~1.3 nm. There is not much difference in size between SRHP-4/GFP lyophilized complex and SRHP-4/H_2O lyophilized complex. The concentration of GFP is low and so the majority of the complexes may not contain GFP. This may account for the poorly fitted summed model. Rather than a bimodal system of two species, three different complexes are present: SRHP-4, SRHP-4/H_2O lyophilized complex, SRHP-4/GFP lyophilized complex.
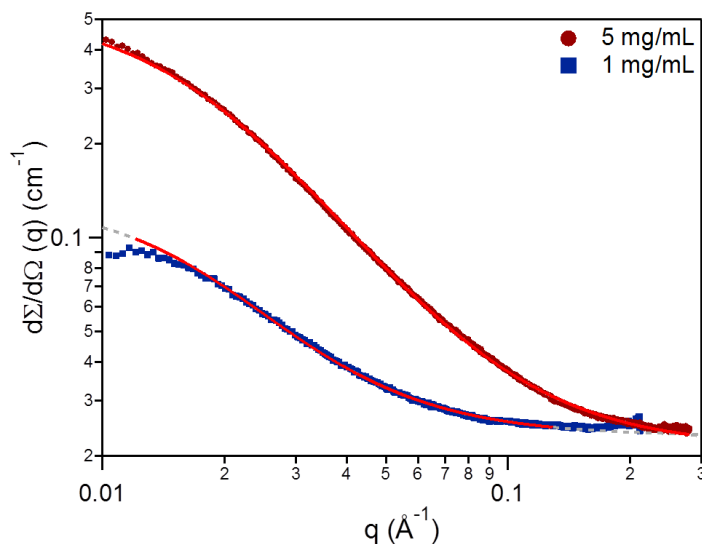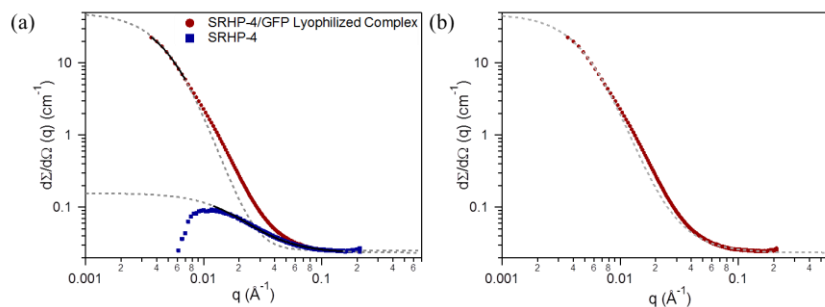

Figure 4.6. SAXS scattering profiles of SRHP-4/GFP lyophilized complexes. (a) Individual fits of SRHP-4/GFP complex and SRHP-4. (b) Combined summed fit.

In Figure 4.7(a-c), fluorescence spectra of SRHP-4/GFP lyophilized complexes, AOT/GFP reverse micelles, and PS-*b*-PEO/GFP reverse micelles were compared over 24 h in toluene respectively. SRHP-4/GFP lyophilized complexes and GFP in water have similar fluorescent emission peak maxima throughout the length of the test (Figure 4.7d). This suggests that the environment of the phenolate/imidizolidone-based moiety found in the interior β-barrel structure remains undisturbed and that there is no solvent penetration that can affect the local environment of the protein core.[24] On the other hand, GFP in AOT reverse micelles and PS-*b*-PEO reverse micelles show a change in peak maxima, indicating a change in dielectric constant experienced by this phenolate/imidizolidone group. This indicates protein unfolding and/or solvent penetration. The intensity of this peak can also be monitored to evaluate GFP tertiary structure. In Figure 4.7e, it is observed that the intensity of GFP when encapsulated in SRHP-4 is retained over 24 h, indicating enhanced stability of GFP. GFP encapsulated in AOT and PS-*b*-PEO decreases to about 55% and 85%, respectively, of their initial fluorescence over 24 h. The interactions between the phenolate/imidizolidone group and basic amino acids lining the interior of the β-barrel enhance electron delocalization causing fluorescence. Any change in the tertiary structure then will make fluorescence intensity decrease, which is seen minimally in SRHP-4/GFP complexes and significantly in the two reverse micelle structures.
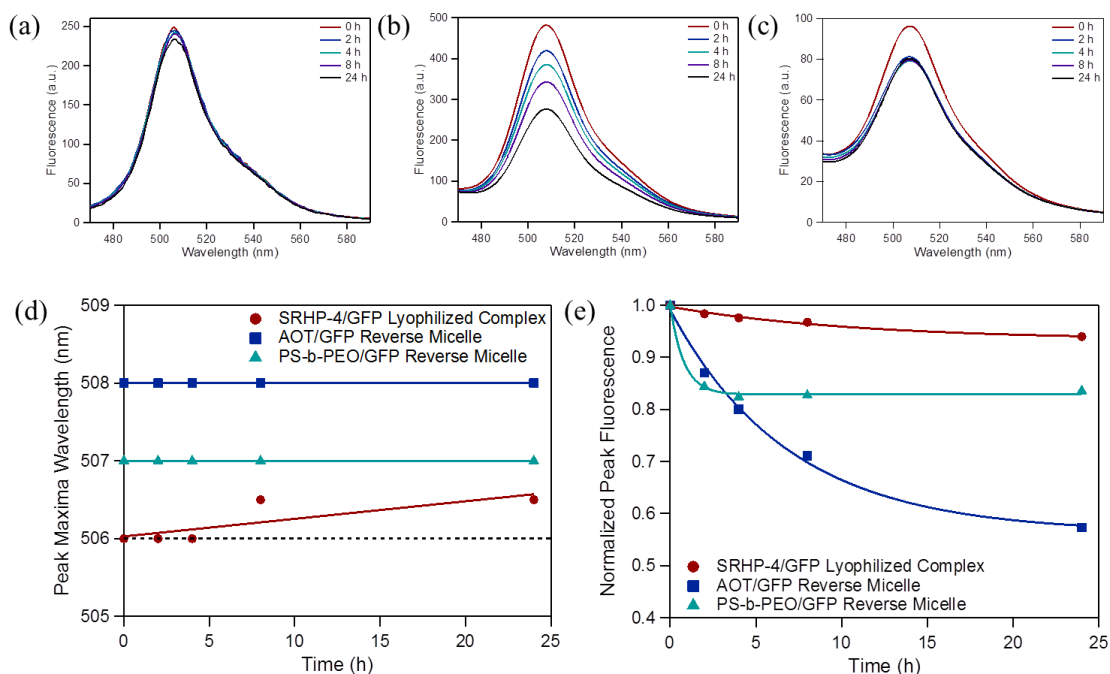
Figure 4.7. Spectroscopic analysis of GFP 3° structure using fluorescence spectroscopy. (a) SRHP-4/GFP lyophilized complex, (b) AOT/GFP reverse micelle, and (c) PS-*b*-PEO/GFP reverse micelle fluorescence spectra. (d) Location of peak maxima over 24 h

when stored in toluene. Dotted line represents location of peak maxima of GFP in water. (e) Normalized absorbance measurement over 24 h when stored in toluene.

For HRP to remain active, an inorganic cofactor, heme, is required.[25] The heme is attracted to a hydrophobic pocket on the exterior of the protein and the presence of histidines provides control of iron oxidation state in heme. This is the active group that is involved in the decomposition of hydrogen peroxide into water. UV-visible absorbance spectra of SRHP-4/HRP lyophilized complex, AOT/HRP reverse micelle, and PS-*b*-PEO/HRP reverse micelle were compared over 24 h in toluene and are shown in Figures 4.8(a-c) respectively. Our measurements indicate that HRP in water has a UV-visible absorbance peak at 403 nm. In Figure 4.8d, no significant deviation from 403 nm was observed for the heme peak in SRHP-4/HRP lyophilized complexes. This suggests that the heme binding pocket is stable and protein tertiary structure is retained over 24 h. AOT/HRP reverse micelles and PS-*b*-PEO/HRP reverse micelles show peak deviation upon encapsulation and a return back to 403 nm over 24 h. The encapsulation process seems to effect the heme-protein interactions. Looking at the peak intensity over time, the SRHP-4/HRP lyophilized complex spectra show little change in absorbance, while AOT/HRP reverse micelle and PS-*b*-PEO/HRP reverse micelle spectra show significant change (Figure 4.8e).
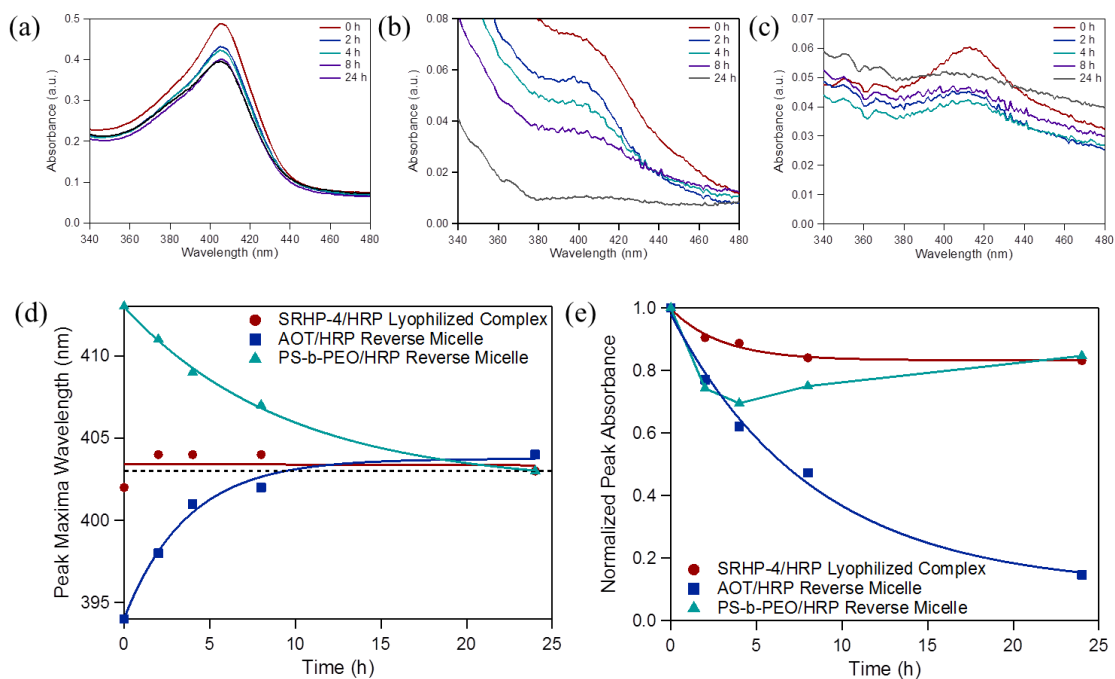
Figure 4.8. Spectroscopic analysis of the heme binding pocket in HRP (a) SRHP-4/HRP lyophilized complex, (b) AOT/HRP reverse micelle, and (c) PS-*b*-PEO/HRP reverse micelle spectra using UV-visible spectroscopy. (d) Location of peak maxima over 24 h when stored in SRHP-4/HRP lyophilized complex, AOT/HRP reverse micelle, and PS-*b*-

PEO/HRP reverse micelle spectra using UV-visible spectroscopy. Dotted line represents location of peak maxima of HRP/heme in water. (e) Normalized absorbance measurement over 24 h when stored in toluene.

When all hierarchical structures are maintained, enzymatic activity should be preserved. Enzymatic assays were used to evaluate activity of HRP function in SRHP-4/HRP lyophilized complexes after suspension in toluene. Over 24 h, aliquots of SRHP-4/HRP lyophilized complexes were dispersed in buffer. This allows us to disrupt SRHP-4/HRP hybridization and extrapolate the effects this process has on solely protein function. As shown in Figure 4.9, over 80% of HRP activity was still maintained (this data was first mentioned in Chapter 3), whereas both reverse micelles only preserved HRP activity to 20% of its original value. HRP encapsulated in small molecule surfactant- and amphiphilic block copolymer-based reverse micelles denature and lose their functionality immediately after encapsulation and this functionality quickly drops off. Other proteins have been encapsulated as well, such as glucose oxidase, and show similar levels of protein function preservation when using SRHP-4 (Appendix A.3.1).
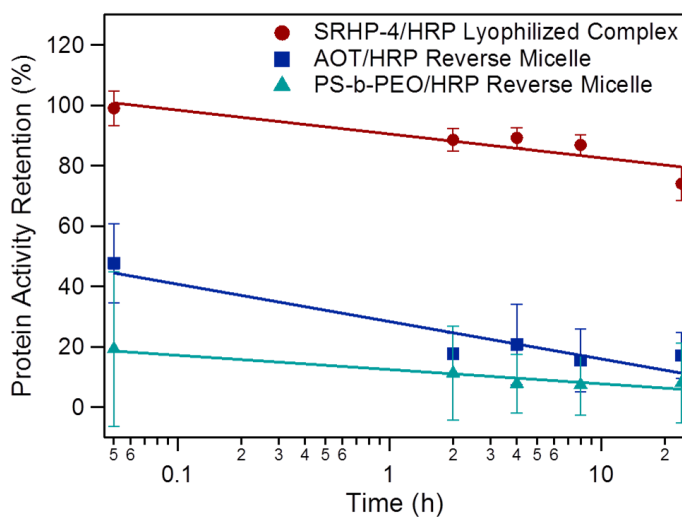
Figure 4.9. Activity of HRP after storage in organic solvent using SRHP-4, AOT, or PS-*b*-PEO and dispersed in aqueous buffer.

Enzymatic activity was evaluated when suspended in organic media. Accessibility of proteins while encapsulated in SRHP-4 provides an approach toward the development of nanoreactors. Tailoring SRHP chemistry can provide tunability of molecular transport across its shell and expulsion of solvent from its core. Tailoring SRHP/protein structure can provide tunability of shell thickness which may provide a kinetic barrier toward penetration. Nanoreactors have advantages over enzyme adsorption on a solid substrate.

Nanoreactors are in constant diffusion in solution, minimizing localized product accumulation near the enzyme.

HRP and chymotrypsin (CT) encapsulated in (SRHP-4)-based complexes were evaluated. HRP has the ability to decompose benzoyl peroxide into benzoic acid in the presence of an electron donor (Figure 4.10a).[26] Benzoyl peroxide is hydrophobic and can be solubilized in toluene, thus allowing us to assess the accessibility of substrates in complexes while proteins remain encapsulated. HRP catalysis was observed by the production of a yellow chromophore in solution, as seen in Figure 4.10b. Although this decomposition of benzoyl peroxide is spontaneous, the presence of HRP does speed up the process, as seen in Figure 4.10c. Individual spectra can be found in Appendix A.3.2. SRHP-4 is able to permit substrates to diffuse into the particle, but from previously shown spectroscopic analysis, organic solvent does not penetrate. It is speculated that the more polar substrate has a lower energetic barrier for penetration in comparison to the more non-polar toluene.
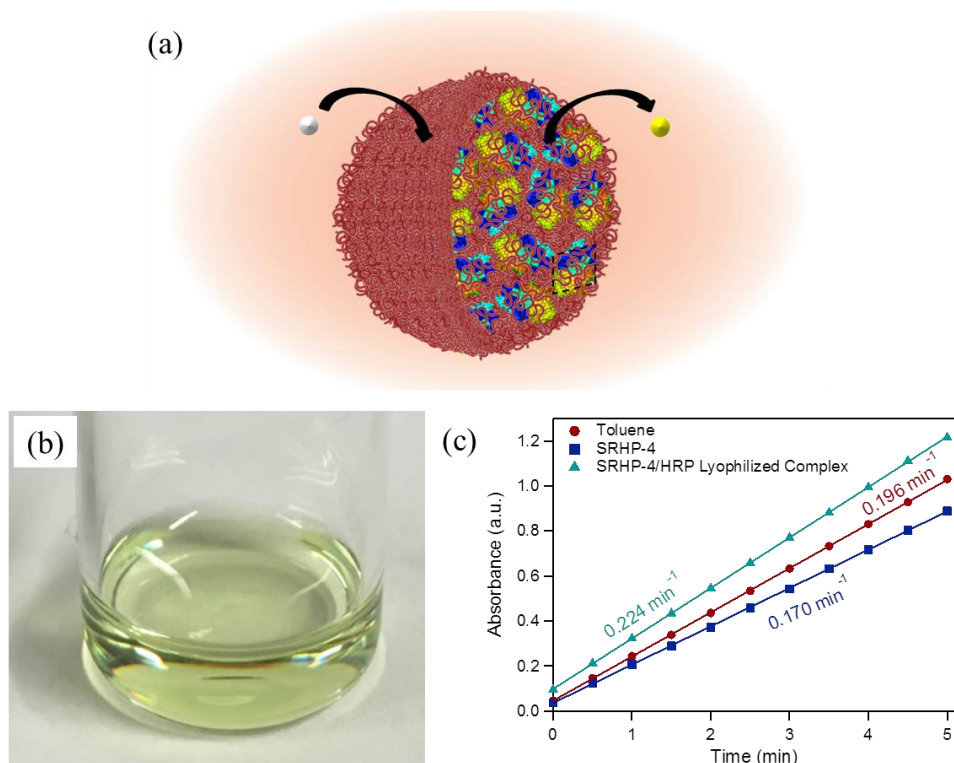
Figure 4.10. Activity and accessibility of HRP while encapsulated in (SRHP-4)-based nanoreactors. (a) Decomposition of hydrophobic benzoyl peroxide into benzoic acid in the presence of SRHP-4/HRP lyophilized complexes. (b) Verification of HRP activity and accessibility in (SRHP-4)-based nanoreactors using colorimetric assays. (c) Activity plots of the catalytic reaction in toluene, in the presence of SRHP-4, and in the presence of SRHP-4/HRP lyophilized complex.

Alternatively, we can encapsulate hydrophilic substrates in reverse micelles. CT, a protease involved in peptide backbone cleavage, has successfully been incorporated into SRHP-4 lyophilized complexes. Their substrate, a short peptide sequence with a colorimetric tag (N-succinyl-Ala-Ala-Pro-Phe p-nitroanilide)[27] has been successfully incorporated into SRHP-4 reverse micelles. By combining the two in solution, we can monitor the interaction of the two different complexes, as shown schematically in Figure 4.11a. Using UV-visible spectroscopy, we see that in the absence of CT, there is no change in absorbance. When SRHP-4/CT lyophilized complexes are introduced, an increase in absorbance is observed, indicating cleavage of p-nitroaniline and activity retention of CT (Figure 4.11b). Individual spectra can be found in Appendix A.3.3. These two methods indicate that substrates can diffuse through SRHP-4 from the surround media, and fusion of complexes can provide delivery of cargo between complexes.
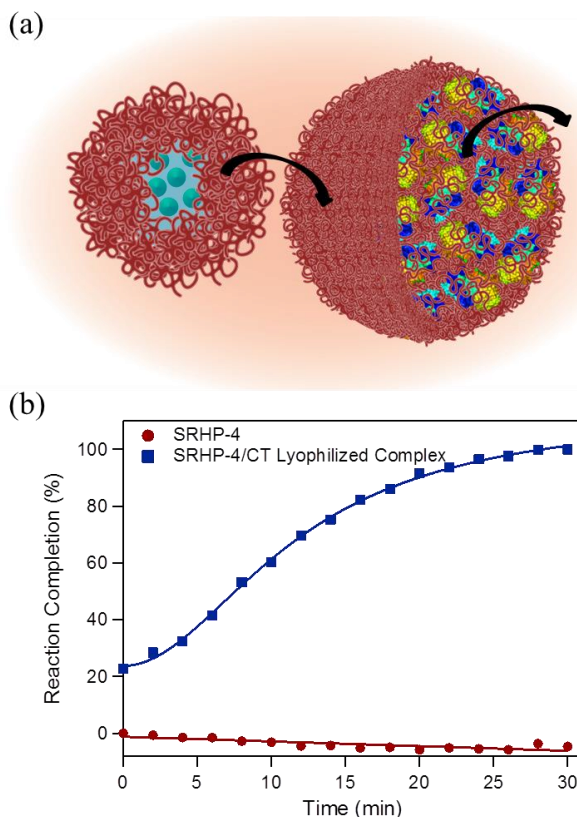
Figure 4.11. Activity and accessibility of CT while encapsulated in (SRHP-4)-based nanoreactors. (a) Proteolysis of hydrophilic peptides encapsulated in (SRHP-4)-based reverse micelles in the presence of SRHP-4/CT lyophilized complexes. (b) Monitoring CT-catalyzed reaction over time.

The significance of CT is that even if proteins are confined in these nanoreactors, protein fluidity is not hindered. In HRP, catalysis stems from oxidation of hydrogen

peroxide at the heme cite. In CT, hydrolysis occurs at the catalytic triad, which involves a mechanical event. If the confinement of CT is too strong, this mechanical event would be hindered and protein activity would be nonexistent. It is speculated that the fluidity arises from the water that is retained within the core of this complex.

§ 4.3. Conclusion

There are many advantages associated with SRHPs. They assist in the encapsulation, solubilization, and stabilization of a variety of proteins in organic solvents. The instability, insolubility, and inability to retain protein function in organic media no longer hold, allowing protein-functionalized materials with increased performance to be generated. Although AOT small molecule surfactants and amphiphilic block copolymers such PS-*b*-PEO do demonstrate the ability to make proteins more processable, their lack of preserving protein function limits their viability. In addition, SRHP-4 provides a vessel that can be used to generate nanoreactors for both hydrophobic and hydrophilic substrates. SRHPs have the potential to pave the path toward improved technologies, such as water detoxification, and shows promise as a modular and general approach toward protein-based material fabrication.

§ 4.4. Experimental Section

4.4.1. Materials

Horseradish peroxidase type II (HRP), glucose oxidase type X-S (GOx), α-chymotrypsin type II (CT), sodium 2-bis(hexylethyl) sulfosuccinate (AOT), α-D-glucose, phenol, 4-aminoantipyrine, N-Succinyl-Ala-Ala-Pro-Phe p-nitroanilide, and magnesium sulfate were obtained from Sigma Aldrich. Benzoyl peroxide was obtained from TCI. TMB Peroxidase EIA Substrate Kit was obtained from Bio-Rad Laboratories. (22 kDa) poly(styrene)-*block*-(21.5 kDa) poly(ethylene oxide) (PS-*b*-PEO) was obtained from Polymer Source. Toluene was obtained from Fisher Scientific, and Milli-Q DI water, green fluorescent protein (GFP), and Amicon Ultra-0.5 mL centrifugal filters with a cutoff molecular weight of 10 kDa were obtained from EMD Millipore. GFP was centrifuge filtrated to remove salts and glycerol using centrifugal filters. GFP was then dissolved in Milli-Q water to a concentration of approximately 1 mg/ml. Benzoyl peroxide was dissolved in toluene and treated with magnesium sulfate to remove water. All other materials were used as received. SRHP-4 was synthesized as previously reported in Chapter 3.

4.4.2. Molecular Dynamic Simulations

The classical molecular dynamics (MD) simulations were performed at the all-atom resolution using the package GROMACS (version 5.0).[28] The latest version of the CHARMM 36 force field was used for all the molecules investigated.[29]

The structure of the protein was downloaded from the RSCB Protein Data Bank with the protein ID 1H55. The degree of polymerization (DP) of 80 was employed for SRHP-4, which is close to the experimental molar weight of 30 kDa. In building a single SRHP-4 chain, random seeds were varied to match the experimental composition ratio of MA:MB:MC:MD = 10:4:5:1, where MA is methyl methacrylate, MB is 2-ethylexyl methacrylate, MC is oligo(ethylene glycol) methacrylate with a degree of polymerization of 9, and MD is 3-sulfopropyl methacrylate. Therefore, each random polymer chain contained 40 MA, 16 MB, 20 MC and 4 MD monomers. In total, 12 different SRHP-4 chains were built using different random seeds so that the ratio of the concentration of polymer to that of protein matched the experimental value.

To investigate the influence of solvent on the encapsulation of proteins by SRHPs two different solvent conditions, aqueous solution and organic (toluene) solution were studied. The compositions of the components are provided in Table 4.2.

Table 4.2. Compositions of SRHP-4/HRP Mixtures in Different Systems

	Protein	Polymer	Toluene	Water
Vacuum	1	12	-	-
Aqueous Solution	1	12	-	92151
Organic Solution	1	12	15430	-

Due to the nature of long polymer chains, the encapsulation kinetics is far beyond the capability of atomistic molecular dynamic simulations. Therefore, some approaches were employed to speed up the polymer/protein aggregation process. The initial structures of the polymer-protein complex were built using the package PACKMOL.[30] The protein molecule was initially put in the center of the box with the edge length of 15 ns in all dimensions. The 12 polymer chains were subsequently arranged surrounding the protein with one out of the four -SO3- groups distributed within the distance of 4 nm from the center of mass of the protein molecule. Note the size of the protein molecule is around $6 \times 4 \times 4$ nm^3. After a short energy minimization using the steepest descent algorithm, the polymer/protein complex was simulated under vacuum conditions for 1 ns. At the end of the simulation, all the polymer chains were aggregated surrounding the protein molecule. In the simulation under the vacuum condition, the NTV ensemble (constant number of particles, temperature and volume) was employed via the V-rescale thermostat (the reference temperature 400 K and the characteristic time of 0.5 ps). It is

noteworthy that the backbone atoms of the protein molecule were constrained at their initial coordinate using a force constant of 1000 kJ/mol/nm^2 to maintain the structure of the protein molecule.

Based on the final frame of the simulation under vacuum condition, the polymer-protein complex was subsequently embedded in organic toluene solution or water solution. See Table 4.1 for the number of solvent molecules added. They were used as the initial structures for the following simulations under the organic or aqueous solutions. In the following simulations, the periodic boundary conditions were imposed in all the three dimensions; neighbor searching was performed for a distance up to 1.2 nm, and was updated every 10 time steps; the short-range van der Waals interactions were truncated at 1.2 nm with the long-range dispersions applied for both the energy and the pressure; the short-range Coulomb interactions was also truncated at 1.2 nm with the long-range interactions calculated using the smooth Particle Mesh Ewald algorithm.[31, 32] Moreover, to speed up the simulations, the simulation time step of 2 fs was employed by constraining the covalent bonds involving hydrogen atoms using the LINCS algorithm.[33] To speed up the process for the optimal polymer-protein aggregate structure, the simulations were first simulated at a high temperature of 400 K. The NTP ensemble (constant number of particle, temperature and pressure) was applied with the temperature coupled via V-rescale algorithm and the isotropic Berendsen barostat (the reference pressure 1 bar). The simulation duration of 40 ns was performed. The calculations of the RMSD of the protein backbone atoms suggest that 40 ns simulations were roughly long enough to equilibrate the polymer-protein complex. Note that the protein backbone atoms were again constrained to maintain the structure.

The production simulations were subsequently performed at room temperature. The position restrain was switched off for the protein molecule, allowing it to fully relax for the optimal structure. The NTP ensemble was imposed with the pressure coupled via the Parrinello-Rahman algorithm (reference pressure 1 bar, characteristic time 4 ps, compressibility of 4.5×10-5 bar-1). The temperatures of protein, polymer and solvent (toluene, or water) were separately coupled via the Nose-Hoover algorithm (reference temperature 298 K, characteristic time 0.5 ps). The frames were saved at a frequency of 50 ps. Each of the simulations was performed for a duration of 200 ns. Calculations support that the simulations have converged, at least within the simulation duration.

4.4.3. Assembly of Protein-Containing Complexes

HRP and GOx were dissolved in DI water to a concentration of 10 mg/mL. CT was dissolved in 0.1 M Tris-HCl with 1 mM CaCl$_2$, pH 7.75, to a concentration of 10 mg/mL GFP was dissolved in DI water to a concentration of approximately 1 mg/ml. SRHP-4 was dissolved in DI water at a concentration of 1 mg/mL. Sodium 2-bis(hexylethyl) sulfosuccinate (AOT, Aldrich) was dissolved in toluene at a concentration of 200 mM. PS-*b*-PEO was dissolved in toluene at a concentration of 1 mg/mL.

HRP solutions were injected into AOT solution at a $[H_2O]/[AOT]$ ratio of $w_0=13$ or injected into PS-*b*-PEO at a volumetric ratio of 1:50 HRP solution to polymer solution. The suspensions were sonicated, mixed, and partially evaporated using a constant stream of N_2 gas until optically clear. Additional toluene was added to compensate for evaporated solvent in order to reobtain original concentrations. SRHP-4/protein complexes were obtained by combining the aqueous SRHP solution with protein solution at a volumetric ratio of 50:1. SRHP/protein mixtures were lyophilized overnight, resuspended with toluene to the original concentration, and subsequently sonicated.

4.4.4. Small Angle X-Ray Scattering

SAXS experiments were carried out at the Advanced Light Source (ALS) at the Lawrence Berkeley National Lab (LBNL), Berkeley, California at the SAXS/WAXS/GISAXS beamline 7.3.3. The instrument was operated using an x-ray energy of 10 keV. For measurements of SRHP-4, SRHP-4/H_2O and SRHP/GFP lyophilized complexes, a sample-to-detector distance of 3.8 m was used. A 2 M Pilatus detector was used to obtain scattering profiles. Samples were contained in standard boron-quartz capillaries situated in a customized sample holder which permitted the sample to be filled and removed using a syringe. This setup allowed for quantitative background subtraction. Absolute intensity calibration was performed using toluene. The capillary thickness was 1.6 mm. Scattering length densities were taken to be the following: $\rho = 8.0 \times 10^{-6}$ Å^{-2} for toluene, $\rho = 9.5 \times 10^{-6}$ Å^{-2} for H_2O, $\rho = 12.3 \times 10^{-6}$ Å^{-2} for GFP, $\rho \sim 9.2 \times 10^{-6}$ Å^{-2} for SRHP-4.

A sum two model function was used to fit the scattering profile associated with SRHP-4/H_2O and SRHP-4/GFP lyophilized complexes in solution. Polydisperse Gaussian Coil[34] was used to model aggregated SRHP-4 and Polydisperse Core with Constant Shell Thickness[35] was used to model the complexes.

4.4.5. Dynamic Light Scattering

Size distributions of SRHP-4/HRP lyophilized complex solutions were measured using a Brookhaven Instruments BI-200SM Research Goniometer and Laser Light Scattering System. Temperature was controlled and set at 25°C. Measurements were sorted by number average and a NNLS function was used to analyze the correlation curves.

4.4.6. Fourier-Transform Infrared Spectroscopy

To enhance the signal-to-noise ratio, solutions of SRHP-4/HRP lyophilized complexes were concentrated 200-fold. Solutions were deposited in a liquid cell composed of CaF_2 windows with a path length of 1 mm. Spectra were collected at 0, 2, 4, 8, and 24 hours after resuspension in toluene on a Thermo Scientific Nicolet 6700. Measurements were conducted at room temperature and the amide I band between 1700

cm^{-1} and 1620 cm^{-1} was monitored. Spectral analysis was performed using the built-in OMNIC Spectra Software.

4.4.7. Fluorescence Spectroscopy

Retention of green fluorescent protein fluorescence was evaluated using a Perkin Elmer LS-55 fluorescence spectrometer. Immediately after encapsulation of GFP, solutions were sealed in a 1-cm path length quartz cuvette and excited at an excitation wavelength of 450 nm. Emission wavelength was monitored between 450 nm and 600 nm. Measurements were conducted at room temperature and taken 0, 2, 4, 8, and 24 hours after resuspension.

4.4.8. Heme Analysis using UV-Visible Spectroscopy

SRHP-4/HRP lyophilized complex solutions in toluene were sealed in a 1-cm path length quartz cuvette. UV-visible spectroscopy was performed on a Hewlett-Packard 8453 Spectrophotometer. Measurements were conducted at room temperature and the location of the heme peak as well as the intensity of this peak were monitored between 350 nm and 800 nm at 0, 2, 4, 8, and 24 hours after resuspension.

4.4.9. Assay of Protein Activity in Aqueous Buffer

HRP activity was assessed using a TMB Peroxidase EIA Substrate Kit. Baseline HRP activity was determined by preparing a stock protein solution in 100 mM KH$_2$PO$_4$/K$_2$HPO$_4$ phosphate buffer at pH 6 and applying a prepared TMB assay solution, as outlined by the manufacturer. Solution was thoroughly mixed and UV-visible spectroscopy was performed on a Hewlett-Packard 8453 Spectrophotometer. A 1-cm path length cuvette was used and absorbance at 370 nm was monitored.

$$(4.1)$$

GOx activity was assessed using an assay containing glucose, phenol, 4-aminoantipyrine, and HRP. Baseline GOx activity was determined by preparing a stock protein solution in 100 mM KH$_2$PO$_4$/K$_2$HPO$_4$ phosphate buffer at pH 6 and applying the colorimetric assay. A 1-cm path length cuvette was used and absorbance at 505 nm was monitored.
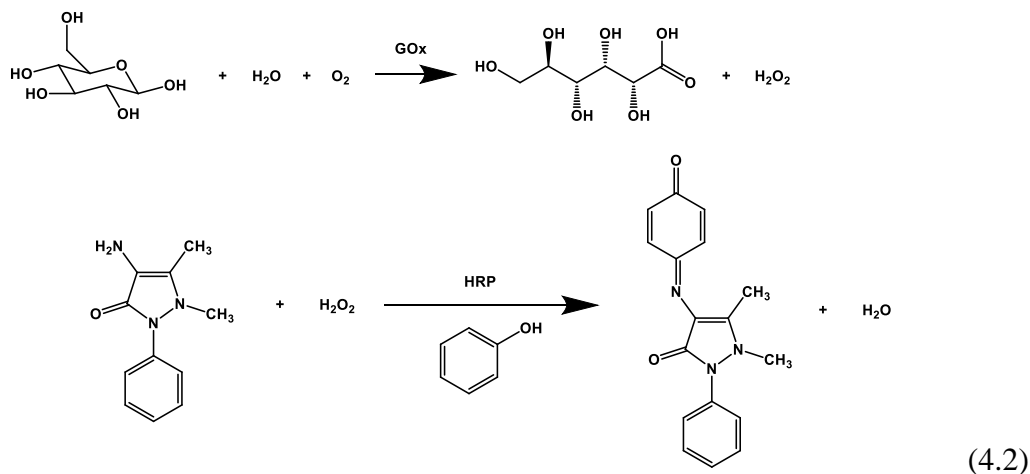
(4.2)

Solutions were left in ambient room temperature conditions for 0, 2, 4, 8, and 24 hours in toluene. After specified times, aliquots were taken and diluted in 100 mM KH_2PO_4/K_2HPO_4 phosphate buffer, pH 6, to disperse the protein and SRHP. After thorough mixing, the assay solution is applied. Activity was quantified using UV-visible spectroscopy by monitoring the conversion of the colorimetric assay.

4.4.10. Assay of Protein Activity in Organic Media

Benzoyl peroxide and 3,3',5,5'-tetramethyl benzidine was introduced into toluene solutions containing SRHP-4/HRP lyophilized complexes. Samples were incubated at room temperature for 30 minutes. Visual analysis and UV-visible spectroscopy were used to determine color change of the colorimetric electron donor (yellow tint). Whole spectra can be found in Appendix A3.3.

(4.3)
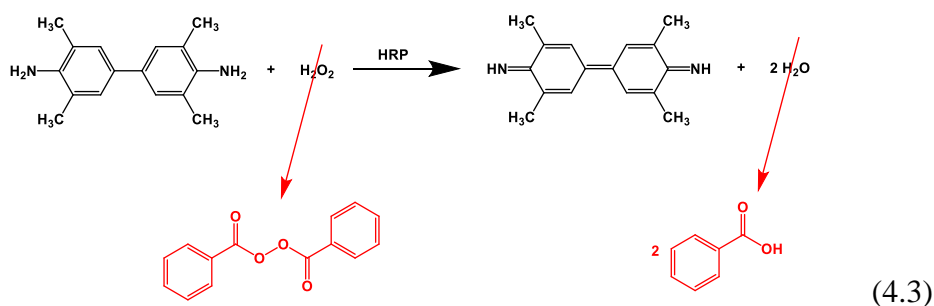
N-Succinyl-Ala-Ala-Pro-Phe p-nitroanilide was used to assay the activity retention of CT in toluene. N-Succinyl-Ala-Ala-Pro-Phe p-nitroanilide was dissolved in 0.1 M Tris-HCl with 1 mM $CaCl_2$, pH 7.75, at a concentration of 1 mM. In order to use N-Succinyl-Ala-Ala-Pro-Phe p-nitroanilide in organic media, the compound was encapsulated in SRHP-4 reverse micelles using an injection emulsion technique, at a volumetric ratio of 50:1 SRHP-4 to assay. After mixing protein and assay, samples were

incubated at room temperature for 30 minutes. Activity was quantified using UV-visible spectroscopy by monitoring the hydrolysis of the p-nitroanilide group at 360 nm.

$$(4.4)$$

<div align="right">**Chapter 5**</div>

Enhanced Thermal Stability of Proteins in Aqueous Solutions Using Rationally Designed Statistically Random Heteropolymers

The use of elevated temperatures for material fabrication and accelerated reaction rates is a common condition for enhanced processing. However, heat and preservation of protein hierarchical structure are two processes that are typically incompatible. Protein denaturation occurs at temperatures exceeding non-native conditions, resulting in diminished functionality and irreversible aggregation. Intramolecular protein interactions are weakened and contributions from entropic penalty dominate. In addition, protein dynamics are accelerated at increased temperatures, allowing proteins to overcome the kinetic barrier between the folded and unfolded state. In this chapter, I will show that the thermal stability of proteins can be improved through incubation with statistically random heteropolymers. Statistically random heteropolymers are amphiphilic and have the ability to form multivalent interactions with a protein's surface. Fluorescence, circular dichroism, and UV-visible spectroscopy were utilized to monitor protein structure at each hierarchical level. In an analogous mechanism to that of chaperones, statistically random heteropolymers provide heterogeneous patches for non-covalent association of partially denatured proteins, offering them the chance to properly refold. The mechanism of statistically random heteropolymer stabilization may provide necessary insight toward the development of artificial cellular machinery and other protein-polymer hybrid materials that can raise the quality of life.

§ 5.1. Introduction

Protein folding is critically sensitive to changes in the local environment. At elevated temperatures, proteins adopt additional non-native conformations, arising from the weakening of hydrogen bond networks and van der Waals forces, the heightened influence of entropic penalty, and the increase in protein dynamics.[1] Unfolded proteins have an increased probability of displaying their hydrophobic regions to the aqueous environment. This drives the formation of protein aggregates to shield these hydrophobic regions from the water. This aggregation process results in irreversible aggregation and loss of activity.

The temperature dependence of protein folding limits the scope of enzyme implementation in both small scale and industrial settings. High temperatures are often required for material and biomolecular processing. Polymer melts are needed for injection molding. Heat is needed to expand components for assembly and for disinfection of medical devices. Additionally, chemical reactors that utilize enzyme catalysis are faced with the challenge of temperature sensitivity at the required reaction or solution viscosity conditions.

In an attempt to preserve protein functionality, both prokaryotic and eukaryotic organisms have adapted molecular aids that prevent protein denaturation at elevated temperatures. Chaperones, a highly conserved class of proteins, play a critical role in maintaining enzyme viability, particularly under conditions of heat shock.[2, 3] Chaperones

assist in the folding of macromolecules or assembly of large complexes. They bind to partially folded or unfolded proteins and prevent irreversible aggregation.[4, 5] By providing a hydrophobic surface for partially unfolded proteins to interact with, chaperones prevent further denaturation, and in turn, aggregation with other unfolded proteins. This provides a reversible mechanism toward renaturation. However, chaperones require the use of ATP binding to drive the transformation between a high affinity state and a low affinity state and may not be compatible with all processing practices.

A particular class of molecular chaperones, chaperonins, has large cylindrical structures that act as folding cages.[6] The interior of this cylinder is lined with hydrophobic residues that act as both a passive and active mechanism toward protein renaturation. These chaperonins block aggregation and accelerate productive folding. Unlike the active mechanism that requires ATP to assist in a high-to-low affinity transition, the passive model provides a protective environment at infinite dilution space, thus preventing the interaction between unfolded proteins and limiting irreversible aggregation.[7]

Mimicking the mechanism of chaperone proteins, thermal denaturation can be deterred through non-covalent interactions with synthetic materials.[8-12] In this chapter, I will show that the thermal stability can be achieved through association with an optimized rationally designed statistically random heteropolymer (SRHP-4). Acting as a synthetic chaperone, SRHP-4 provides stabilizing interactions that protect a protein from thermal denaturation, preserving native folding and functionality. Colorimetric assays were used to measure protein activity retention, and protein hierarchical structure was evaluated using spectroscopic techniques. As will be discussed in this chapter, thermal stability is achieved in both aqueous and organic media, but there are clear differences in the mechanism used to stabilize the protein in each case.

§ 5.2. Results and Discussion

Small angle x-ray scattering was used to evaluate SRHP-4 as a function of concentration. In water, an SRHP-4 concentration where aggregation does not occur is ideal; polymer-polymer interactions that occur during aggregation may hinder a polymer's ability to interact with the protein and prevent denaturation. Figure 5.1 shows scattering profiles of SRHP-4 at 0.05, 0.1, 0.5, and 1 w/v % fitted to a polydispersed core-constant shell model. Since the polymer has both hydrophobic and hydrophobic components, the polymer is expected to have a core-shell structure, where the majority of the hydrophobic residues are in the core and the majority of hydrophilic residues are in the shell. All scattering profiles show similar shapes, with slight offsets caused by differences in scaling factor. Similarities in scattering profile shape indicate that the structure of the polymer in solution is not concentration dependent within the evaluated

concentration range. Fits were conducted at high-q in order to decouple the form factor scattering contributions from the structure factor scattering contributions found at low-q. Each fit was done independently from one another.
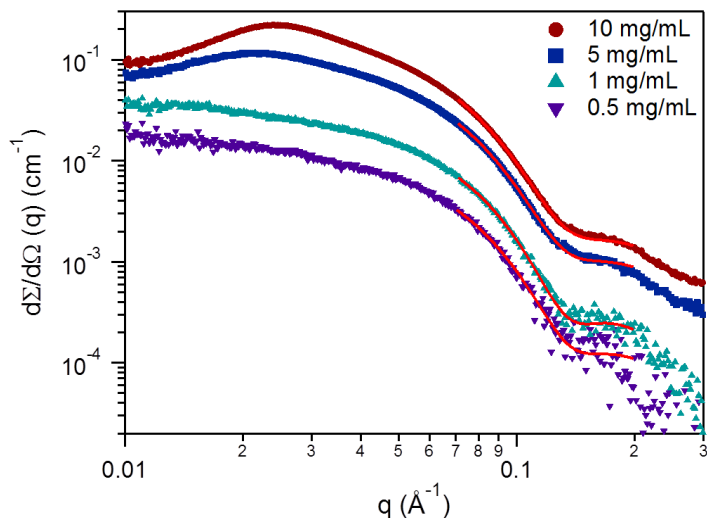
Figure 5.1. SAXS scattering profiles of SRHP-4 in water at different concentrations. Red solid lines represent PolyCore fits.

Table 5.1 summarizes information obtained from SAXS. Both the core radius and shell thickness of SRHP-4 do not change as a function of concentration. The core radius is maintained at 0.7 nm and the shell thickness at 2.5 nm. With the known molecular weight of the polymer, it is assumed that the polymers exist as a unimeric state and do not aggregate at this concentration. The affinity the polymers have with one another is fairly weak. The relative scaling factors used are shown in the fourth column and are good agreement with the changes in concentration. This provides verification that our individual fits are reasonable. At low-q, an autocorrelation peak is observed and becomes more pronounced as concentration is increased. Indexing the peak provides information on the interparticle dispersion distance between SRHP-4. As SRHP-4 concentration is increased, the autocorrelation peak shifts right, indicating a decrease in polymer-to-polymer distance in water.

Table 5.1. Summary of SAXS Results

Concentration (mg/mL)	r_{core} (nm)	t_{shell} (nm)	Scaling Factor	Autocorrelation Peak (nm)
10	0.7	2.5	9.64	25.6
5	0.7	2.5	5.15	28.5
1	0.7	2.5	1	40.9
0.5	0.7	2.5	0.57	—

By graphing interparticle distance as a function of SRHP-4 concentration, it is possible to observe particle interactions. If polymer-to-polymer interactions are not observed within this concentration range, a linear dependence between concentration and interparticle distance should be observed. In Figure 5.2, as concentration increases, an exponential decay that levels off at around 25 nm occurs. This indicates that at distances less than 25 nm, the repulsion force between particles becomes too great and prevents SRHP-4 from getting closer.
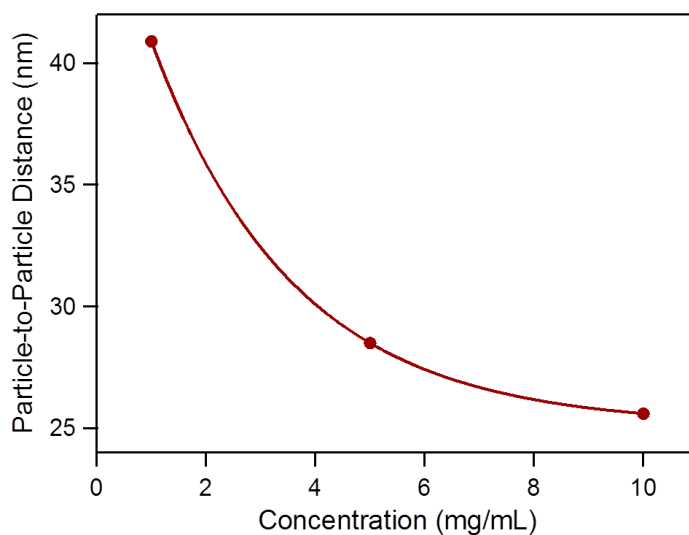
Figure 5.2. Relationship between SRHP-4 concentration and particle-to-particle distance in water.

Interactions between HRP and polymer where evaluated using dynamic light scattering. In Figure 5.3a, histogram distributions of HRP alone, SRHP-4 alone, and both are shown in aqueous solution. If complexation occurs between the two macromolecules, an increase in size should occur. Initially, this was not observed. The sample was then allowed to incubate at room temperature for 1 h (Figure 5.3b), 2 h (Figure 5.3c), and 3 h (Figure 5.3d). The hydrodynamic diameter of the particle did not change within this time range. This indicates that the interaction between the protein and polymer are either nonexistent and do not have an affinity for one another or are short lived and cannot be observed by DLS. Complexation between protein and polymer was also not observed at 70°C (Appendix A.4.1).
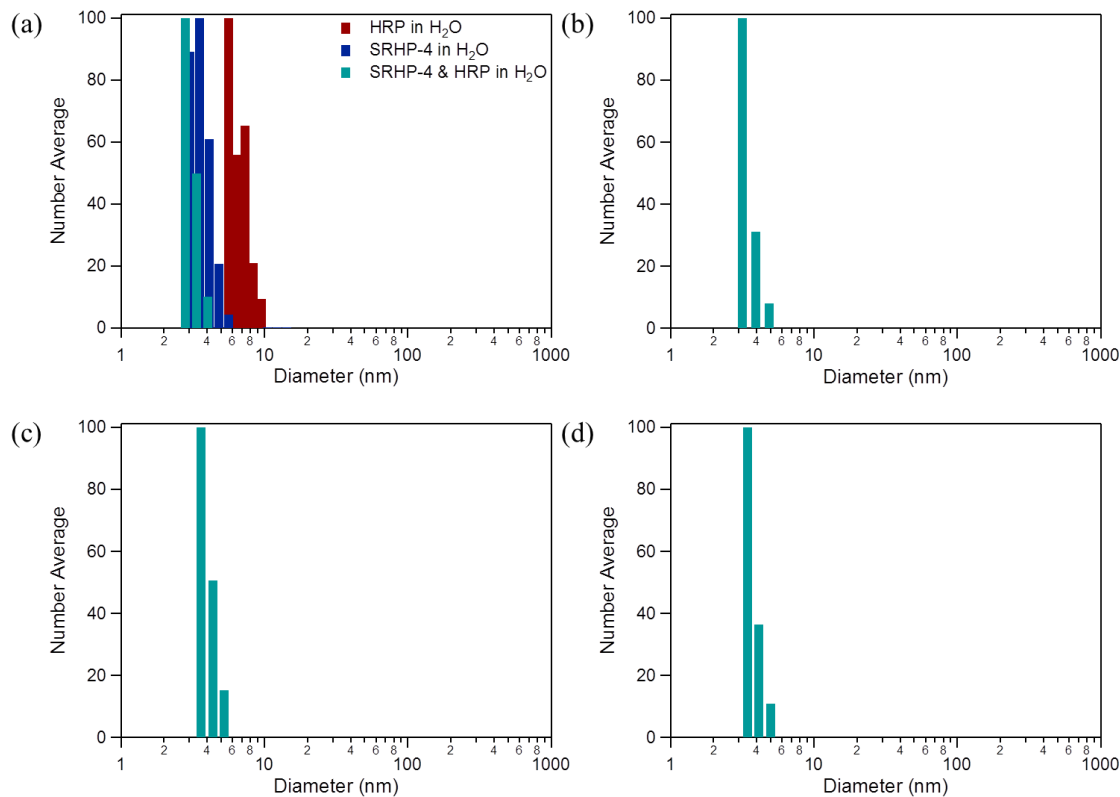
Figure 5.3. DLS histograms of SRHP-4 and HRP in water. (a) SRHP-4 and HRP in water after storage in water for (a) 0 h, (b) 1 h, (c) 2 h, and (d) 3 h at room temperature. DLS distributions of HRP and SRHP-4 alone are overlaid at time 0 h.

In this study, a low polymer concentration and high polymer concentration solution was used to evaluate protein thermal stability as a function of SRHP-4 concentration. Two extremes were chosen – [SRHP-4]:[HRP] molar concentration of 11:1 and 110:1. To further evaluate the presence of complexation, SAXS was employed. Scattering profiles were obtained individually for HRP, 1 mg/mL SRHP-4, and 10 mg/mL SRHP-4 (Figures 5.4(a-b)). In addition, scattering profiles were obtained for a mixed HRP/SRHP-4 solution at the two different SRHP-4 concentrations. It was observed that no complexation occurs after 20-24 h post-sonication. Summation of the two individual scattering profiles – protein and polymer – resulted in replication of the mixed system. This indicates that each scattering profile is independent of one another and that there is no complex formation; proteins and polymers do not hybridize with one another at room temperature in water. If complexation does occur, the scattering profile should change to indicate a new form factor.
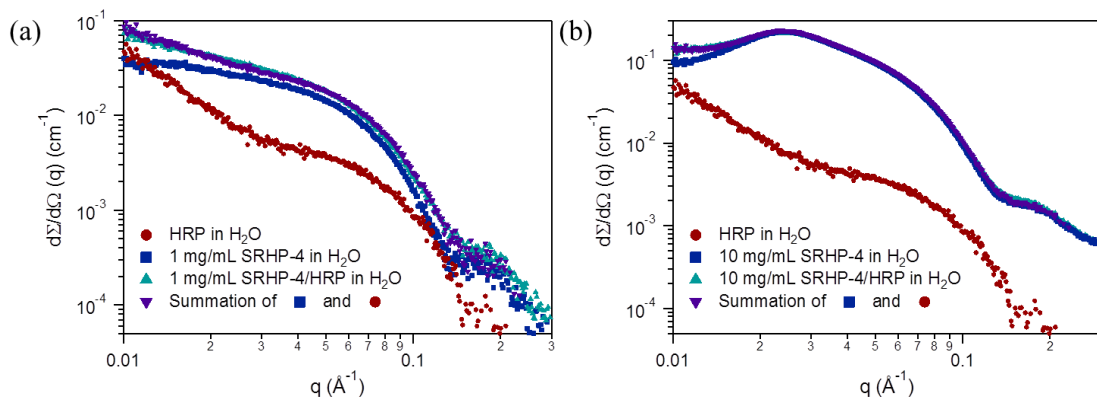
Figure 5.4. SAXS scattering profiles of SRHP-4 and HRP. (a) SRHP-4 to HRP molar ratio of 11:1. (b) SRHP-4 to HRP molar ratio of 110:1.

HRP hierarchical structure was first monitored at room temperature. As a reference, (100 kDa) poly(ethylene oxide) (PEG) was used as a control. Using PEG will allow us to evaluate the effects of having chemical complexity (SRHP-4) and a heterogeneous surface on protein stability. The volume fraction of PEG in solution was kept at percentage between the volume percent of 1 mg/mL and 10 mg/mL SRHP-4 solutions (1 mg/mL SRHP-4 at 0.8 v %, 10 mg/mL at 7.5 v %, 1 mg/mL PEG at 1.5 v %). These values are kept low to eliminate the molecular crowding effect that occurs at higher volume fractions.

Circular dichroism spectroscopy was used to evaluate protein secondary structure. By using circularly polarized light, the amount of α-helix, β-sheets, and turns can be quantified. The difference in absorbance between left- and right-handed circularly polarized light will change depending on the secondary structure composition of HRP. The structure of HRP is primarily helical, as observed by x-ray diffraction.[13] The spectra found in Appendix A.4.2 show a strong the α-helix signal. Over 24 h, the 222 nm is monitored, as it is a characteristic peak for the α-helical 2° structure. At room temperature, PEG provides slight increase in helicity (Figure 5.5a). 1 mg/mL and 10 mg/mL SRHP-4 result in more helical characteristics. Over the span of this test, all samples did not show a reduction in activity, even solutions containing no polymer. More studies must conducted to determine why initial 222 nm signal increases in the presence of polymer. It is not known if the addition of polymers alters secondary structure or if the polymer renatures unfolded proteins found in solution. At 70°C, α-helical characteristic was maintained to a much greater extent in the SRHP-4 solutions over 24 h (Figure 5.5b). It is speculated that the chemical heterogeneity of the random heteropolymer provides HRP with better secondary structure stability than PEG alone.
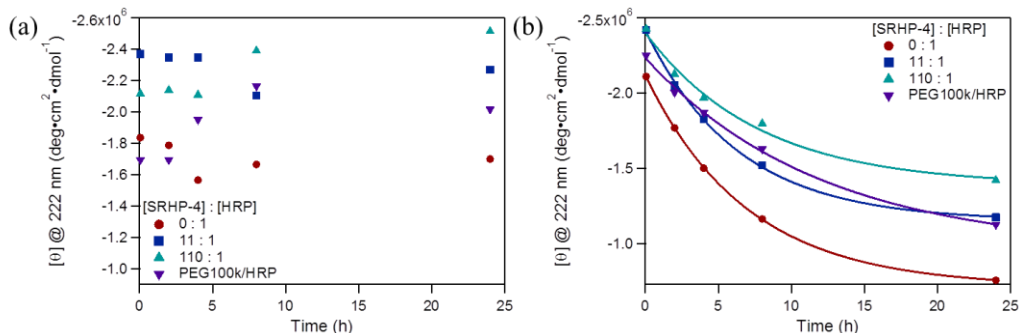
Figure 5.5. CD spectroscopic analysis of HRP hierarchical structure in the presence of SRHP-4 or PEG at (a) room temperature and (b) 70°C.

Fluorescence spectroscopy was used to evaluate protein tertiary structure. By using an excitation wavelength of 280 nm, the change in emission wavelength spectra can be used to monitor the environment of tyrosine, tryptophan, and disulfide bonds within HRP. As the protein unfolds, these amino acids that were once in the core of the protein would become exposed to the solvent. This results in a change in the dielectric constant of the local environment, changing the electronic properties of these chemical bonds. Looking at the spectra in Appendix A.4.3, the intensity appears random. Typically for HRP, as the protein unfolds, the heme which quenches the fluorescence gets removed locally and the fluorescence should increase; however, fluorescence is heavily influenced by temperature, making intensity an unreliable indicator for tertiary structure change. The change in peak position can be monitored instead, as changes in the local environment around the aromatic and disulfide moieties will cause shifts in this peak. Over 24 h at room temperature, no significant change was observed, indicating retention of 3° structure (Figure 5.6a). The peak maxima only changed within a percent of the initial location of the peak. Less peak shift was observed with the inclusion of SRHP-4 in comparison to PEG. At 70°C, HRP in SRHP-4 solutions were stabilized to a much greater extent than proteins in PEG solutions (Figure 5.6b).
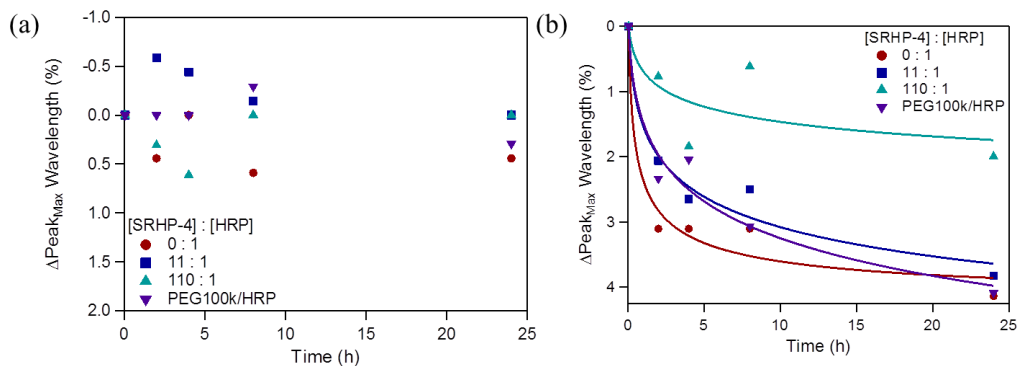
Figure 5.6. Fluorescence spectroscopic analysis of HRP hierarchical structure in the presence of SRHP-4 or PEG at (a) room temperature and (b) 70°C.

As previously discussed in Chapter 4, HRP requires an inorganic cofactor, heme, to be present. UV-visible spectra found in Appendix A.4.4 indicate an absence in peak maximum shift as a function of time, but a change in intensity at 400 nm was observed. By monitoring this wavelength, it is possible to see any changes to the heme molar extinction coefficient. This indicates a change in the local dielectric environment of heme. At room temperature, there was little change over 24 h (Figure 5.7a); however, intensity increased in the presence of SRHP-4 and PEG. It is speculated that the SRHP-4 and PEG may help reform unfolded HRP in solution, but further investigation must be conducted. At elevated temperatures, proteins in a 10 mg/mL solution were stabilized to a much greater extent and protein in a 1 mg/mL solution retained tertiary structure to a higher degree than protein in a solution of PEG.
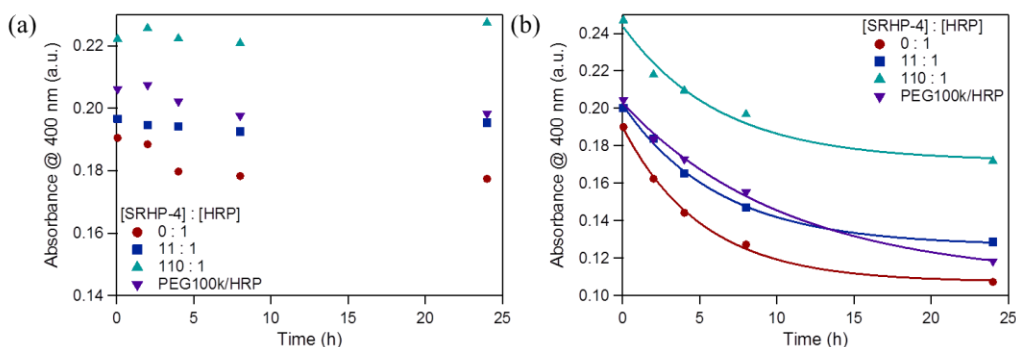
Figure 5.7. UV-visible spectroscopic analysis of HRP hierarchical structure in the presence of SRHP-4 or PEG at (a) room temperature and (b) 70°C.

When all hierarchical levels are preserved, activity is retained. Using the same colorimetric assay discussed in previous chapters, retention of protein activity as a function of time, temperature, and polymer concentration was evaluated. At room temperature, activity did not change over time (Figure 5.8a). A slight increase in activity was observed with addition of polymer. At elevated temperatures, there is a drastic decrease in HRP activity without polymer additives. As SRHP-4 is introduced, protein activity is preserved and is improved to a much greater extent when more SRHP-4 is introduced. PEG, which provides great initial activity retention, decays at a much more drastic rate (Figure 5.8b).
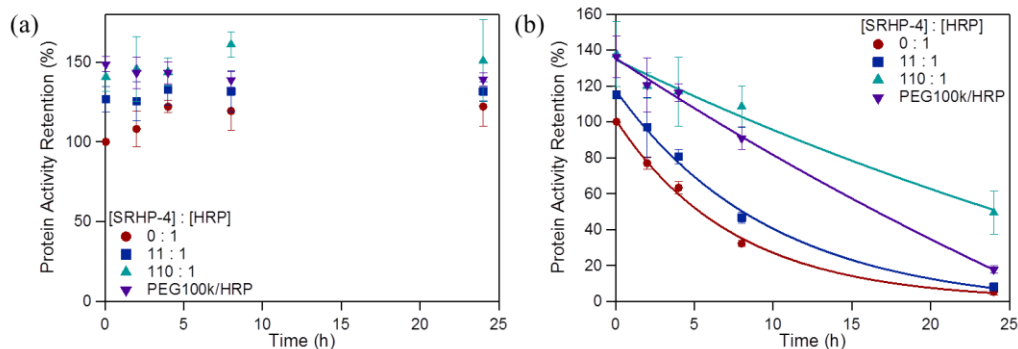
Figure 5.8. Colorimetric assay analyses of HRP function in the presence of SRHP-4 at (a) room temperature and (b) 70°C.

Typically, additives are included to slow down the motion of the system or crowd proteins to restrict conformational change. However, volume percent of polymers used in these solutions are kept to a minimum. This indicates that SRHP-4 does not act as a molecular crowder but participate in interactions that prevent protein denaturation. In addition, this interaction is short-lived, as indicated by the structural tests performed; there is no complex formation. We speculate that the statistically random heteropolymers provide a heterogeneous surface that provides proteins with an environment to fold back to their native state when partially unfolded. By increasing the amount of SRHP-4, the probability of finding a chemically patchy surface is increased. When no polymer is added, unfolded proteins find other unfolded proteins and undergo irreversible aggregation, resulting in activity loss.

Unlike samples in water, SRHP-4/HRP lyophilized complexes in toluene provide nanoscopic confinement for HRP. This nanoconfinement provides an enclosed space that restricts conformational change and provides a driving force for retaining native structure.[14] This is seen in Figure 5.9. Proteins both encapsulated in (SRHP-4)-based complexes and AOT-based reverse micelles both exhibit higher protein activity after 24 h in comparison to proteins in aqueous media at 70°C. Proteins in SRHP-4 complexes seem to be more conformationally restricted; the protein-polymer network found in lyophilized complexes may provide more confinement in comparison to a fluid reverse micelle structure.

In addition, when temperature is increased, the subunit exchange of surfactants typically increases,[15] thus leading to solvent penetration. To see this effect, AOT was used as a benchmark. In the case of AOT, a drastic drop in activity retention was observed, whereas HRP encapsulated in SRHP-4 was able to retain around 50% of its initial activity at 70°C. This information reveals that SRHP-4 possibly has a higher complex affinity than small molecule surfactants in organic solvent. The multivalent interaction that SRHP-4 polymers exhibit prevents long range diffusion of the surfactant and reduces SRHP-4 desorption from the complex. Further investigation must be conducted to decouple the effects of nanocaonfinement and impeded micelle dynamics.
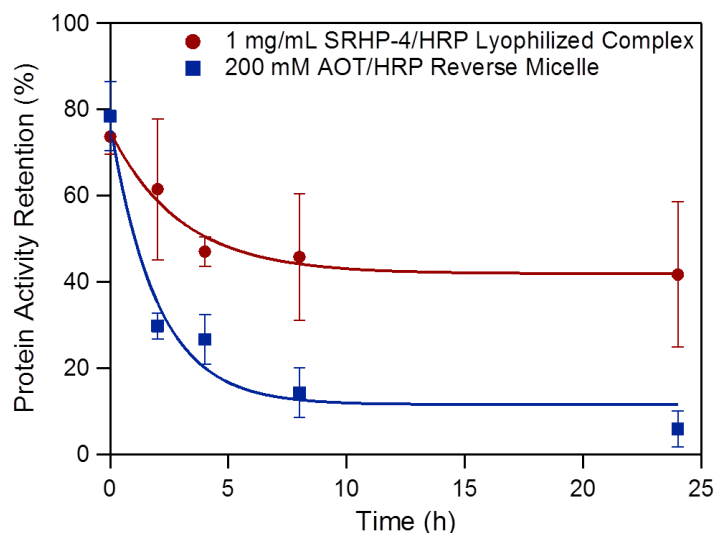
Figure 5.9. Activity of HRP after storage in organic solvent using SRHP-4 or AOT surfactant and dispersed in aqueous buffer. Samples were stored at 70°C.

§ 5.3. Conclusion

There are many advantages associated with SRHPs. Not only do they encapsulate, solubilize, and stabilize proteins in organic solvents but can also stabilize proteins at elevated temperatures (70°C) in both water and organic media. This provides routes that can benefit both the field of material processing and nanoreactors. By increasing temperature, proteins can be introduced into polymer melts, for example, or be incorporated in a catalytic reaction where temperature can increase the rate of reaction. Although PEG can be used as a commercially available substitute for thermal stability, the chemical heterogeneity of SRHP-4 produces far greater stability without the need for high polymer concentrations. High polymer concentrations are needed for molecular crowding, which may not be cost-effective route toward protein stabilization in industry. In addition, the use of heat in organic solvents allowed us to monitor micelle dynamics. Proof that the interaction per SRHP-4 surfactant has a greater binding affinity than the interaction per AOT small molecule surfactant was obtained.

§ 5.4. Experimental Section

5.4.1. Materials

Horseradish peroxidase type II (HRP), 2-bis(hexylethyl) sulfosuccinate (AOT), and (100 kDa) poly(ethylene oxide) (PEO) were obtained from Sigma Aldrich. TMB Peroxidase EIA Substrate Kit was obtained from Bio-Rad Laboratories. Toluene was obtained from Fisher Scientific, and Milli-Q water was obtained from EMD Millipore.

All other materials were used as received. SRHP-4 was synthesized as previously reported in Chapter 3.

5.4.2. Preparation of SRHP-4/HRP Solutions

For aqueous solutions composed of SRHP-4 and HRP, SRHP-4 was dissolved in DI water at a concentration of 0.1 w/v % or 1 w/v % and HRP was dissolved in DI water at a concentration of 1 w/v %. Aqueous SRHP-4 solution was combined and sonicated with HRP solution at a volumetric ratio of 50:1. For aqueous solutions composed of PEO and HRP, PEO was dissolved in DI water at a concentration of 0.1 w/v %. Aqueous PEO solution was combined and sonicated with HRP solution at a volumetric ratio of 50:1.

For SRHP-4/HRP lyophilized complexes, SRHP-4 was dissolved separately in DI water at a concentration of 0.1 w/v % and HRP was dissolved in DI water to a concentration of 1 w/v %. Aqueous SRHP-4 solution was combined and sonicated with HRP solution at a volumetric ratio of 50:1. SRHP-4/HRP mixtures were lyophilized overnight, resuspended with toluene to the original concentration, and subsequently sonicated. For AOT/HRP reverse micelles, AOT was dissolved in toluene at a concentration of 200 mM. HRP was individually dissolved in DI water to a concentration of 2 w/v %. Injection emulsion was used to create AOT-HRP reverse micelles. The suspension was sonicated, mixed, and partially evaporated using a constant stream of N_2 gas until optically clear. Additional toluene was added to compensate for evaporated solvent in order to reestablish the original concentration.

5.4.3. Small Angle X-Ray Scattering

SAXS experiments were carried out at the Advanced Light Source (ALS) at the Lawrence Berkeley National Lab (LBNL), Berkeley, California at the SAXS/WAXS/GISAXS beamline 7.3.3. The instrument was operated using an x-ray energy of 10 keV. Measurements were done at a sample-to-detector distance of 1.8 m. A 2 M Pilatus detector was used to obtain scattering profiles. Samples were contained in standard boron-quartz capillaries situated in a customized sample holder which permitted the sample to be filled and removed using a syringe. This setup allowed for quantitative background subtraction of both the capillary and the solvent. Absolute intensity calibration was performed using toluene. The capillary thickness was 1.6 mm. Scattering length densities were taken to be the following: $\rho = 9.5 \times 10^{-6}$ $Å^{-2}$ for H_2O, $\rho \sim 9.2 \times 10^{-6}$ $Å^{-2}$ for SRHP-4. Polydisperse Core with Constant Shell Thickness[16] was used to determine SRHP-4 morphology in water as a function of concentration.

5.4.4. Dynamic Light Scattering

Size distributions of aqueous SRHP-4/HRP solutions were measured using a Brookhaven Instruments BI-200SM Research Goniometer and Laser Light Scattering

System. Temperature was controlled and set at 25°C. Measurements were sorted by number average and a NNLS function was used to analyze the correlation curves.

5.4.5. Circular Dichroism

SRHP-4/HRP aqueous solutions were stored at room temperature or in an oven at 70°C. Samples were allowed to equilibrate back to room temperature. Circular dichroism measurements were taken 0, 2, 4, 8, or 24 h after sonication of solutions on a Jasco J-815 Spectropolarimeter. Solutions were sealed in a 1-mm path length quartz cuvette and ellipticity was monitored between 190 nm and 250 nm. Background subtractions were performed post-measurements using an SRHP-4 solution with the corresponding concentration. Measurements were conducted at 20°C.

5.4.6. Fluorescence Spectroscopy

Retention of HRP tertiary structure was evaluated using a Perkin Elmer LS-55 fluorescence spectrometer. SRHP-4/HRP aqueous solutions were stored at room temperature or in an oven at 70°C. Samples were allowed to equilibrate back to room temperature. Measurements were taken 0, 2, 4, 8, or 24 h after sonication of solutions. Solutions were sealed in a 1-cm path length quartz cuvette and excited at an excitation wavelength of 280 nm. Emission wavelength was monitored between 310 nm and 400 nm. Measurements were conducted at room temperature.

5.4.7. Heme Analysis using UV-Visible Spectroscopy

SRHP-4/HRP aqueous solutions were stored at room temperature or in an oven at 70°C. Samples were sealed in a 1-cm path length quartz cuvette. Samples were allowed to equilibrate back to room temperature. UV-visible spectroscopy was performed on a Hewlett-Packard 8453 Spectrophotometer. Measurements were conducted at room temperature and the location of the heme peak as well as the intensity of this peak were monitored between 270 nm and 450 nm at 0, 2, 4, 8, and 24 hours after sonication

5.4.8. Assay of Protein Activity in Aqueous Buffer or Organic Solvent

HRP activity was assessed using a TMB Peroxidase EIA Substrate Kit (Bio-Rad). Baseline HRP activity was determined by preparing a stock protein solution in 100 mM KH_2PO_4/K_2HPO_4 phosphate buffer at pH 6 and applying a prepared TMB assay solution, as outlined by the manufacturer. Solution was thoroughly mixed and UV-visible spectroscopy was performed on a Hewlett-Packard 8453 Spectrophotometer. A 1-cm path length cuvette was used and absorbance at 370 nm was monitored.

$$\text{(structure: } H_3C, CH_3 \text{ substituted diaminobiphenyl)} + H_2O_2 \xrightarrow{\text{HRP}} \text{(oxidized quinone diimine structure)} + 2\,H_2O \tag{3.5}$$
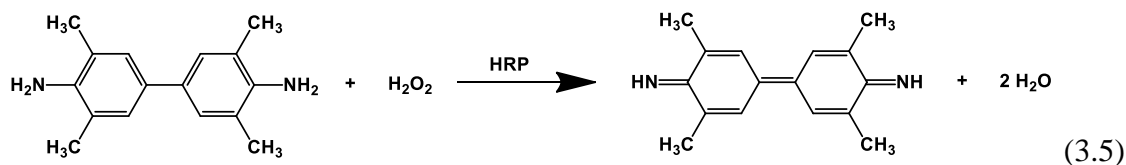
SRHP-4/HRP, PEG/HRP, or AOT/HRP solutions were left at ambient room or elevated temperature conditions for 0, 2, 4, 8, and 24 hours in DI water or toluene. After specified times, aliquots were taken and diluted in 100 mM KH_2PO_4/K_2HPO_4 phosphate buffer, pH 6, to disperse the protein and SRHP-4. After thorough mixing, the assay solution is applied. Activity was quantified using UV-visible spectroscopy by monitoring the conversion of the colorimetric assay.

Chapter 6

Generating Protein-Based Nanoassemblies via Rationally Designed Statistically Random Heteropolymers

Protein-functionalized materials with persistent nanoscale ordering can improve a variety of applications. A combination of protein and block copolymer offers a bottom-up approach toward materials with unique and specific functionality coupled with controlled nano-patterned assemblies. In this chapter, I will report on the co-processing of horseradish peroxidase-containing reverse micelles and block copolymers in organic media. Statistically random heteropolymers were used to first encapsulate proteins, providing a vessel for increased processability, enhanced retention of protein activity, and a modular platform to tune protein-block copolymer interactions in organic solvent. Subsequently, reverse micelles are co-assembled with poly(styrene)-block-poly(ethylene oxide) and spin-cast into block copolymer thin films. Sequestration of proteins into one of the domains was observed, and protein functionality was retained throughout the fabrication process.

§ 6.1. Introduction

Nanostructured materials exhibiting biofunctionality over defined, controllable length-scales can improve a variety of technological sectors. This may include catalysis,[1] sensors,[2] molecular transport,[3] energy,[4] and medical therapeutics.[5] Synergistic integration of protein and synthetic block copolymer (BCP) is of particular interest. There is a preexisting library of proteins rich in chemical, structural, and functional diversity, where each individual protein possesses an unmatched level of specificity and efficiency.[6] Synthetic biomimetic reproductions have generally not been able to replicate the same level of performance proteins possess, such as those involved in photosynthesis.[7] Block copolymers, alternatively, have the capacity to form well-defined nanoscale morphologies with long range ordering.[8] They are highly robust and processable and have a diverse set of tunable properties (e.g. glass transition temperature, hydrophobicity, degradability, mechanical strength). Rather than developing fully synthetic biomaterials, combining proteins and block copolymers, which have proved to be valuable on their own scientific merits, may provide even greater utility in tandem.

However, it remains a significant challenge to produce protein-based functional materials without compromising protein structure and accordingly, protein activity. Proteins have a narrow window of conditions where they remain functional. Specific temperatures, pH, salt concentrations, and solvent polarities are needed to provide the necessary intra- and intermolecular interactions that govern native protein conformation. Consequently, polymers require their own set of conditions that may prove to be incompatible with protein activity preservation. By limiting the media to strictly water – a condition generally required for protein solubilization and stability – the type of polymers and applications that can be accessed becomes greatly restricted. Protein processability in organic solvents would increase the breadth of obtainable materials.

Co-assembly of block copolymers and proteins in organic solvents provides a bottom-up approach that benefit from enhanced processability, increased protein loading, and the ability to incorporate proteins with greater hierarchical complexities.[9, 10] In addition, block copolymer-based nanocomposites can be fabricated into various macroscopic structures. These structures include thin films, bulk gels, nanofibers, and colloidal particles. Depending on the type of application, the chemistry, microstructure, and macrostructure of the block copolymer composite can be tailored to obtain the most desirable performance.

The main limitation, however, is the ability to find processing conditions that facilitate block copolymer microphase separation and protein solubility and stability. Solubilizing and stabilizing proteins in organic solvents can be achieved using small molecule surfactants[11-14] or through PEGylation,[9] as discussed in Chapter 2. These methods have been shown to facilitate further material processing. Small molecule surfactants, however, are dynamic and lend themselves to protein denaturation. PEGylation requires specific chemistries to be present on the protein surface. In addition, the chemical tunability of both small molecule surfactants and polymer conjugation is limited, contributing to potential conflicts between protein-solvent-block copolymer interactions during processing.

Statistically random heteropolymers (SRHPs) provide a modular platform for protein solubilization, stabilization, and processability. Their amphiphilic nature and ability to multivalently hybridize with the protein's surface enables protein usability in organic solvents. Furthermore, SRHP amphiphilicity and its interaction with the environment can be tuned through modulation of its monomer selection and monomer ratio. Monomers can be chosen to interact favorably with one domain of the block copolymer and unfavorably with the other.

In this chapter, I will report the use of SRHP-4/HRP reverse micelles to increase the breadth of conceivable hybrid materials, facilitating compatibility between proteins and block copolymers. We demonstrate that SRHP-4 can encapsulate proteins in spherical reverse micelles, a vessel for enhanced solubility, stability, and processability in organic solvents. These SRHP-4/HRP reverse micelles are then co-assembled with block copolymers during thin film spin-casting. Proteins remain active and functional throughout the entire process, block copolymer microphase separation remains unhindered, and proteins are nanoscopically arranged in controllable hierarchical structures. The next step involves incorporation of proteins into BCP electrospun fibers.

§ 6.2. Results and Discussion

Injection emulsion induces encapsulation of HRP in (SRHP-4)-based reverse micelles, as stated in Chapter 3. These reverse micelles appear spherical under TEM with a bimodal diameter distribution centering around 20 nm and 50 nm. The 20 nm size arises

from free polymer and the 50 nm size arises from SRHP-4/HRP reverse micelles. Co-solubilization of SRHP-4/HRP reverse micelles and poly(styrene)-*block*-poly(ethylene oxide) (PS-*b*-PEO) block copolymer in toluene resulted in no disruption of SRHP-4/HRP reverse micelles prior to spin-casting. Intensity average was used for dynamic light scattering (DLS) size distribution analysis, as seen in Figure 6.1. Mixtures of SRHP-4/HRP reverse micelles and PS-*b*-PEO resulted in shifts of the 200 nm and 1500 nm peaks of the BCP solution. Scattering contributions from the SRHP-4/HRP reverse micelles can account for this deviation to lower sizes; the peak is influenced by scattering contributions from the BCP as well as the SRHP-4/HRP reverse micelles.
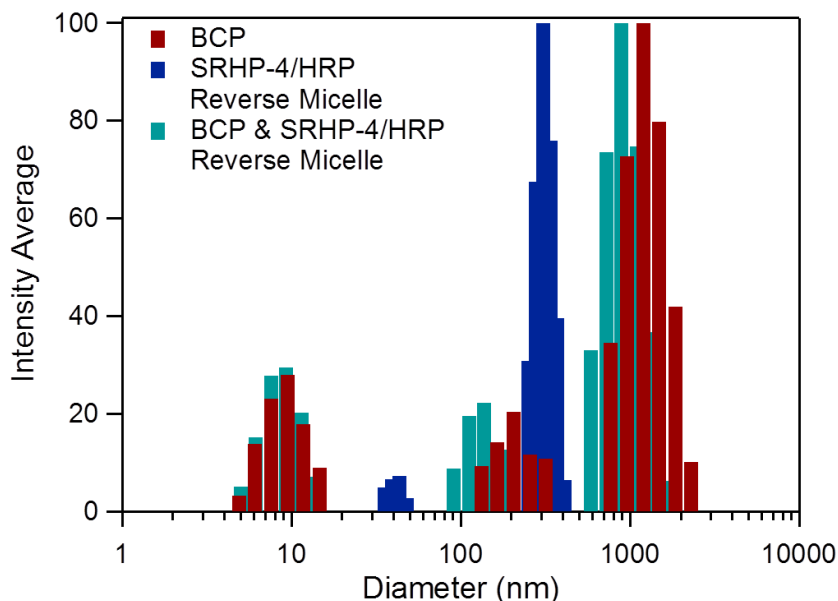
Figure 6.1. Intensity-averaged DLS histogram of PS-*b*-PEO and SRHP-4/HRP reverse micelle solution prior to spin-casting.

The chemical synergy of the system allows us to direct the assembly of proteins into nanoscale patterns. The Flory-Huggins parameter, χ, between PS and PEO is high, providing us with well-ordered nanostructures through microphase separation. SRHP-4 is primarily composed of PMMA and PEO chains, chemical moieties that are miscible in PEO and not in PS. The χ between PMMA and PEO is around -0.005 to -0.001 and the χ between PMMA and PS is around 0.08. Because of this, we believe that the SRHP-4/HRP reverse micelle will be directed into the PEO domain of the block copolymer thin film. This is summarized in Scheme 6.1, where the red-depicted statistically random heteropolymer is complementary to the red-depicted PEO domain of the block copolymer hybrid material.
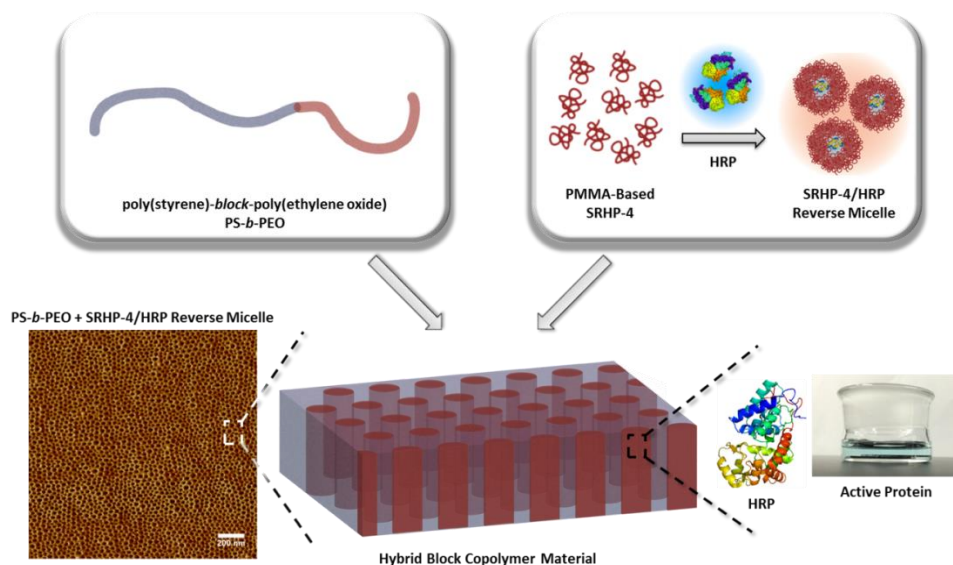
Scheme 6.1. Summary of hybrid block copolymer materials via co-assembly of block copolymer and SRHP-4/HRP reverse micelles. AFM is used to evaluate morphology, and chromophoric assays are used to evaluate protein activity.

After spin-casting, atomic force microscopy (AFM) was used to evaluate the as cast protein-BCP composite thin films. The phase image (Figure 6.2a) shows cylindrical PEO domains, where the softer PEO domains are depicted black and the higher modulus PS are depicted tan. The image shows some of the PEO domains appearing tan. It is speculated that SRHP-4/HRP reverse micelles were incorporated into the PEO domain and the packing of extra material accounts for the increase in modulus. The height image (Figure 6.2b) reveals a slight increase in height at the center of the cylindrical PEO domains. This further suggests that SRHP-4/HRP reverse micelles were sequestered by PEO during the spin-casting process.
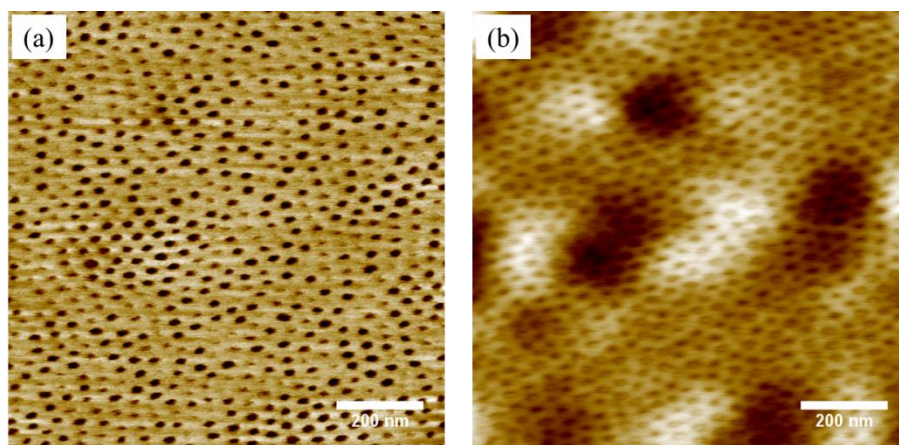
Figure 6.2. AFM images of an as cast thin film composed of PS-*b*-PEO and SRHP-4/HRP reverse micelles (a) Phase and (b) height images of block copolymer-protein hybrid thin film prior to solvent annealing.

95

Solvent annealing was used to increase the order in block copolymer thin films. Pre-swelling with water allowed for selective annealing of the PEO domain, and subsequent co-solvent annealing with water and benzene provided mobility for the entire BCP thin film.[15] After annealing, PS-*b*-PEO (Figure 6.3a) and PS-*b*-PEO thin films containing SRHP-4 (Figure 6.3b) and SRHP-4/HRP reverse micelles (Figure 6.4c) all showed ordered films with perpendicular PEO cylindrical domains. BCP alone showed an average PEO domain diameter of 23.7 nm (Figure 6.3d). Slight increase in average PEO domain diameter was observed upon inclusion of SRHP-4 to 31.2 nm (Figure 6.3e). Significant average PEO domain diameter was observed upon incorporation of SRHP-4/HRP reverse micelles to 40.6 nm (Figure 6.3f). The addition of proteins is speculated to cause an increase in PEO domain size as a way to accommodate for the extra material. Although the average size increased, the incorporation of SRHP-4 increased the frequency of PEO domain sizes that are 19 nm. This collapse in some of the PEO domain was unusual and further investigation must be conducted. One possible theory on this occurrence is that the PMMA mediates the interactions that occur at the interface.
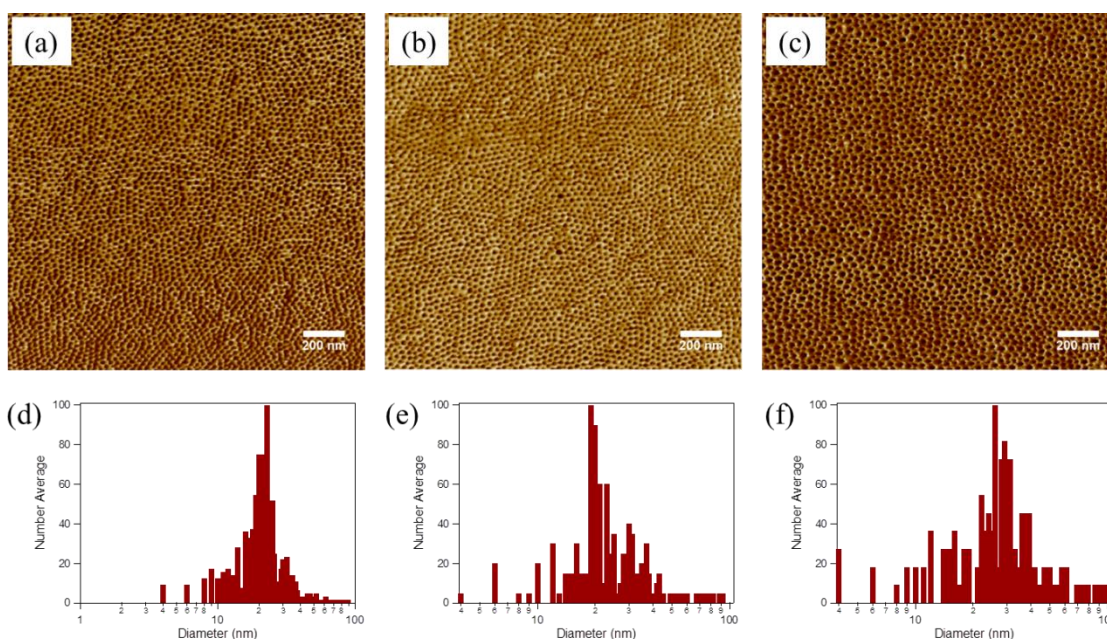
Figure 6.3. AFM phase images of solvent annealed thin films of (a) PS-*b*-PEO, (b) PS-*b*-PEO with SRHP-4, and (c) PS-*b*-PEO with SRHP-4/HRP reverse micelles. Image analysis of PEO domain diameters of (d) PS-*b*-PEO, (e) PS-*b*-PEO with SRHP-4, and (f) PS-*b*-PEO with SRHP-4/HRP reverse micelles.

Grazing-incidence small angle x-ray scattering (GISAXS) was used to determine changes in periodicity upon incorporation of SRHP-4 and SRHP-4/HRP reverse micelles. Two-dimensional scattering profiles for each thin film can be found in Figures 6.4(a-c). Taking q_x line cuts, it was observed that the structure factor peak shifts to lower q as

SRHP-4 is added, and lowered further after addition of SRHP-4/HRP reverse micelles (Figure 6.4d). This indicated an increase in periodicity. The natural periodicity of this block copolymer system is 31 nm. Addition of SRHP-4 increased the periodicity to 33 nm, and addition of SRHP-4/HRP reverse micelles increased the periodicity to 39 nm. The ratio between the first order peak and second order peak in all three samples is 1:√3, verifying that these PEO cylinders are hexagonally packed and perpendicular to the substrate.
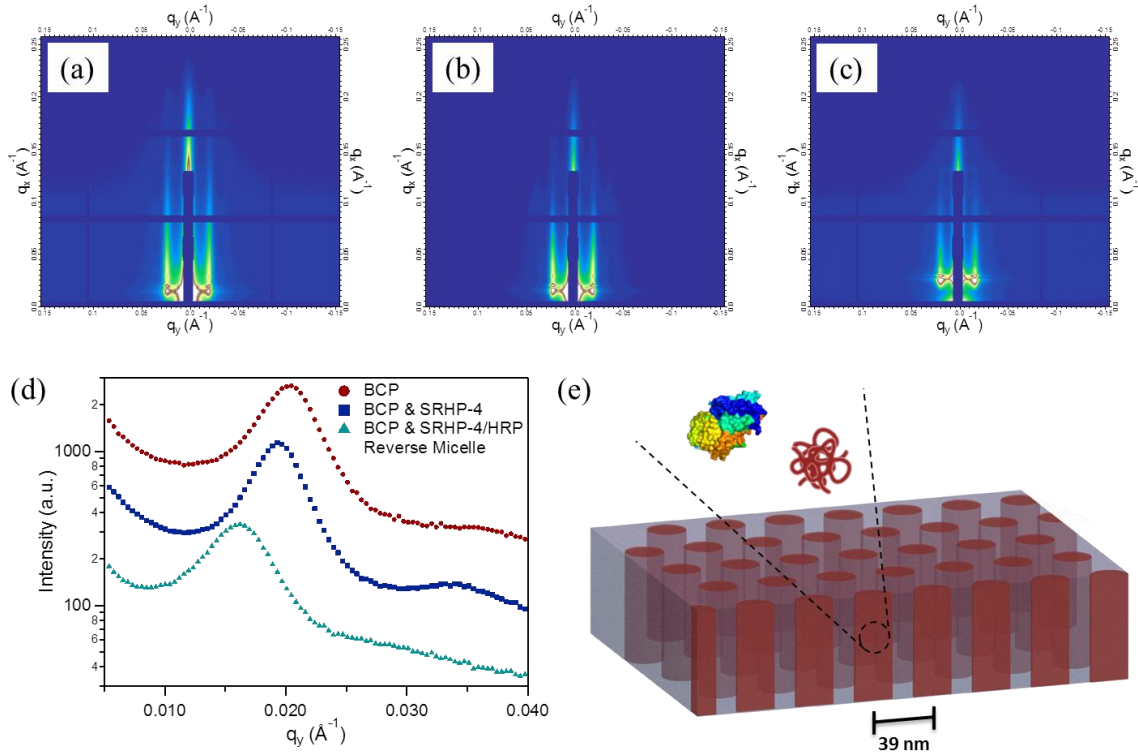
Figure 6.4. GISAXS scattering profiles of solvent annealed thin films of (a) PS-*b*-PEO, (b) PS-*b*-PEO with SRHP-4, and (c) PS-*b*-PEO with SRHP-4/HRP reverse micelles. (d) GISAXS q_x line cuts. (e) Schematic of block copolymer thin film with locations of HRP and SRHP-4.

Increase in periodicity and increase in domain size suggest directed assembly of HRP into the PEO domains. As previously stated however, SRHP-4/HRP reverse micelles have a diameter of around 50 nm. In order to accommodate for this material into a PEO domain with a diameter of 40.6 nm, there must be a disassembly of the reverse micelle. It is hypothesized that during annealing, the SRHP-4/HRP reverse micelle is disrupted and reside in the PEO domains as smaller complexes or as individual components. This may explain why after annealing, the phase discrepancies observed in as cast films were no longer present. Within the PEO domain, the driving force for reverse micelle stability – the interface between two immiscible media – is no longer present. SRHP-4 and its cargo both have favorable interactions with PEO, resulting in the

disruption of the reverse micelle. Figure 6.4e is a schematic that illustrates this hypothesis, where both HRP and SRHP-4 are sequestered into the PEO domain; however, they exist as individual components.

In order to directly verify directed assembly of proteins into the PEO domain, resonant soft x-ray scattering (RSoXS) was attempted. This technique allows us to change the x-ray energy in order to enhance the contrast for specific elements. Targeting the nitrogen-edge would allow us to see the periodicity of HRP since SRHP-4 and PS-*b*-PEO do not contain nitrogen. However, RSoXS did not reveal information on the protein arrangement, as shown in Appendix A.5.1. HRP loading may not be high enough. Not all PEO cylinders contained a sufficient amount of protein. This would result in a lack of lateral auto correlation of the nitrogen signal.

Retention of HRP activity post-annealing was evaluated using a colorimetric assay of H_2O_2 and 3,3',5,5'-tetramethylbenzidine (TMB). The conversion of TMB into its diimine species indicates retention of HRP activity, which can be visually observed by the appearance of a blue chromophore in solution. Upon submergence of HRP-containing thin films in a phosphate buffered solution containing the assay, the appearance of the blue tint after 30 min at room temperature verified active HRP (Figure 6.5).

Figure 6.5. Photo of solution containing colorimetric assay in buffer after submergence of an HRP-containing hybrid thin film.

Over the course of processing HRP into block copolymer thin films, from encapsulation into (SRHP-4)-based reverse micelles, to mixing with a BCP solution, to spin-casting, HRP is able to retain 50% of its original activity (Figure 6.6). Data was normalized by HRP concentration, where HRP concentration in the film was calculated by assuming a film density similar to the density of the PS-*b*-PEO (~1 g/mL) and measuring the dimensions of the film to determine film volume (1.7 cm × 1.7 cm × 31 nm). However, after solvent annealing, protein activity retention drops significantly, down to 5%. The disassembly of the complex is speculated to be the cause for drastic protein denaturation during solvent annealing. As there is no longer a protective barrier around the protein, benzene is allowed to interact with the protein and cause a reduction in protein activity. Future systems are currently under investigation where protein-polymer complexes are kept intact during the entire processing procedure.
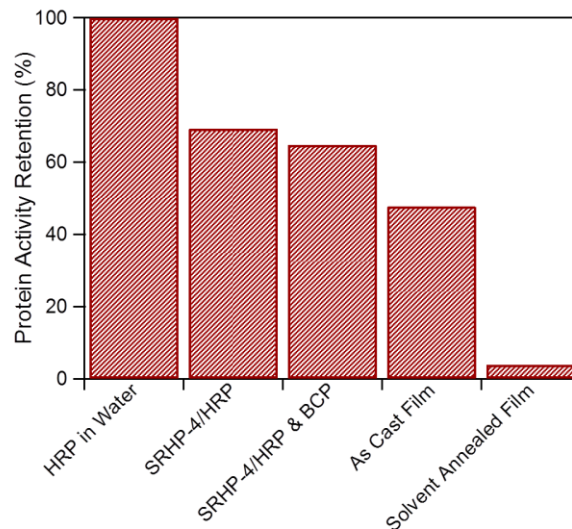
Figure 6.6. Activity of HRP during the film casting process.

When proteins were stored in block copolymer thin films, activity was drastically diminished when stored at room temperature after 1 h. This was unusual since the block copolymer is in solid form. However, when SRHP-4/HRP reverse micelles were directly spin-cast onto a silicon wafer without the BCP, HRP was able to retain about 70% of its activity after 2 weeks when stored at ambient conditions, as seen in Figure 6.7. SRHP-4 was able to provide HRP with a confined environment that allowed HRP to retain activity after 2 weeks. When co-processed with PS-*b*-PEO, this ability is compromised. The PEO domain may be too fluid. In addition, it is speculated that the interface between PS and PEO may be the origin of this quick denaturation phenomenon. More studies must be conducted to investigate the mechanism that is occurring to optimize this bottom-up approach toward protein patterning.
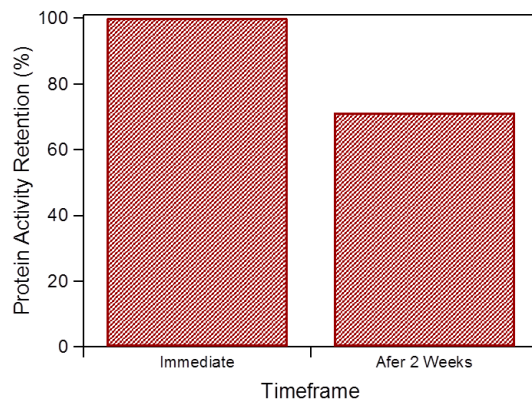
Figure 6.7. Activity of HRP after spin-casting of SRHP-4/HRP reverse micelles directly onto a silicon wafer. Activity was evaluated immediately after spin-casting and after 2 weeks at room temperature. Protein activity is normalized by protein concentration.

With this enhanced processability, electrospinning was employed in an attempt to develop protein-based fiber materials from organic media. Because electrospinning generates fibers with extremely large surface area-to-volume ratios, electrospinning is a desirable technique for fabricating catalytic fiber mats. SRHP-4/HRP complexes were mixed with poly(methyl methacrylate) (PMMA). PMMA was chosen because it is wettable yet still hydrophobic enough to retain its structural integrity in water. In addition, PMMA is chemically compatible with SRHP-4. Hybrid electrospun fiber mats with loaded SRHP-4/HRP lyophilized complexes were successfully fabricated, as seen in Figure 6.7(a-b), and exhibited excellent activity in aqueous buffer solution, as verified by the conversion of a blue chromophoric assay (Figure 6.7c). As PMMA is hydrophobic, electrospun fiber mats are expected to repel water without inhibiting assay transport. This is schematically portrayed in Figure 6.7d. The next step is to exchange PMMA with either poly(styrene)-*block*-poly(ethylene oxide) or poly(styrene)-*block*-poly(methyl methacrylate) as a way to generate electrospun fibers with internal nanoscale ordering.
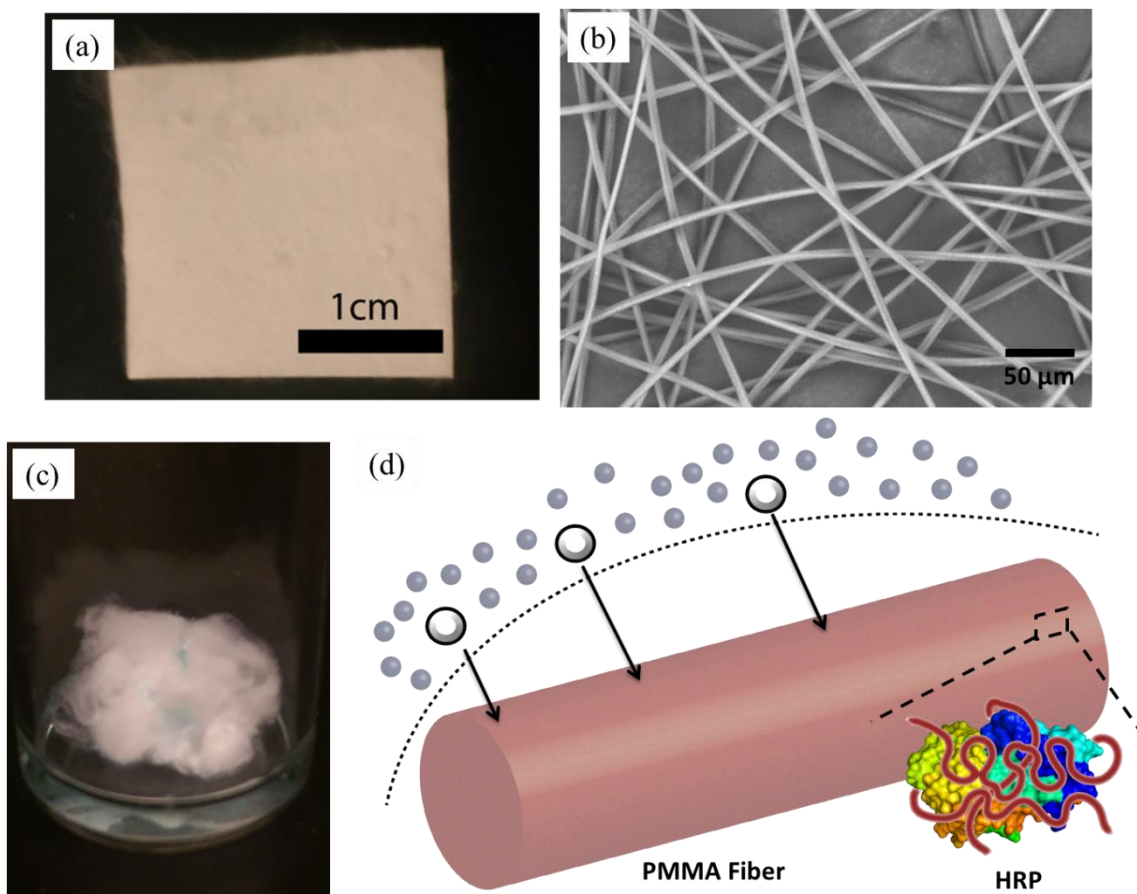
Figure 6.8. Processing of proteins using SRHP-4. (a) Electrospun PMMA fiber mat. (b) SEM image of electrospun PMMA fibers containing SRHP-4/HRP complexes. (c) Verification of HRP activity and accessibility in electrospun fiber mat using colorimetric

assays. (d) Schematic of HRP-containing fibers where substrates are permeable but water is excluded out.

§ 6.3. Conclusion

The combination of SRHPs and BCPs hold great promise in providing a general approach toward nanostructured protein-based materials. SRHPs allow for water-soluble proteins to disperse in organic solvents in nano-sized vehicles. They preserve protein functionality during the fabrication of these nanocomposites to a significantly high degree. Lastly, the ability to modulate SRHP chemistry allows for manipulation and fine tuning of protein-block copolymer interactions. BCPs, on the other hand, provide a good platform for protein nanoassemblies in complex, hierarchical, three dimensional structures. Their ability to arrange proteins in very precise patterns with very minimal human interference provides a processable and scalable technique for future technological advancements. Future directions include incorporation of other proteins, as seen in Appendix A.5.2. Incorporation of insulin into synthetic materials will allow us to store protein therapeutic at room temperature and create biodegradable patches. Computationally designed three helix bundles[16] can be used to create two dimensional arrays with hierarchically-decorated surfaces using high temperatures.

§ 6.4. Experimental Section

6.4.1. Materials

Horseradish peroxidase type II (HRP), phosphotungstic acid, and poly(methyl methacrylate) (PMMA) (MW = 350,000 Da) were obtained from Sigma Aldrich. were obtained from Sigma Aldrich. TMB Peroxidase EIA Substrate Kit was obtained from Bio-Rad Laboratories. (23 kDa) poly(styrene)-block-(7 kDa) poly(ethylene oxide) (PS-b-PEO) was obtained from Polymer Source with a PDI of 1.07. Toluene and benzene were obtained from Fisher Scientific, and Milli-Q DI water was obtained from EMD Millipore. TEM carbon grids were obtained from Ted Pella. Silicon wafers were obtained from International Wafer Service. All materials were used as received. SRHP-4 was synthesized as reported in Chapter 3.

6.4.2. Assembly of Protein-Containing Reverse Micelles

SRHP-4 was dissolved in toluene at a concentration of 0.1 w/v % and HRP was dissolved in DI water to a concentration of 1 w/v %. Injection emulsion was used to create SRHP-4/HRP reverse micelles, where the resultant solution contained a volumetric ratio of 50:1 SRHP-4 solution to HRP solution. The suspension was sonicated, mixed, and partially evaporated using a constant stream of N_2 gas until optically clear.

Additional toluene was added to compensate for evaporated solvent in order to reestablish the original concentration.

6.4.3. Fabrication of HRP-Containing Thin Films

Prior to spin casting, SRHP-4/HRP reverse micelles were co-solubilized with a solution containing 1 w/v % PS-*b*-PEO. The final spin casting solution was 0.002 wt % HRP. Two other solutions were created as controls: PS-*b*-PEO only, PS-*b*-PEO with SRHP-4. These samples were prepared to possess similar concentrations to the HRP-containing solution. Solutions were spin-cast for 20 s at 3000 RPM onto a silicon wafer. Film thickness was assessed using a Filmetrics F20 interferometer and ranged between 30-40 nm.

Samples were solvent annealed using a mixture of water and benzene. Samples were placed in a 2.6-L cylindrical aluminum chamber equipped with an O-ring-sealed lid. Samples were pre-swelled with water (6 mL) for 2 hrs. Benzene (6 mL) was then added to the chamber, where the samples continued to anneal for 2 hrs.

Formation of SRHP-4/HRP thin films, SRHP-4/HRP reverse micelles were directly spin-cast for 20 s at 3000 RPM onto a silicon wafer.

6.4.4. Dynamic Light Scattering

Size distributions of SRHP-4/HRP reverse micelle solution, PS-*b*-PEO solution, and a solution containing a mixture of the two were measured using a Brookhaven Instruments BI-200SM Research Goniometer and Laser Light Scattering System. Temperature was controlled and set at 25°C. Measurements were sorted by intensity average and a NNLS function was used to analyze the correlation curves.

6.4.5. Atomic Force Microscopy

Thin films were imaged using atomic force microscopy. AFM was performed on a Molecular Imaging PicoSPM II with a PicoScan 2500 controller. A scan rate of 2 Hz and a resonant frequency ranging between 300-400 kHz were used.

6.4.6. Grazing-Incidence Small Angle X-Ray Scattering

GISAXS experiments were carried out at the ALS beamline 7.3.3. The instrument was operated using an x-ray energy of 10 keV and a sample-to-detector distance of 2.3 m. Scattering profiles were collected on a 2 M Pilatus detector, at an incident angle of 0.20°.

6.4.7. Analysis of HRP Activity during Processing

HRP activity was assessed using a TMB Peroxidase EIA Substrate Kit. Baseline HRP activity was determined by preparing a stock protein solution in 100 mM

KH_2PO_4/K_2HPO_4 phosphate buffer at pH 6 and applying a prepared TMB assay solution, as outlined by the manufacturer. Solution was thoroughly mixed and UV-visible spectroscopy was performed on a Hewlett-Packard 8453 Spectrophotometer. A 1-cm path length cuvette was used and absorbance at 370 nm was monitored.

(6.1)
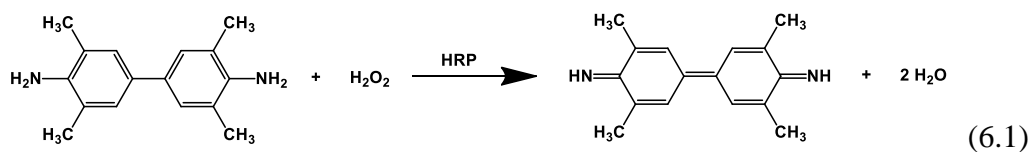
After each step during spin-cast processing, an aliquot of each solution was taken and dispensed into the previously outlined buffer. TMB was immediately applied and UV-visible spectroscopy was used to monitor HRP activity. The film was placed in the buffer for at least 20 s to release all the HRP prior to TMB assay introduction and UV-visible spectroscopy analysis.

6.4.8. Visual Analysis of HRP Activity Post-Annealing

Thin films were submerged for 30 min in 100 mM KH_2PO_4/K_2HPO_4 phosphate buffer at pH 6 containing TMB assay. Presence of blue color indicates HRP activity.

6.4.9. Electrospinning HRP-Containing Fibers

PMMA was dissolved in chloroform to achieve a 7.5 wt% concentration. 200 uL of toluene containing the SRHP/HRP complex was mixed with 800 uL of the PMMA/chloroform solution. The mixture was stirred for 5 min at 350 RPM immediately prior to electrospinning. The solution was then electrospun from a 1 mL syringe and a 20 gauge needle. An aluminum collector plate was placed 18 cm away from the needle tip in a horizontal setup. The solution was pumped at a rate of 0.45 mL/h. A voltage of 8 kV was applied to the solution.

6.4.10. Scanning Electron Microscopy

A Hitachi TM-1000 scanning electron microscope was used to acquire images of the electrospun fibers. The samples were mounted on conductive carbon tape. A 15 kV accelerating voltage was used to acquire the SEM images.

6.4.11. Visual Analysis of HRP Activity Post-Electrospinning

Electrospun fiber mats were submerged for 30 min in 100 mM KH_2PO_4/K_2HPO_4 phosphate buffer at pH 6 containing TMB assay. Presence of blue color indicates HRP activity.

Afterword

Protein-functional nanomaterials are an interesting and exciting class of new materials with applicable translation into catalysis, sensing, filtration, medicine, energy, and beyond. As the interactions that govern protein folding, polymer conformation, solvent solubility, and the interactions between these three components are all along the same energy length scale, the research that is conducted within this field lies at both the physical interfaces of this system as well as the scientific interfaces of many disciplines. The work that is described in this dissertation provides a comprehensive analysis of protein-polymer interactions and possible applications. From a science perspective, evaluation of interactions using spectroscopic technique and determination of structure using scattering provides intellectual wealth. From an engineering perspective, the design of the polymer, the optimization of processing techniques, and the incorporation into a model application provides potential in enhancing society. This strong relationship between chemistry, structure, and performance and the ability to manipulate these three core aspects provides a modular approach toward protein-based nanomaterials.

Future work will continue to further characterize and analyze this polymer chemistry-protein stability relationship. The world of random heteropolymers is an emerging field and the chemistry and structure of this exciting class of tailorable materials is appealing. In addition, the road has been paved for a variety of applications. Water and gas filtration of chemical warfare agents is one key avenue that is in current development in our lab. By incorporating organophosphorus hydrolase into electrospun nanofiber mats, smart fabrics can be created to enhance the lives of both soldiers and civilians. Expansion into different molecular systems is another avenue of interest as we delve deeper into the world of statistically random heteropolymers. Current directions that are now in progress is to apply SRHPs to larger systems, such as stabilizing

molecular machinery (ribosomes), creating transmembrane-decorated liposomes, and finally, making mammalian cells into viable material building blocks.

References

R.1. Chapter 1

1. Leader, B., Baca, Q.J. & Golan, D.E. Protein therapeutics: A summary and pharmacological classification. *Nature Reviews Drug Discovery* **7**, 21-39 (2008).
2. de la Rica, R. & Matsui, H. Applications of peptide and protein-based materials in bionanotechnology. *Chemical Society Reviews* **39**, 3499-3509 (2010).
3. Shu, J.Y., Panganiban, B. & Xu, T. in Annual Review of Physical Chemistry, Vol 64, Vol. 64. (eds. M.A. Johnson & T.J. Martinez) 631-6572013).
4. Duncan, R. The dawning era of polymer therapeutics. *Nature Reviews Drug Discovery* **2**, 347-360 (2003).
5. Harris, J.M. & Chess, R.B. Effect of pegylation on pharmaceuticals. *Nature Reviews Drug Discovery* **2**, 214-221 (2003).
6. Borner, H.G. & Schlaad, H. Bioinspired functional block copolymers. *Soft Matter* **3**, 394-408 (2007).
7. Klok, H.A. et al. Peptide mediated formation of hierarchically organized solution and solid state polymer nanostructures. *Faraday Discussions* **128**, 29-41 (2005).
8. Deming, T.J. Polypeptide materials: New synthetic methods and applications. *Advanced Materials* **9**, 299-& (1997).
9. Petka, W.A., Harden, J.L., McGrath, K.P., Wirtz, D. & Tirrell, D.A. Reversible hydrogels from self-assembling artificial proteins. *Science* **281**, 389-392 (1998).
10. Wang, C., Stewart, R.J. & Kopecek, J. Hybrid hydrogels assembled from synthetic polymers and coiled-coil protein domains. *Nature* **397**, 417-420 (1999).
11. Hartgerink, J.D., Beniash, E. & Stupp, S.I. Self-assembly and mineralization of peptide-amphiphile nanofibers. *Science* **294**, 1684-1688 (2001).
12. Nowak, A.P. et al. Rapidly recovering hydrogel scaffolds from self-assembling diblock copolypeptide amphiphiles. *Nature* **417**, 424-428 (2002).
13. Sarikaya, M., Tamerler, C., Schwartz, D.T. & Baneyx, F.O. Materials assembly and formation using engineered polypeptides. *Annual Review of Materials Research* **34**, 373-408 (2004).
14. Vandermeulen, G.W.M. et al. Structure and dynamics of self-assembled poly(ethylene glycol) based coiled-coil Nano objects. *Chemphyschem* **5**, 488-494 (2004).
15. Shu, J.Y., Tan, C., DeGrado, W.F. & Xu, T. New design of helix bundle peptide-polymer conjugates. *Biomacromolecules* **9**, 2111-2117 (2008).
16. Haupt, K. & Mosbach, K. Molecularly imprinted polymers and their use in biomimetic sensors. *Chemical Reviews* **100**, 2495-2504 (2000).
17. Ye, L. & Haupt, K. Molecularly imprinted polymers as antibody and receptor mimics for assays, sensors and drug discovery. *Analytical and Bioanalytical Chemistry* **378**, 1887-1897 (2004).
18. Wulff, G. Enzyme-like catalysis by molecularly imprinted polymers. *Chemical Reviews* **102**, 1-27 (2002).

19. Gust, D., Moore, T.A. & Moore, A.L. Solar Fuels via Artificial Photosynthesis. *Accounts of Chemical Research* **42**, 1890-1898 (2009).

20. Griebenow, K. & Klibanov, A.M. On protein denaturation in aqueous-organic mixtures but not in pure organic solvents. *Journal of the American Chemical Society* **118**, 11695-11700 (1996).

21. Klibanov, A.M. Improving enzymes by using them in organic solvents. *Nature* **409**, 241-246 (2001).

22. Mattos, C. & Ringe, D. Proteins in organic solvents. *Current Opinion in Structural Biology* **11**, 761-764 (2001).

23. Castro, G.R. Enzymatic activities of proteases dissolved in organic solvents. *Enzyme Microb. Technol.* **25**, 689-694 (1999).

24. Schmid, A. et al. Industrial biocatalysis today and tomorrow. *Nature* **409**, 258-268 (2001).

25. Dordick, J.S. ENZYMATIC CATALYSIS IN MONOPHASIC ORGANIC-SOLVENTS. *Enzyme Microb. Technol.* **11**, 194-211 (1989).

26. Bornscheuer, U.T. et al. Engineering the third wave of biocatalysis. *Nature* **485**, 185-194 (2012).

27. Shoulders, M.D. & Raines, R.T. in Annual Review of Biochemistry, Vol. 78 929-9582009).

28. Hubbard, S.R. & Till, J.H. Protein tyrosine kinase structure and function. *Annu. Rev. Biochem.* **69**, 373-398 (2000).

29. Dyson, H.J. & Wright, P.E. Intrinsically unstructured proteins and their functions. *Nat. Rev. Mol. Cell Biol.* **6**, 197-208 (2005).

30. Perutz, M.F. et al. STRUCTURE OF HAEMOGLOBIN - 3-DIMENSIONAL FOURIER SYNTHESIS AT 5.5-A RESOLUTION, OBTAINED BY X-RAY ANALYSIS. *Nature* **185**, 416-422 (1960).

31. Yusupov, M.M. et al. Crystal structure of the ribosome at 5.5 angstrom resolution. *Science* **292**, 883-896 (2001).

32. Kuriyan, J., Konforti, B. & Wemmer, D. The Molecules of Life: Physical and Chemical Principles. (Garland Science, 2013).

33. Carter, P. & Wells, J.A. DISSECTING THE CATALYTIC TRIAD OF A SERINE PROTEASE. *Nature* **332**, 564-568 (1988).

34. Kirk, O., Borchert, T.V. & Fuglsang, C.C. Industrial enzyme applications. *Current Opinion in Biotechnology* **13**, 345-351 (2002).

35. Veitch, N.C. Horseradish peroxidase: a modern view of a classic enzyme. *Phytochemistry* **65**, 249-259 (2004).

36. Spiess, C., Beil, A. & Ehrmann, M. A temperature-dependent switch from chaperone to protease in a widely conserved heat shock protein. *Cell* **97**, 339-347 (1999).

37. Jeffery, C.J. Moonlighting proteins. *Trends in Biochemical Sciences* **24**, 8-11 (1999).

38. Dill, K.A. DOMINANT FORCES IN PROTEIN FOLDING. *Biochemistry* **29**, 7133-7155 (1990).

39. Dordick, J.S. DESIGNING ENZYMES FOR USE IN ORGANIC-SOLVENTS. *Biotechnol. Prog.* **8**, 259-267 (1992).

40. Stepankova, V. et al. Strategies for Stabilization of Enzymes in Organic Solvents. *Acs Catalysis* **3**, 2823-2836 (2013).

41. Liszka, M.J., Clark, M.E., Schneider, E. & Clark, D.S. in Annual Review of Chemical and Biomolecular Engineering, Vol 3, Vol. 3. (ed. J.M. Prausnitz) 77-1022012).

42. Santoro, M.M., Liu, Y.F., Khan, S.M.A., Hou, L.X. & Bolen, D.W. INCREASED THERMAL-STABILITY OF PROTEINS IN THE PRESENCE OF NATURALLY-OCCURRING OSMOLYTES. *Biochemistry* **31**, 5278-5283 (1992).

43. Arakawa, T. & Timasheff, S.N. THE STABILIZATION OF PROTEINS BY OSMOLYTES. *Biophysical Journal* **47**, 411-414 (1985).

44. Gekko, K. & Timasheff, S.N. MECHANISM OF PROTEIN STABILIZATION BY GLYCEROL - PREFERENTIAL HYDRATION IN GLYCEROL-WATER MIXTURES. *Biochemistry* **20**, 4667-4676 (1981).

45. Liu, Y.F. & Bolen, D.W. THE PEPTIDE BACKBONE PLAYS A DOMINANT ROLE IN PROTEIN STABILIZATION BY NATURALLY-OCCURRING OSMOLYTES. *Biochemistry* **34**, 12884-12891 (1995).

46. Back, J.F., Oakenfull, D. & Smith, M.B. INCREASED THERMAL-STABILITY OF PROTEINS IN THE PRESENCE OF SUGARS AND POLYOLS. *Biochemistry* **18**, 5191-5196 (1979).

47. Kim, B., Lam, C.N. & Olsen, B.D. Nanopatterned Protein Films Directed by Ionic Complexation with Water-Soluble Diblock Copolymers. *Macromolecules* **45**, 4572-4580 (2012).

48. Shan, W.J., He, P.L. & Hu, N.F. Electrocatalytic reduction of nitric oxide and other substrates on hydrogel triblock copolymer Pluronic films containing hemoglobin or myoglobin based on protein direct electrochemistry. *Electrochimica Acta* **51**, 432-440 (2005).

49. Jia, S.S., Fei, J.J., Deng, J.J., Cai, Y.L. & Li, J.A. Direct electrochemistry and electrocatalysis of hemoglobin immobilized in an amphiphilic diblock copolymer film. *Sensors and Actuators B-Chemical* **138**, 244-250 (2009).

50. Jain, N.K. & Roy, I. Effect of trehalose on protein structure. *Protein Science* **18**, 24-36 (2009).

51. Grasmeijer, N., Stankovic, M., de Waard, H., Frijlink, H.W. & Hinrichs, W.L.J. Unraveling protein stabilization mechanisms: Vitrification and water replacement in a glass transition temperature controlled system. *Biochimica Et Biophysica Acta-Proteins and Proteomics* **1834**, 763-769 (2013).

52. Wang, W. Lyophilization and development of solid protein pharmaceuticals. *International Journal of Pharmaceutics* **203**, 1-60 (2000).

53. Romero, P.A. & Arnold, F.H. Exploring protein fitness landscapes by directed evolution. *Nat. Rev. Mol. Cell Biol.* **10**, 866-876 (2009).

54. Arnold, F.H. Design by directed evolution. *Accounts of Chemical Research* **31**, 125-131 (1998).

55. DeGrado, W.F., Summa, C.M., Pavone, V., Nastri, F. & Lombardi, A. De novo design and structural characterization of proteins and metalloproteins. *Annu. Rev. Biochem.* **68**, 779-819 (1999).

56. Bornscheuer, U.T. & Pohl, M. Improved biocatalysts by directed evolution and rational protein design. *Current Opinion in Chemical Biology* **5**, 137-143 (2001).

57. Cedrone, F., Menez, A. & Quemeneur, E. Tailoring new enzyme functions by rational redesign. *Current Opinion in Structural Biology* **10**, 405-410 (2000).

58. Bolon, D.N., Voigt, C.A. & Mayo, S.L. De novo design of biocatalysts. *Current Opinion in Chemical Biology* **6**, 125-129 (2002).

59. Greenfield, N.J., Stafford, W.F. & Hitchcockdegregori, S.E. THE EFFECT OF N-TERMINAL ACETYLATION ON THE STRUCTURE OF AN N-TERMINAL TROPOMYOSIN PEPTIDE AND ALPHA-ALPHA-TROPOMYOSIN. *Protein Science* **3**, 402-410 (1994).

60. Veronese, F.M. Peptide and protein PEGylation: a review of problems and solutions. *Biomaterials* **22**, 405-417 (2001).

61. Gil, E.S. & Hudson, S.M. Stimuli-reponsive polymers and their bioconjugates. *Progress in Polymer Science* **29**, 1173-1222 (2004).

62. Dube, N., Presley, A.D., Shu, J.Y. & Xu, T. Amphiphilic Peptide-Polymer Conjugates with Side-Conjugation. *Macromolecular Rapid Communications* **32**, 344-353 (2011).

63. Pechar, M., Kopeckova, P., Joss, L. & Kopecek, J. Associative diblock copolymers of poly(ethylene glycol) and coiled-coil peptides. *Macromolecular Bioscience* **2**, 199-206 (2002).

64. Vandermeulen, G.W.M., Tziatzios, C., Duncan, R. & Klok, H.A. PEG-based hybrid block copolymers containing alpha-helical coiled coil peptide sequences: Control of self-assembly and preliminary biological evaluation. *Macromolecules* **38**, 761-769 (2005).

65. Vandermeulen, G.W.M., Tziatzios, C. & Klok, H.A. Reversible self-organization of poly(ethylene glycol)-based hybrid block copolymers mediated by a De Novo four-stranded alpha-helical coiled coil motif. *Macromolecules* **36**, 4107-4114 (2003).

66. Shu, J.Y. et al. Amphiphilic Peptide-Polymer Conjugates Based on the Coiled-Coil Helix Bundle. *Biomacromolecules* **11**, 1443-1452 (2010).

67. Presley, A.D., Chang, J.J. & Xu, T. Directed co-assembly of heme proteins with amphiphilic block copolymers toward functional biomolecular materials. *Soft Matter* **7**, 172-179 (2011).

68. Tidor, B. & Karplus, M. THE CONTRIBUTION OF CROSS-LINKS TO PROTEIN STABILITY - A NORMAL MODE ANALYSIS OF THE

CONFIGURATIONAL ENTROPY OF THE NATIVE-STATE. *Proteins-Structure Function and Genetics* **15**, 71-79 (1993).

69.   Singh, R.K., Tiwari, M.K., Singh, R. & Lee, J.K. From Protein Engineering to Immobilization: Promising Strategies for the Upgrade of Industrial Enzymes. *International Journal of Molecular Sciences* **14**, 1232-1277 (2013).

70.   Dennis, P.B., Walker, A.Y., Dickerson, M.B., Kaplan, D.L. & Naik, R.R. Stabilization of Organophosphorus Hydrolase by Entrapment in Silk Fibroin: Formation of a Robust Enzymatic Material Suitable for Surface Coatings. *Biomacromolecules* **13**, 2037-2045 (2012).

71.   Fishman, A., Levy, I., Cogan, U. & Shoseyov, O. Stabilization of horseradish peroxidase in aqueous-organic media by immobilization onto cellulose using a cellulose-binding-domain. *Journal of Molecular Catalysis B-Enzymatic* **18**, 121-131 (2002).

72.   Wang, Z.G., Wan, L.S., Liu, Z.M., Huang, X.J. & Xu, Z.K. Enzyme immobilization on electrospun polymer nanofibers: An overview. *Journal of Molecular Catalysis B-Enzymatic* **56**, 189-195 (2009).

73.   Avnir, D., Braun, S., Lev, O. & Ottolenghi, M. ENZYMES AND OTHER PROTEINS ENTRAPPED IN SOL-GEL MATERIALS. *Chemistry of Materials* **6**, 1605-1614 (1994).

74.   Hartl, F.U. Molecular chaperones in cellular protein folding. *Nature* **381**, 571-580 (1996).

75.   Lei, C.H., Shin, Y.S., Liu, J. & Ackerman, E.J. Entrapping enzyme in a functionalized nanoporous support. *Journal of the American Chemical Society* **124**, 11242-11243 (2002).

76.   Helenius, A. & Simons, K. SOLUBILIZATION OF MEMBRANES BY DETERGENTS. *Biochimica Et Biophysica Acta* **415**, 29-79 (1975).

77.   Geiger, S. & Mandel, M. INTERACTIONS BETWEEN POLYMERS AND INVERTED MICELLES IN APOLAR MEDIA. *Journal of Physical Chemistry* **93**, 4195-4198 (1989).

78.   Moller, J.V. & Lemaire, M. DETERGENT BINDING AS A MEASURE OF HYDROPHOBIC SURFACE-AREA OF INTEGRAL MEMBRANE-PROTEINS. *Journal of Biological Chemistry* **268**, 18659-18672 (1993).

79.   Tribet, C., Audebert, R. & Popot, J.L. Amphipols: Polymers that keep membrane proteins soluble in aqueous solutions. *Proceedings of the National Academy of Sciences of the United States of America* **93**, 15047-15050 (1996).

80.   Gohon, Y. & Popot, J.L. Membrane protein-surfactant complexes. *Current Opinion in Colloid & Interface Science* **8**, 15-22 (2003).

81.   Popot, J.L. et al. Amphipols: polymeric surfactants for membrane biology research. *Cellular and Molecular Life Sciences* **60**, 1559-1574 (2003).

82.   Pocanschi, C.L. et al. Amphipathic polymers: Tools to fold integral membrane proteins to their active form. *Biochemistry* **45**, 13954-13961 (2006).

83. Popot, J.L. et al. in Annual Review of Biophysics, Vol 40, Vol. 40. (eds. D.C. Rees, K.A. Dill & J.R. Williamson) 379-4082011).

84. Herricks, T.E. et al. Direct fabrication of enzyme-carrying polymer nanofibers by electrospinning. *Journal of Materials Chemistry* **15**, 3241-3245 (2005).

85. Bates, F.S. & Fredrickson, G.H. BLOCK COPOLYMER THERMODYNAMICS - THEORY AND EXPERIMENT. *Annual Review of Physical Chemistry* **41**, 525-557 (1990).

86. Fu, J.L., Liu, M.H., Liu, Y., Woodbury, N.W. & Yan, H. Interenzyme Substrate Diffusion for an Enzyme Cascade Organized on Spatially Addressable DNA Nanostructures. *Journal of the American Chemical Society* **134**, 5516-5519 (2012).

87. Khmelnitsky, Y.L. et al. Synthesis of water-soluble paclitaxel derivatives by enzymatic acylation. *Journal of the American Chemical Society* **119**, 11554-11555 (1997).

88. DiMasi, J.A., Grabowski, H.G. & Hansen, R.W. Innovation in the pharmaceutical industry: New estimates of R&D costs. *Journal of Health Economics* **47**, 20-33 (2016).

89. Hamblett, K.J. et al. Effects of drug loading on the antitumor activity of a monoclonal antibody drug conjugate. *Clinical Cancer Research* **10**, 7063-7070 (2004).

90. Himmel, M.E. et al. Biomass recalcitrance: Engineering plants and enzymes for biofuels production. *Science* **315**, 804-807 (2007).

91. Klein-Marcuschamer, D., Oleskowicz-Popiel, P., Simmons, B.A. & Blanch, H.W. The challenge of enzyme cost in the production of lignocellulosic biofuels. *Biotechnology and Bioengineering* **109**, 1083-1087 (2012).

92. Li, L. et al. N-terminal PEGylated cellulase: a high stability enzyme in 1-butyl-3-methylimidazolium chloride. *Green Chemistry* **15**, 1624-1630 (2013).

93. LeBlanc, G., Chen, G.P., Gizzie, E.A., Jennings, G.K. & Cliffel, D.E. Enhanced Photocurrents of Photosystem I Films on p-Doped Silicon. *Advanced Materials* **24**, 5959-+ (2012).

94. Yan, X., Faulkner, C.J., Jennings, G.K. & Cliffel, D.E. Photosystem I in Langmuir-Blodgett and Langmuir-Schaefer Monolayers. *Langmuir* **28**, 15080-15086 (2012).

95. Gunther, D. et al. Photosystem I on Graphene as a Highly Transparent, Photoactive Electrode. *Langmuir* **29**, 4177-4180 (2013).

96. LeBlanc, G., Gizzie, E., Yang, S.Y., Cliffel, D.E. & Jennings, G.K. Photosystem I Protein Films at Electrode Surfaces for Solar Energy Conversion. *Langmuir* **30**, 10990-11001 (2014).

97. Kim, J., Jia, H.F. & Wang, P. Challenges in biocatalysis for enzyme-based biofuel cells. *Biotechnology Advances* **24**, 296-308 (2006).

98. Leech, D., Kavanagh, P. & Schuhmann, W. Enzymatic fuel cells: Recent progress. *Electrochimica Acta* **84**, 223-234 (2012).

99. Kim, M. et al. Enhanced activity and stability of organophosphorus hydrolase via interaction with an amphiphilic polymer. *Chemical Communications* **50**, 5345-5348 (2014).

100. Mulchandani, A., Chen, W., Mulchandani, P., Wang, J. & Rogers, K.R. Biosensors for direct determination of organophosphate pesticides. *Biosensors & Bioelectronics* **16**, 225-230 (2001).

101. Richins, R.D., Kaneva, I., Mulchandani, A. & Chen, W. Biodegradation of organophosphorus pesticides by surface-expressed organophosphorus hydrolase. *Nature Biotechnology* **15**, 984-987 (1997).

102. Sogorb, M.A. & Vilanova, E. Enzymes involved in the detoxification of organophosphorus, carbamate and pyrethroid insecticides through hydrolysis. *Toxicology Letters* **128**, 215-228 (2002).

103. Lund, R., Shu, J. & Xu, T. A Small-Angle X-ray Scattering Study of alpha-helical Bundle-Forming Peptide-Polymer Conjugates in Solution: Chain Conformations. *Macromolecules* **46**, 1625-1632 (2013).

104. Shu, J.Y., Lund, R. & Xu, T. Solution Structural Characterization of Coiled-Coil Peptide-Polymer Side-Conjugates. *Biomacromolecules* **13**, 1945-1955 (2012).

105. Xu, T. & Shu, J. Coiled-coil helix bundle, a peptide tertiary structural motif toward hybrid functional materials. *Soft Matter* **6**, 212-217 (2010).

R.2. Chapter 2

1. Romanov, V. et al. A critical comparison of protein microarray fabrication technologies. *Analyst* **139**, 1303-1326 (2014).

2. Mammen, M., Choi, S.K. & Whitesides, G.M. Polyvalent interactions in biological systems: Implications for design and use of multivalent ligands and inhibitors. *Angewandte Chemie-International Edition* **37**, 2755-2794 (1998).

3. Mrksich, M. & Whitesides, G.M. Using self-assembled monolayers to understand the interactions of man-made surfaces with proteins and cells. *Annual Review of Biophysics and Biomolecular Structure* **25**, 55-78 (1996).

4. Perham, R.N. Swinging arms and swinging domains in multifunctional enzymes: Catalytic machines for multistep reactions. *Annual Review of Biochemistry* **69**, 961-1004 (2000).

5. Bates, F.S. & Fredrickson, G.H. BLOCK COPOLYMER THERMODYNAMICS - THEORY AND EXPERIMENT. *Annual Review of Physical Chemistry* **41**, 525-557 (1990).

6. Lin, Y. et al. Self-directed self-assembly of nanoparticle/copolymer mixtures. *Nature* **434**, 55-59 (2005).

7. Koizumi, S., Hasegawa, H. & Hashimoto, T. ORDERED STRUCTURES OF BLOCK COPOLYMER/HOMOPOLYMER MIXTURES .5. INTERPLAY OF

MACROPHASE AND MICROPHASE TRANSITIONS. *Macromolecules* **27**, 6532-6540 (1994).

8. Stoykovich, M.P. et al. Directed assembly of block copolymer blends into nonregular device-oriented structures. *Science* **308**, 1442-1446 (2005).

9. Tung, S.H., Kalarickal, N.C., Mays, J.W. & Xu, T. Hierarchical assemblies of block-copolymer-based supramolecules in thin films. *Macromolecules* **41**, 6453-6462 (2008).

10. Kao, J., Tingsanchali, J. & Xu, T. Effects of Interfacial Interactions and Film Thickness on Nonequilibrium Hierarchical Assemblies of Block Copolymer-Based Supramolecules in Thin Films. *Macromolecules* **44**, 4392-4400 (2011).

11. Rancatore, B.J., Mauldin, C.E., Frechet, J.M.J. & Xu, T. Small Molecule-Guided Thermoresponsive Supramolecular Assemblies. *Macromolecules* **45**, 8292-8299 (2012).

12. Leader, B., Baca, Q.J. & Golan, D.E. Protein therapeutics: A summary and pharmacological classification. *Nature Reviews Drug Discovery* **7**, 21-39 (2008).

13. Lee, K.B., Kim, E.Y., Mirkin, C.A. & Wolinsky, S.M. The use of nanoarrays for highly sensitive and selective detection of human immunodeficiency virus type 1 in plasma. *Nano Letters* **4**, 1869-1872 (2004).

14. Lee, K.B., Park, S.J., Mirkin, C.A., Smith, J.C. & Mrksich, M. Protein nanoarrays generated by dip-pen nanolithography. *Science* **295**, 1702-1705 (2002).

15. Tinazli, A., Piehler, J., Beuttler, M., Guckenberger, R. & Tampe, R. Native protein nanolithography that can write, read and erase. *Nature Nanotechnology* **2**, 220-225 (2007).

16. Doh, J. & Irvine, D.J. Photogenerated polyelectrolyte bilayers from an aqueous-processible photoresist for multicomponent protein patterning. *Journal of the American Chemical Society* **126**, 9170-9171 (2004).

17. Lahiri, J., Ostuni, E. & Whitesides, G.M. Patterning ligands on reactive SAMs by microcontact printing. *Langmuir* **15**, 2055-2060 (1999).

18. Presley, A.D., Chang, J.J. & Xu, T. Directed co-assembly of heme proteins with amphiphilic block copolymers toward functional biomolecular materials. *Soft Matter* **7**, 172-179 (2011).

19. Xu, T. et al. Subnanometer Porous Thin Films by the Co-assembly of Nanotube Subunits and Block Copolymers. *Acs Nano* **5**, 1376-1384 (2011).

20. Cresce, A.V., Silverstein, J.S., Bentley, W.E. & Kofinas, P. Nanopatterning of recombinant proteins using block copolymer templates. *Macromolecules* **39**, 5826-5829 (2006).

21. Kumar, N. & Hahm, J.I. Nanoscale protein patterning using self-assembled diblock copolymers. *Langmuir* **21**, 6652-6655 (2005).

22. Kumar, N., Parajuli, O. & Hahm, J.I. Two-dimensionally self-arranged protein nanoarrays on diblock copolymer templates. *Journal of Physical Chemistry B* **111**, 4581-4587 (2007).

23. Wong, M., Thomas, J.K. & Nowak, T. STRUCTURE AND STATE OF H2O IN REVERSED MICELLES .3. *Journal of the American Chemical Society* **99**, 4730-4736 (1977).

24. Luisi, P.L. ENZYMES HOSTED IN REVERSE MICELLES IN HYDROCARBON SOLUTION. *Angewandte Chemie-International Edition in English* **24**, 439-450 (1985).

25. Luisi, P.L., Giomini, M., Pileni, M.P. & Robinson, B.H. REVERSE MICELLES AS HOSTS FOR PROTEINS AND SMALL MOLECULES. *Biochimica Et Biophysica Acta* **947**, 209-246 (1988).

26. Pileni, M.P. REVERSE MICELLES AS MICROREACTORS. *Journal of Physical Chemistry* **97**, 6961-6973 (1993).

27. Taleb, A., Petit, C. & Pileni, M.P. Synthesis of highly monodisperse silver nanoparticles from AOT reverse micelles: A way to 2D and 3D self-organization. *Chemistry of Materials* **9**, 950-959 (1997).

28. Leser, M.E. & Luisi, P.L. APPLICATION OF REVERSE MICELLES FOR THE EXTRACTION OF AMINO-ACIDS AND PROTEINS. *Chimia* **44**, 270-282 (1990).

29. Paradkar, V.M. & Dordick, J.S. MECHANISM OF EXTRACTION OF CHYMOTRYPSIN INTO ISOOCTANE AT VERY-LOW CONCENTRATIONS OF AEROSOL OT IN THE ABSENCE OF REVERSED MICELLES. *Biotechnology and Bioengineering* **43**, 529-540 (1994).

30. De, T.K. & Maitra, A. SOLUTION BEHAVIOR OF AEROSOL OT IN NONPOLAR-SOLVENTS. *Advances in Colloid and Interface Science* **59**, 95-193 (1995).

31. Matzke, S.F., Creagh, A.L., Haynes, C.A., Prausnitz, J.M. & Blanch, H.W. MECHANISMS OF PROTEIN SOLUBILIZATION IN REVERSE MICELLES. *Biotechnology and Bioengineering* **40**, 91-102 (1992).

32. Kao, J. et al. Nanoparticle Assemblies in Thin Films of Supramolecular Nanocomposites. *Nano Letters* **12**, 2610-2618 (2012).

33. Kao, J., Bai, P., Lucas, J.M., Alivisatos, A.P. & Xu, T. Size-Dependent Assemblies of Nanoparticle Mixtures in Thin Films. *Journal of the American Chemical Society* **135**, 1680-1683 (2013).

34. Huang, W.H., Chen, P.Y. & Tung, S.H. Effects of Annealing Solvents on the Morphology of Block Copolymer-Based Supramolecular Thin Films. *Macromolecules* **45**, 1562-1569 (2012).

35. Fu, J.L., Liu, M.H., Liu, Y., Woodbury, N.W. & Yan, H. Interenzyme Substrate Diffusion for an Enzyme Cascade Organized on Spatially Addressable DNA Nanostructures. *Journal of the American Chemical Society* **134**, 5516-5519 (2012).

36. Idan, O. & Hess, H. Origins of Activity Enhancement in Enzyme Cascades on Scaffolds. *Acs Nano* **7**, 8658-8665 (2013).

37. Novick, S.J. & Dordick, J.S. Protein-containing hydrophobic coatings and films. *Biomaterials* **23**, 441-448 (2002).

38. Wnek, G.E., Carr, M.E., Simpson, D.G. & Bowlin, G.L. Electrospinning of nanofiber fibrinogen structures. *Nano Letters* **3**, 213-216 (2003).

39. Li, D. & Xia, Y.N. Electrospinning of nanofibers: Reinventing the wheel? *Advanced Materials* **16**, 1151-1170 (2004).

40. Megelski, S., Stephens, J.S., Chase, D.B. & Rabolt, J.F. Micro- and nanostructured surface morphology on electrospun polymer fibers. *Macromolecules* **35**, 8456-8466 (2002).

41. Reneker, D.H. & Chun, I. Nanometre diameter fibres of polymer, produced by electrospinning. *Nanotechnology* **7**, 216-223 (1996).

42. Frenot, A. & Chronakis, I.S. Polymer nanofibers assembled by electrospinning. *Current Opinion in Colloid & Interface Science* **8**, 64-75 (2003).

43. Ruotsalainen, T. et al. Towards internal structuring of electrospun fibers by hierarchical self-assembly of polymeric comb-shaped supramolecules. *Advanced Materials* **17**, 1048-+ (2005).

44. Ruotsalainen, T. et al. Tailoring of the hierarchical structure within electrospun fibers due to supramolecular comb-coil block copolymers: polystyrene-block-poly(4-vinyl pyridine) plasticized by hydrogen bonded pentadecylphenol. *Soft Matter* **3**, 978-985 (2007).

45. Herricks, T.E. et al. Direct fabrication of enzyme-carrying polymer nanofibers by electrospinning. *Journal of Materials Chemistry* **15**, 3241-3245 (2005).

R.3. Chapter 3

1. Gao, J.Y. & Dubin, P.L. Binding of proteins to copolymers of varying hydrophobicity. *Biopolymers* **49**, 185-193 (1999).

2. Cooper, C.L., Dubin, P.L., Kayitmazer, A.B. & Turksen, S. Polyelectrolyte-protein complexes. *Curr. Opin. Colloid Interface Sci.* **10**, 52-78 (2005).

3. Petit, F., Audebert, R. & Iliopoulos, I. INTERACTIONS OF HYDROPHOBICALLY-MODIFIED POLY(SODIUM ACRYLATE) WITH GLOBULAR-PROTEINS. *Colloid and Polymer Science* **273**, 777-781 (1995).

4. Xia, J.L., Dubin, P.L. & Kokufuta, E. DYNAMIC AND ELECTROPHORETIC LIGHT-SCATTERING OF A WATER-SOLUBLE COMPLEX FORMED BETWEEN PEPSIN AND POLY(ETHYLENE GLYCOL). *Macromolecules* **26**, 6688-6690 (1993).

5. Tribet, C., Audebert, R. & Popot, J.L. Amphipols: Polymers that keep membrane proteins soluble in aqueous solutions. *Proceedings of the National Academy of Sciences of the United States of America* **93**, 15047-15050 (1996).

6.   Hsieh, E.T. & Randall, J.C. MONOMER SEQUENCE DISTRIBUTIONS IN ETHYLENE 1-HEXENE COPOLYMERS. *Macromolecules* **15**, 1402-1406 (1982).

7.   Leser, M.E. & Luisi, P.L. APPLICATION OF REVERSE MICELLES FOR THE EXTRACTION OF AMINO-ACIDS AND PROTEINS. *Chimia* **44**, 270-282 (1990).

8.   Luisi, P.L. ENZYMES HOSTED IN REVERSE MICELLES IN HYDROCARBON SOLUTION. *Angewandte Chemie-International Edition in English* **24**, 439-450 (1985).

9.   Paradkar, V.M. & Dordick, J.S. MECHANISM OF EXTRACTION OF CHYMOTRYPSIN INTO ISOOCTANE AT VERY-LOW CONCENTRATIONS OF AEROSOL OT IN THE ABSENCE OF REVERSED MICELLES. *Biotechnology and Bioengineering* **43**, 529-540 (1994).

10.   Luisi, P.L., Giomini, M., Pileni, M.P. & Robinson, B.H. REVERSE MICELLES AS HOSTS FOR PROTEINS AND SMALL MOLECULES. *Biochimica Et Biophysica Acta* **947**, 209-246 (1988).

11.   Miller, A.C. et al. Block Copolymer Micelles as Nanocontainers for Controlled Release of Proteins from Biocompatible Oil Phases. *Biomacromolecules* **10**, 732-741 (2009).

12.   Jones, M.C. et al. Self-assembled nanocages for hydrophilic guest molecules. *Journal of the American Chemical Society* **128**, 14599-14605 (2006).

13.   Presley, A.D., Chang, J.J. & Xu, T. Directed co-assembly of heme proteins with amphiphilic block copolymers toward functional biomolecular materials. *Soft Matter* **7**, 172-179 (2011).

14.   Israelachvili, J.N., Mitchell, D.J. & Ninham, B.W. THEORY OF SELF-ASSEMBLY OF HYDROCARBON AMPHIPHILES INTO MICELLES AND BILAYERS. *Journal of the Chemical Society-Faraday Transactions Ii* **72**, 1525-1568 (1976).

15.   Castelletto, V., Krysmann, M., Kelarakis, A. & Jauregi, P. Complex formation of bovine serum albumin with a poly(ethylene glycol) lipid conjugate. *Biomacromolecules* **8**, 2244-2249 (2007).

16.   Chen, H.T. et al. Release of hydrophobic molecules from polymer micelles into cell membranes revealed by Forster resonance energy transfer imaging. *Proceedings of the National Academy of Sciences of the United States of America* **105**, 6596-6601 (2008).

17.   Kastantin, M. et al. Thermodynamic and Kinetic Stability of DSPE-PEG(2000) Micelles in the Presence of Bovine Serum Albumin. *Journal of Physical Chemistry B* **114**, 12632-12640 (2010).

18.   Nicolai, T., Colombani, O. & Chassenieux, C. Dynamic polymeric micelles versus frozen nanoparticles formed by block copolymers. *Soft Matter* **6**, 3111-3118 (2010).

19. Shu, J.Y., Panganiban, B. & Xu, T. in Annual Review of Physical Chemistry, Vol 64, Vol. 64. (eds. M.A. Johnson & T.J. Martinez) 631-6572013).

20. Dube, N., Presley, A.D., Shu, J.Y. & Xu, T. Amphiphilic Peptide-Polymer Conjugates with Side-Conjugation. *Macromolecular Rapid Communications* **32**, 344-353 (2011).

21. Shu, J.Y. et al. Amphiphilic Peptide-Polymer Conjugates Based on the Coiled-Coil Helix Bundle. *Biomacromolecules* **11**, 1443-1452 (2010).

22. Lund, R., Shu, J. & Xu, T. A Small-Angle X-ray Scattering Study of alpha-helical Bundle-Forming Peptide-Polymer Conjugates in Solution: Chain Conformations. *Macromolecules* **46**, 1625-1632 (2013).

23. Lutz, J.F., Ouchi, M., Liu, D.R. & Sawamoto, M. Sequence-Controlled Polymers. *Science* **341**, 628-+ (2013).

24. Candau, F. & Selb, J. Hydrophobically-modified polyacrylamides prepared by micellar polymerization. *Advances in Colloid and Interface Science* **79**, 149-172 (1999).

25. Laschewsky, A. in Polysoaps/Stabilizers/Nitrogen-15 Nmr, Vol. 124 1-861995).

26. Morishima, Y., Nomura, S., Ikeda, T., Seki, M. & Kamachi, M. CHARACTERIZATION OF UNIMOLECULAR MICELLES OF RANDOM COPOLYMERS OF SODIUM 2-(ACRYLAMIDO)-2-METHYLPROPANESULFONATE AND METHACRYLAMIDES BEARING BULKY HYDROPHOBIC SUBSTITUENTS. *Macromolecules* **28**, 2874-2881 (1995).

27. Kuroda, K., Fujimoto, K., Sunamoto, J. & Akiyoshi, K. Hierarchical self-assembly of hydrophobically modified pullulan in water: Gelation by networks of nanoparticles. *Langmuir* **18**, 3780-3786 (2002).

28. Petit, F., Iliopoulos, I. & Audebert, R. Aggregation of associating polymers studied by F-19 nmr. *Polymer* **39**, 751-753 (1998).

29. Petit-Agnely, F., Iliopoulos, I. & Zana, R. Hydrophobically modified sodium polyacrylates in aqueous solutions: Association mechanism and characterization of the aggregates by fluorescence probing. *Langmuir* **16**, 9921-9927 (2000).

30. Gorzelle, B.M. et al. Amphipols can support the activity of a membrane enzyme. *Journal of the American Chemical Society* **124**, 11594-11595 (2002).

31. Sanders, C.R., Hoffmann, A.K., Grayn, D.N., Keyes, M.H. & Ellis, C.D. French swimwear for membrane proteins. *Chembiochem* **5**, 423-426 (2004).

32. Popot, J.L. et al. Amphipols: polymeric surfactants for membrane biology research. *Cellular and Molecular Life Sciences* **60**, 1559-1574 (2003).

33. Berglund, G.I. et al. The catalytic pathway of horseradish peroxidase at high resolution. *Nature* **417**, 463-468 (2002).

34. Lu, J., Bates, F.S. & Lodge, T.P. Remarkable Effect of Molecular Architecture on Chain Exchange in Triblock Copolymer Micelles. *Macromolecules* **48**, 2667-2676 (2015).

35. Chiefari, J. et al. Living free-radical polymerization by reversible addition-fragmentation chain transfer: The RAFT process. *Macromolecules* **31**, 5559-5562 (1998).

36. Frokjaer, S. & Otzen, D.E. Protein drug stability: A formulation challenge. *Nature Reviews Drug Discovery* **4**, 298-306 (2005).

37. Brandrup, J. & Immergut, E.H. Polymer Handbook. (Interscience Publishers, 1966).

38. Barton, A.F.M. Handbook of Polymer-Liquid Interaction Parameters and Solubility Parameters. (Taylor & Francis, 1990).

39. Somasundaran, P., Krishnakumar, S. & Mehta, S.C. A new model to describe the sorption of surfactants on solids in non-aqueous media. *Journal of Colloid and Interface Science* **292**, 373-380 (2005).

40. Kontogeorgis, G.M. & Folas, G.K. Thermodynamic Models for Industrial Applications: From Classical and Advanced Mixing Rules to Association Theories. (Wiley, 2009).

41. Israelachvili, J.N. Intermolecular and Surface Forces: Revised Third Edition. (Elsevier Science, 2011).

42. Shanbhag, V.P. & Axelsson, C.G. HYDROPHOBIC INTERACTION DETERMINED BY PARTITION IN AQUEOUS 2-PHASE SYSTEMS - PARTITION OF PROTEINS IN SYSTEMS CONTAINING FATTY-ACID ESTERS OF POLY(ETHYLENE GLYCOL). *European Journal of Biochemistry* **60**, 17-22 (1975).

43. Perrier, S., Takolpuckdee, P., Westwood, J. & Lewis, D.M. Versatile chain transfer agents for reversible addition fragmentation chain transfer (RAFT) polymerization to synthesize functional polymeric architectures. *Macromolecules* **37**, 2709-2717 (2004).

44. Beaucage, G. Approximations leading to a unified exponential power-law approach to small-angle scattering. *Journal of Applied Crystallography* **28**, 717-728 (1995).

45. Bartlett, P. & Ottewill, R.H. A NEUTRON-SCATTERING STUDY OF THE STRUCTURE OF A BIMODAL COLLOIDAL CRYSTAL. *Journal of Chemical Physics* **96**, 3306-3318 (1992).

46. Guinier, A. & Fournet, G. Small-angle scattering of X-rays. (Wiley, 1955).

47. Higgins, J.S., Benoit, H.C. & Benoît, H. Polymers and Neutron Scattering. (Clarendon Press, 1994).

R.4. Chapter 4

1. Bornscheuer, U.T. et al. Engineering the third wave of biocatalysis. *Nature* **485**, 185-194 (2012).

2.   Castillo, J. et al. Biosensors for life quality - Design, development and applications. *Sens. Actuator B-Chem.* **102**, 179-194 (2004).

3.   Leader, B., Baca, Q.J. & Golan, D.E. Protein therapeutics: A summary and pharmacological classification. *Nature Reviews Drug Discovery* **7**, 21-39 (2008).

4.   Leech, D., Kavanagh, P. & Schuhmann, W. Enzymatic fuel cells: Recent progress. *Electrochimica Acta* **84**, 223-234 (2012).

5.   Ma, X., Hortelão, A.C., Patiño, T. & Sánchez, S. Enzyme Catalysis To Power Micro/Nanomachines. *ACS Nano* **10**, 9111-9122 (2016).

6.   Baneyx, F. & Schwartz, D.T. Selection and analysis of solid-binding peptides. *Curr. Opin. Biotechnol.* **18**, 312-317 (2007).

7.   Shu, J.Y., Panganiban, B. & Xu, T. in Annual Review of Physical Chemistry, Vol 64, Vol. 64. (eds. M.A. Johnson & T.J. Martinez) 631-6572013).

8.   Dube, N., Presley, A.D., Shu, J.Y. & Xu, T. Amphiphilic Peptide-Polymer Conjugates with Side-Conjugation. *Macromolecular Rapid Communications* **32**, 344-353 (2011).

9.   Shu, J.Y. et al. Amphiphilic Peptide-Polymer Conjugates Based on the Coiled-Coil Helix Bundle. *Biomacromolecules* **11**, 1443-1452 (2010).

10.   Leser, M.E. & Luisi, P.L. APPLICATION OF REVERSE MICELLES FOR THE EXTRACTION OF AMINO-ACIDS AND PROTEINS. *Chimia* **44**, 270-282 (1990).

11.   Luisi, P.L. ENZYMES HOSTED IN REVERSE MICELLES IN HYDROCARBON SOLUTION. *Angewandte Chemie-International Edition in English* **24**, 439-450 (1985).

12.   Paradkar, V.M. & Dordick, J.S. MECHANISM OF EXTRACTION OF CHYMOTRYPSIN INTO ISOOCTANE AT VERY-LOW CONCENTRATIONS OF AEROSOL OT IN THE ABSENCE OF REVERSED MICELLES. *Biotechnology and Bioengineering* **43**, 529-540 (1994).

13.   Luisi, P.L., Giomini, M., Pileni, M.P. & Robinson, B.H. REVERSE MICELLES AS HOSTS FOR PROTEINS AND SMALL MOLECULES. *Biochimica Et Biophysica Acta* **947**, 209-246 (1988).

14.   Castelletto, V., Krysmann, M., Kelarakis, A. & Jauregi, P. Complex formation of bovine serum albumin with a poly(ethylene glycol) lipid conjugate. *Biomacromolecules* **8**, 2244-2249 (2007).

15.   Chen, H.T. et al. Release of hydrophobic molecules from polymer micelles into cell membranes revealed by Forster resonance energy transfer imaging. *Proceedings of the National Academy of Sciences of the United States of America* **105**, 6596-6601 (2008).

16.   Kastantin, M. et al. Thermodynamic and Kinetic Stability of DSPE-PEG(2000) Micelles in the Presence of Bovine Serum Albumin. *Journal of Physical Chemistry B* **114**, 12632-12640 (2010).

17.   Gorzelle, B.M. et al. Amphipols can support the activity of a membrane enzyme. *Journal of the American Chemical Society* **124**, 11594-11595 (2002).

18.   Sanders, C.R., Hoffmann, A.K., Grayn, D.N., Keyes, M.H. & Ellis, C.D. French swimwear for membrane proteins. *Chembiochem* **5**, 423-426 (2004).

19.   Popot, J.L. et al. Amphipols: polymeric surfactants for membrane biology research. *Cellular and Molecular Life Sciences* **60**, 1559-1574 (2003).

20.   Tribet, C., Audebert, R. & Popot, J.L. Amphipols: Polymers that keep membrane proteins soluble in aqueous solutions. *Proceedings of the National Academy of Sciences of the United States of America* **93**, 15047-15050 (1996).

21.   Degrado, W.F. & Lear, J.D. INDUCTION OF PEPTIDE CONFORMATION AT APOLAR WATER INTERFACES .1. A STUDY WITH MODEL PEPTIDES OF DEFINED HYDROPHOBIC PERIODICITY. *Journal of the American Chemical Society* **107**, 7684-7689 (1985).

22.   Jackson, A.M., Myerson, J.W. & Stellacci, F. Spontaneous assembly of subnanometre-ordered domains in the ligand shell of monolayer-protected nanoparticles. *Nature Materials* **3**, 330-336 (2004).

23.   Yang, H.Y., Yang, S.N., Kong, J.L., Dong, A.C. & Yu, S.N. Obtaining information about protein secondary structures in aqueous solution using Fourier transform IR spectroscopy. *Nature Protocols* **10** (2015).

24.   Tsien, R.Y. The green fluorescent protein. *Annual Review of Biochemistry* **67**, 509-544 (1998).

25.   Veitch, N.C. Horseradish peroxidase: a modern view of a classic enzyme. *Phytochemistry* **65**, 249-259 (2004).

26.   Avila, G.P., Salvador, A. & de la Guardia, M. Enzymic determination of peroxides in non-aqueous media. *Analyst* **122**, 1543-1547 (1997).

27.   DelMar, E.G., Largman, C., Brodrick, J.W. & Geokas, M.C. A sensitive new substrate for chymotrypsin. *Analytical Biochemistry* **99**, 316-320 (1979).

28.   Van der Spoel, D. et al. GROMACS: Fast, flexible, and free. *Journal of Computational Chemistry* **26**, 1701-1718 (2005).

29.   Klauda, J.B. et al. Update of the CHARMM All-Atom Additive Force Field for Lipids: Validation on Six Lipid Types. *Journal of Physical Chemistry B* **114**, 7830-7843 (2010).

30.   Martinez, L., Andrade, R., Birgin, E.G. & Martinez, J.M. PACKMOL: A Package for Building Initial Configurations for Molecular Dynamics Simulations. *Journal of Computational Chemistry* **30**, 2157-2164 (2009).

31.   Essmann, U. et al. A SMOOTH PARTICLE MESH EWALD METHOD. *Journal of Chemical Physics* **103**, 8577-8593 (1995).

32.   Darden, T., York, D. & Pedersen, L. PARTICLE MESH EWALD - AN N.LOG(N) METHOD FOR EWALD SUMS IN LARGE SYSTEMS. *Journal of Chemical Physics* **98**, 10089-10092 (1993).

33.   Hess, B. P-LINCS: A parallel linear constraint solver for molecular simulation. *Journal of Chemical Theory and Computation* **4**, 116-122 (2008).

34.   Higgins, J.S., Benoit, H.C. & Benoît, H. Polymers and Neutron Scattering. (Clarendon Press, 1994).

35.   Bartlett, P. & Ottewill, R.H. A NEUTRON-SCATTERING STUDY OF THE STRUCTURE OF A BIMODAL COLLOIDAL CRYSTAL. *Journal of Chemical Physics* **96**, 3306-3318 (1992).

R.5. Chapter 5

1.   Dill, K.A. DOMINANT FORCES IN PROTEIN FOLDING. *Biochemistry* **29**, 7133-7155 (1990).
2.   Hartl, F.U. Molecular chaperones in cellular protein folding. *Nature* **381**, 571-580 (1996).
3.   Bukau, B. & Horwich, A.L. The Hsp70 and Hsp60 chaperone machines. *Cell* **92**, 351-366 (1998).
4.   Gething, M.-J. & Sambrook, J. Protein folding in the cell. *Nature* **355**, 33-45 (1992).
5.   Hendrick, J.P. & Hartl, F.U. MOLECULAR CHAPERONE FUNCTIONS OF HEAT-SHOCK PROTEINS. *Annual Review of Biochemistry* **62**, 349-384 (1993).
6.   Sigler, P.B. et al. Structure and function in GroEL-mediated protein folding. *Annual Review of Biochemistry* **67**, 581-608 (1998).
7.   Kuriyan, J., Konforti, B. & Wemmer, D. The Molecules of Life: Physical and Chemical Principles. (Garland Science, 2013).
8.   De, M. & Rotello, V.M. Synthetic "chaperones": nanoparticle-mediated refolding of thermally denatured proteins. *Chemical Communications*, 3504-3506 (2008).
9.   Nomura, Y., Ikeda, M., Yamaguchi, N., Aoyama, Y. & Akiyoshi, K. Protein refolding assisted by self-assembled nanogels as novel artificial molecular chaperone. *FEBS Letters* **553**, 271-276 (2003).
10.   Kameta, N., Masuda, M. & Shimizu, T. Soft Nanotube Hydrogels Functioning As Artificial Chaperones. *Acs Nano* **6**, 5249-5258 (2012).
11.   Cleland, J.L., Hedgepeth, C. & Wang, D.I.C. POLYETHYLENE-GLYCOL ENHANCED REFOLDING OF BOVINE CARBONIC ANHYDRASE-B - REACTION STOICHIOMETRY AND REFOLDING MODEL. *Journal of Biological Chemistry* **267**, 13327-13334 (1992).
12.   Back, J.F., Oakenfull, D. & Smith, M.B. INCREASED THERMAL-STABILITY OF PROTEINS IN THE PRESENCE OF SUGARS AND POLYOLS. *Biochemistry* **18**, 5191-5196 (1979).
13.   Berglund, G.I. et al. The catalytic pathway of horseradish peroxidase at high resolution. *Nature* **417**, 463-468 (2002).
14.   Sirur, A., Knott, M. & Best, R.B. Effect of interactions with the chaperonin cavity on protein folding and misfolding. *Physical Chemistry Chemical Physics* **16**, 6358-6366 (2014).
15.   Israelachvili, J.N. Intermolecular and Surface Forces. (Elsevier Science, 2015).

16. Bartlett, P. & Ottewill, R.H. A NEUTRON-SCATTERING STUDY OF THE STRUCTURE OF A BIMODAL COLLOIDAL CRYSTAL. *Journal of Chemical Physics* **96**, 3306-3318 (1992).

R.6. Chapter 6

1. Bornscheuer, U.T. et al. Engineering the third wave of biocatalysis. *Nature* **485**, 185-194 (2012).
2. Castillo, J. et al. Biosensors for life quality - Design, development and applications. *Sensors and Actuators B-Chemical* **102**, 179-194 (2004).
3. Ma, X., Hortelão, A.C., Patiño, T. & Sánchez, S. Enzyme Catalysis To Power Micro/Nanomachines. *ACS Nano* **10**, 9111-9122 (2016).
4. Leech, D., Kavanagh, P. & Schuhmann, W. Enzymatic fuel cells: Recent progress. *Electrochimica Acta* **84**, 223-234 (2012).
5. Leader, B., Baca, Q.J. & Golan, D.E. Protein therapeutics: A summary and pharmacological classification. *Nature Reviews Drug Discovery* **7**, 21-39 (2008).
6. de la Rica, R. & Matsui, H. Applications of peptide and protein-based materials in bionanotechnology. *Chemical Society Reviews* **39**, 3499-3509 (2010).
7. McConnell, I., Li, G.H. & Brudvig, G.W. Energy Conversion in Natural and Artificial Photosynthesis. *Chemistry & Biology* **17**, 434-447 (2010).
8. Bates, F.S. & Fredrickson, G.H. BLOCK COPOLYMER THERMODYNAMICS - THEORY AND EXPERIMENT. *Annual Review of Physical Chemistry* **41**, 525-557 (1990).
9. Presley, A.D., Chang, J.J. & Xu, T. Directed co-assembly of heme proteins with amphiphilic block copolymers toward functional biomolecular materials. *Soft Matter* **7**, 172-179 (2011).
10. Xu, T. et al. Subnanometer Porous Thin Films by the Co-assembly of Nanotube Subunits and Block Copolymers. *ACS Nano* **5**, 1376-1384 (2011).
11. Leser, M.E. & Luisi, P.L. APPLICATION OF REVERSE MICELLES FOR THE EXTRACTION OF AMINO-ACIDS AND PROTEINS. *Chimia* **44**, 270-282 (1990).
12. Luisi, P.L. ENZYMES HOSTED IN REVERSE MICELLES IN HYDROCARBON SOLUTION. *Angewandte Chemie-International Edition in English* **24**, 439-450 (1985).
13. Paradkar, V.M. & Dordick, J.S. MECHANISM OF EXTRACTION OF CHYMOTRYPSIN INTO ISOOCTANE AT VERY-LOW CONCENTRATIONS OF AEROSOL OT IN THE ABSENCE OF REVERSED MICELLES. *Biotechnology and Bioengineering* **43**, 529-540 (1994).
14. Luisi, P.L., Giomini, M., Pileni, M.P. & Robinson, B.H. REVERSE MICELLES AS HOSTS FOR PROTEINS AND SMALL MOLECULES. *Biochimica Et Biophysica Acta* **947**, 209-246 (1988).

15. Kim, T.H., Hwang, J., Acharya, H. & Park, C. Ordered Nanostructure of PS-b-PEO Copolymer by Solvent Annealing with Mixture of Benzene/Water Vapor and Its Micropattern Fabrication. *J. Nanosci. Nanotechnol.* **10**, 6883-6887 (2010).

16. Huang, P.S. et al. High thermodynamic stability of parametrically designed helical bundles. *Science* **346**, 481-485 (2014).

Appendix

A.1. Supporting Information for Chapter 2
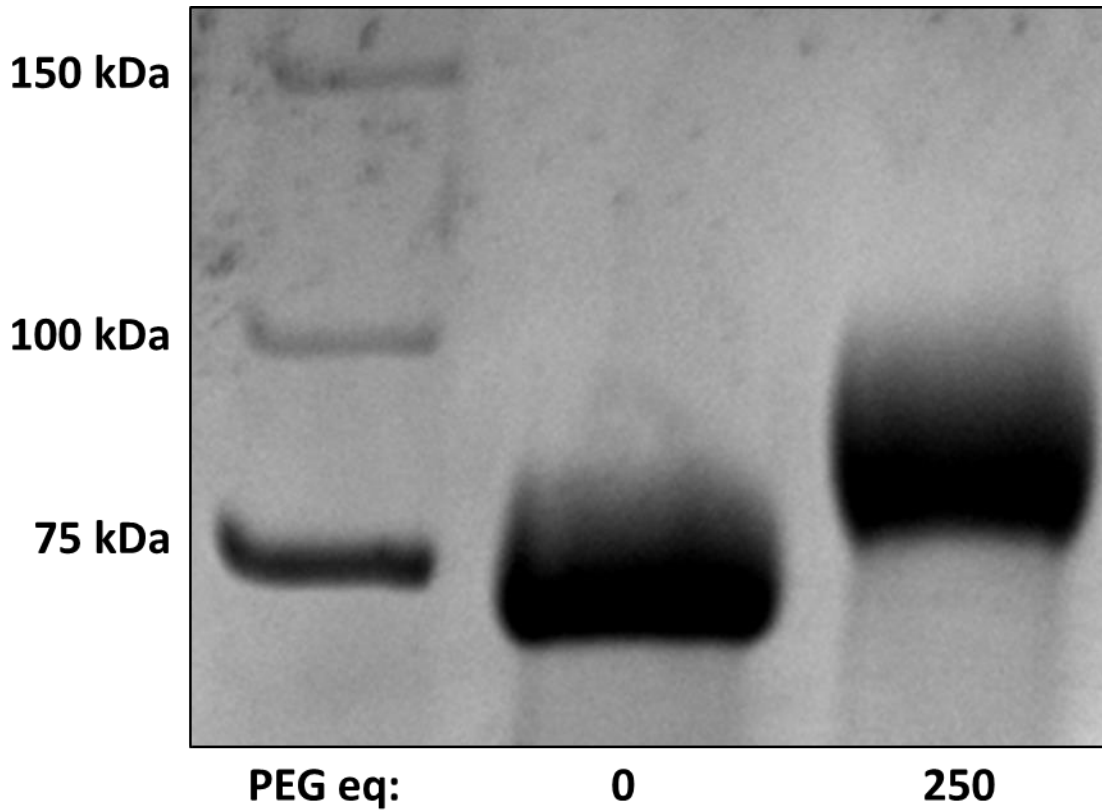
A.1.1. Conjugation of poly(ethylene glycol) was verified through gel electrophoresis. Maleimide-functionalized PEG with a molecular weight of 2000 Da was reacted with glucose oxidase in a phosphate buffered solution. An excess of PEG was introduced. Glucose oxidase has a molecular weight of 80 kDa. The molecular weight increase observed in the right lane verifies conjugation of PEG.

A.1.2. Glucose oxidase-PEG conjugates were dissolved in either water, 80% methanol, or a 2:1 benzene to methanol solution. A colorimetric assay was used to assess the degree to which protein activity was retained. It was observed that at 80% methanol, activity of glucose oxidase had diminished in comparison to pure water. When glucose oxidase-PEG conjugates dissolved in a benzene/methanol mixture, the protein was completely deactivated.
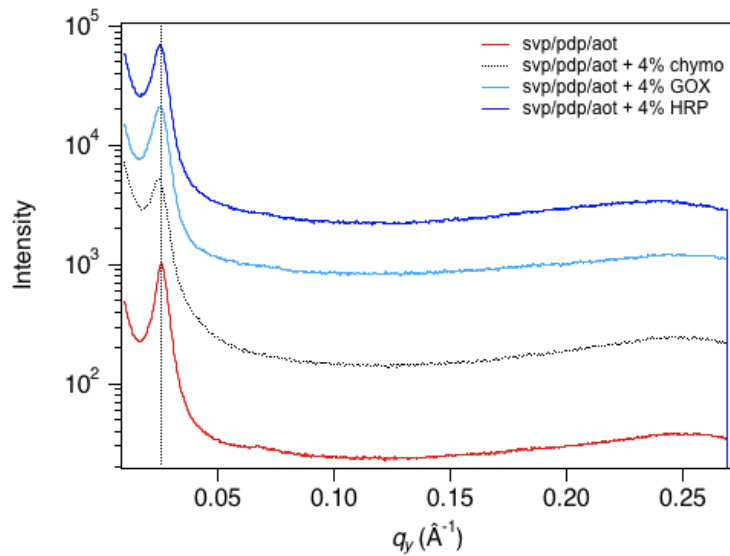
A.1.3. GISAXS scattering profiles of polymer thin films containing AOT or AOT/protein reverse micelles. Films are unstructured beneath the surface and the periodicity of the cylindrical domains did not change based on protein incorporation.
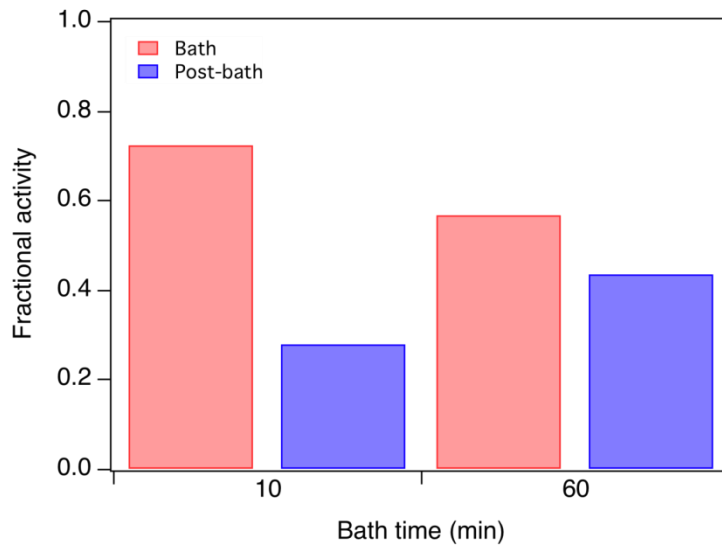
A.1.4. Comparison of chymotrypsin activity in hybrid thin film. Enzyme activity was assessed based on proteolysis of N-succinyl-Ala-Ala-Pro-Phe-p-nitroanilide. PS-*b*-P4VP/PDP thin films contain 0.25% (w/w) chymotrypsin. Protein was incorporated as a charge-paired surfactant complex (P4VP:AOT = 1:0.15). Leaching was monitored 10 and 60 min after submergence in an aqueous bath.
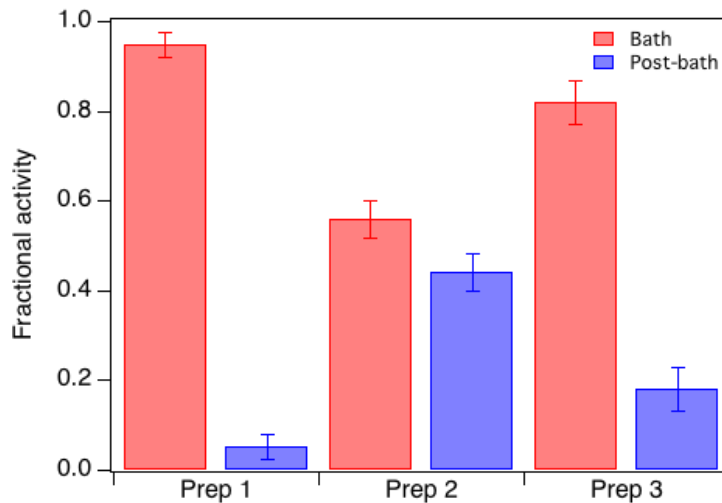
A.1.5. Comparison of horseradish peroxidase activity in hybrid thin film. Enzyme activity was assessed as a function of reverse micelle buffer and assay reaction buffer after a 30 min bath. Prep 1 involves a reverse micelle core containing buffer pH of 4.6 and a reaction buffer pH of 4.6. Prep 2 involves a reverse micelle core containing buffer pH of 4.6 and a reaction buffer pH of 6. Prep 3 involves a reverse micelle core containing buffer pH of 6 and a reaction buffer pH of 6.
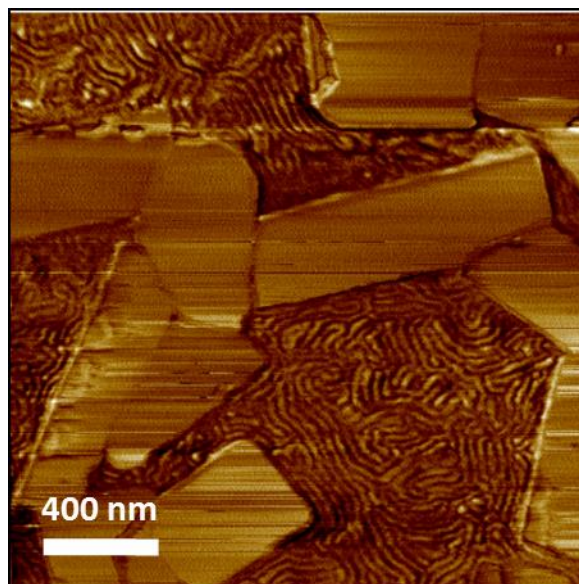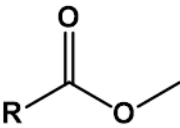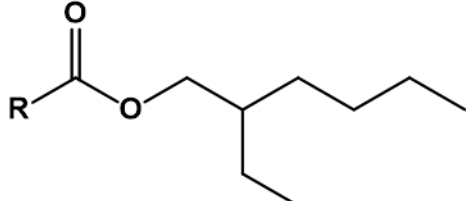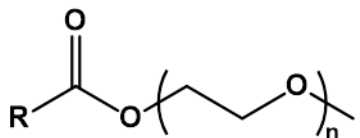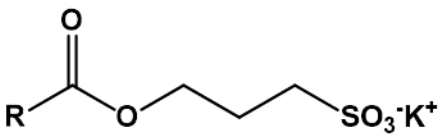
A.1.6. Fabrication of chymotrypsin hybrid thin film using (24 kDa)PS-b-(9 kDa)P4VP(PDP) (P4VP:PDP = 1:1) and CTAB. Protein was incorporated as a charge-paired surfactant complex (P4VP:CTAB = 1:0.36).
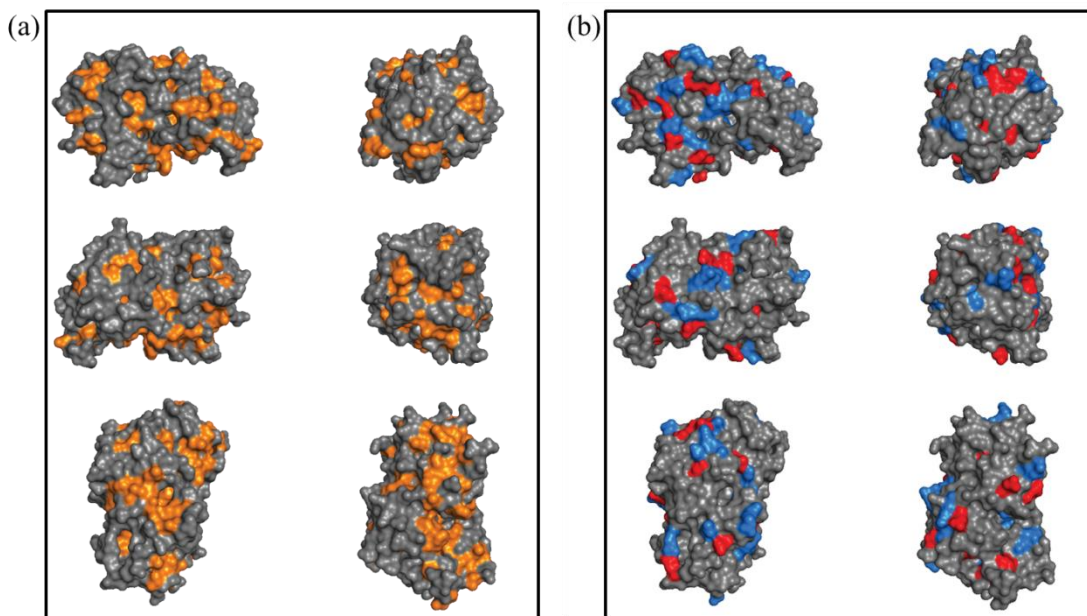
A.2.1. Protein crystal structure of horseradish peroxidase (1H55). (a) Hydrophilic surface map where orange represents areas with hydrophobic residues and gray represents areas with hydrophilic residues. (b) Charge surface map where blue represents areas with positive residues, red represents areas with negative residues, and gray represents areas with non-charged residues.

A.2.2. Hildebrand Solubility Parameters for Monomers and Solvents

Component	δ (cal/cm^3)$^{1/2}$
	8.93
	8.40
	n=5: 18.0 to 23.7 n=9: 18.0 to 20.5
	~20
Toluene	8.9
H_2O	23.4
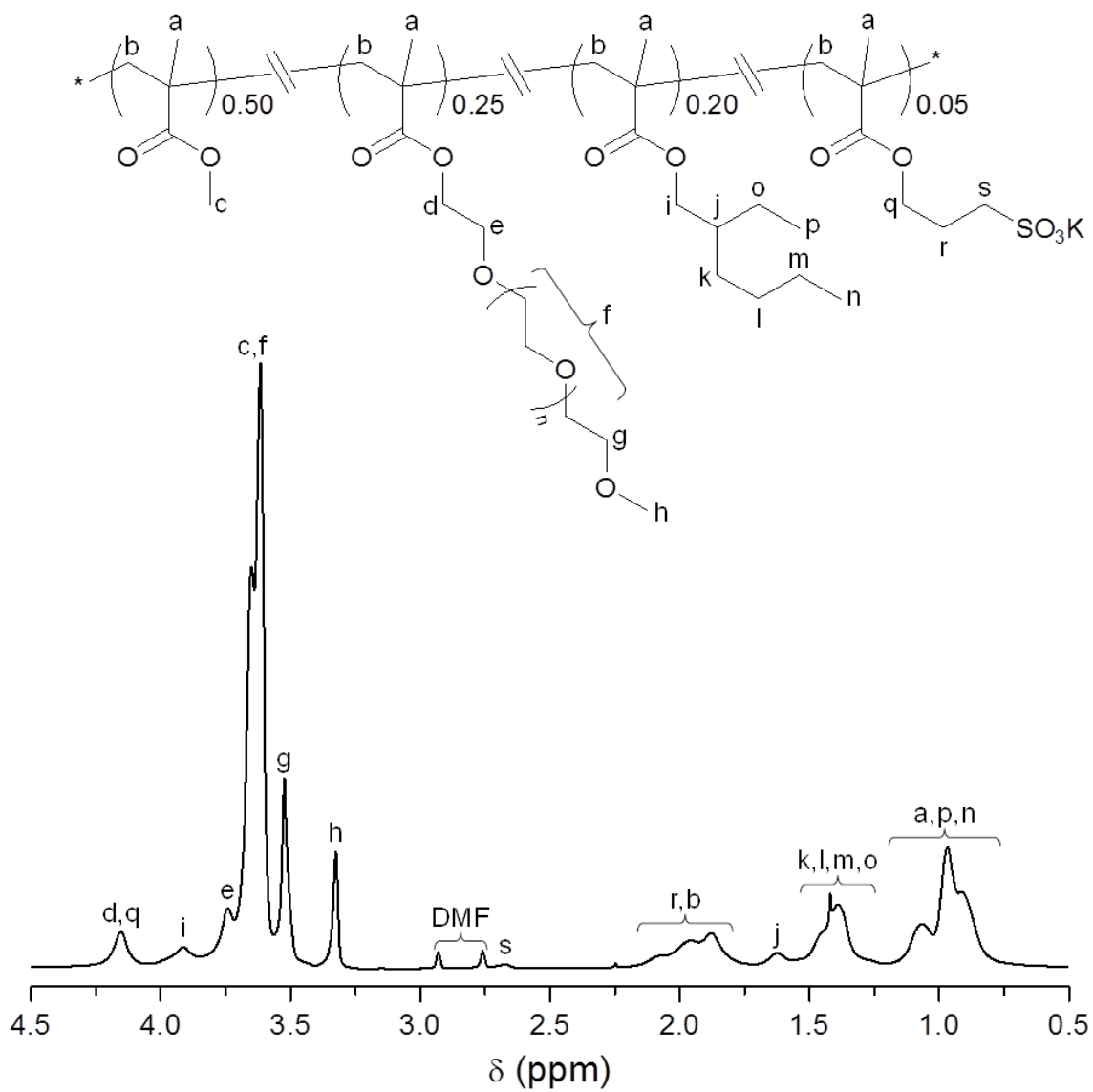
A.3.3. 1H NMR (DMF-d$_7$, 400 MHz) of SRHP-4.
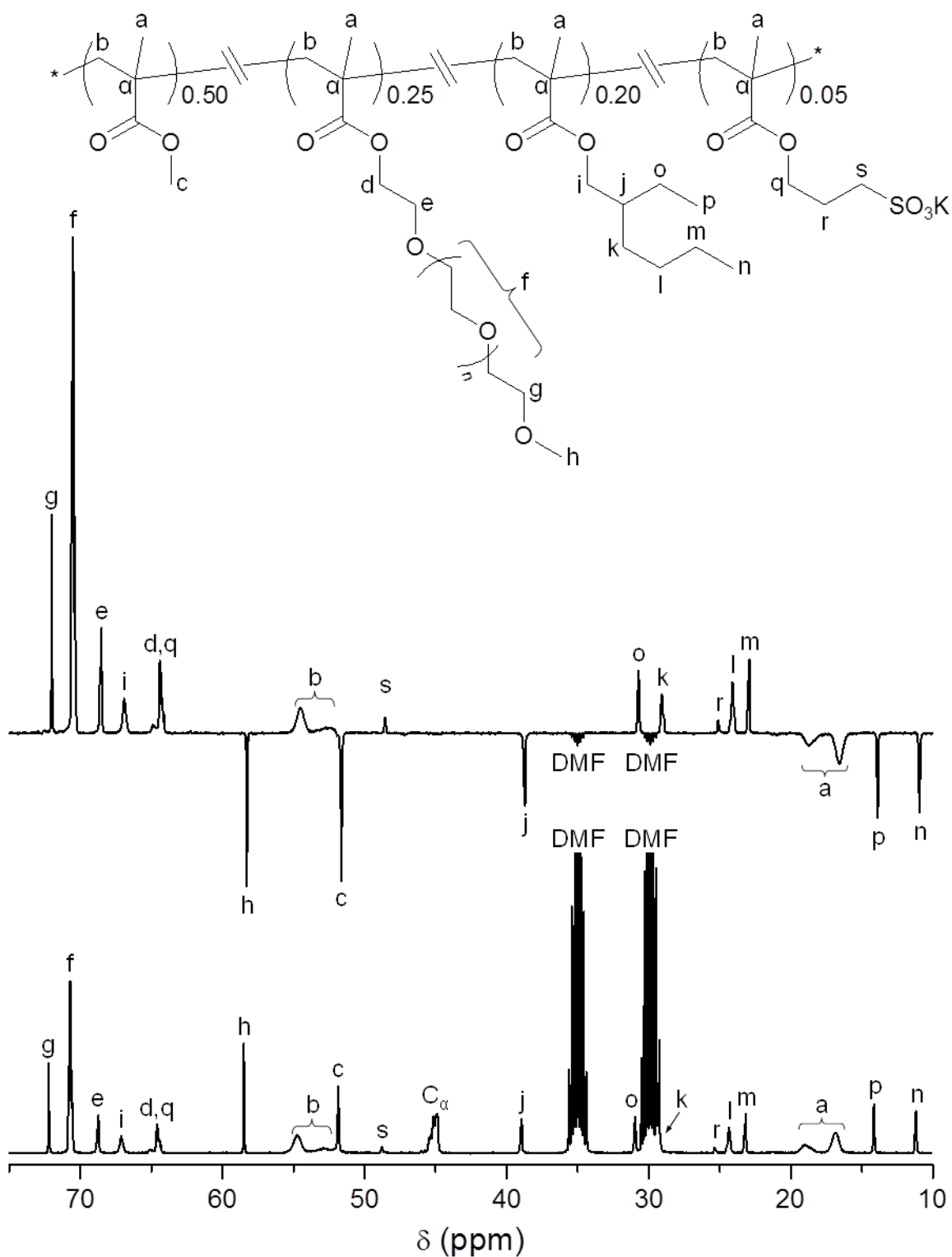
A.3.4. DEPT ^{13}C NMR and quantitative ^{13}C NMR (DMF-d$_7$, 100 MHz) of SRHP-4.
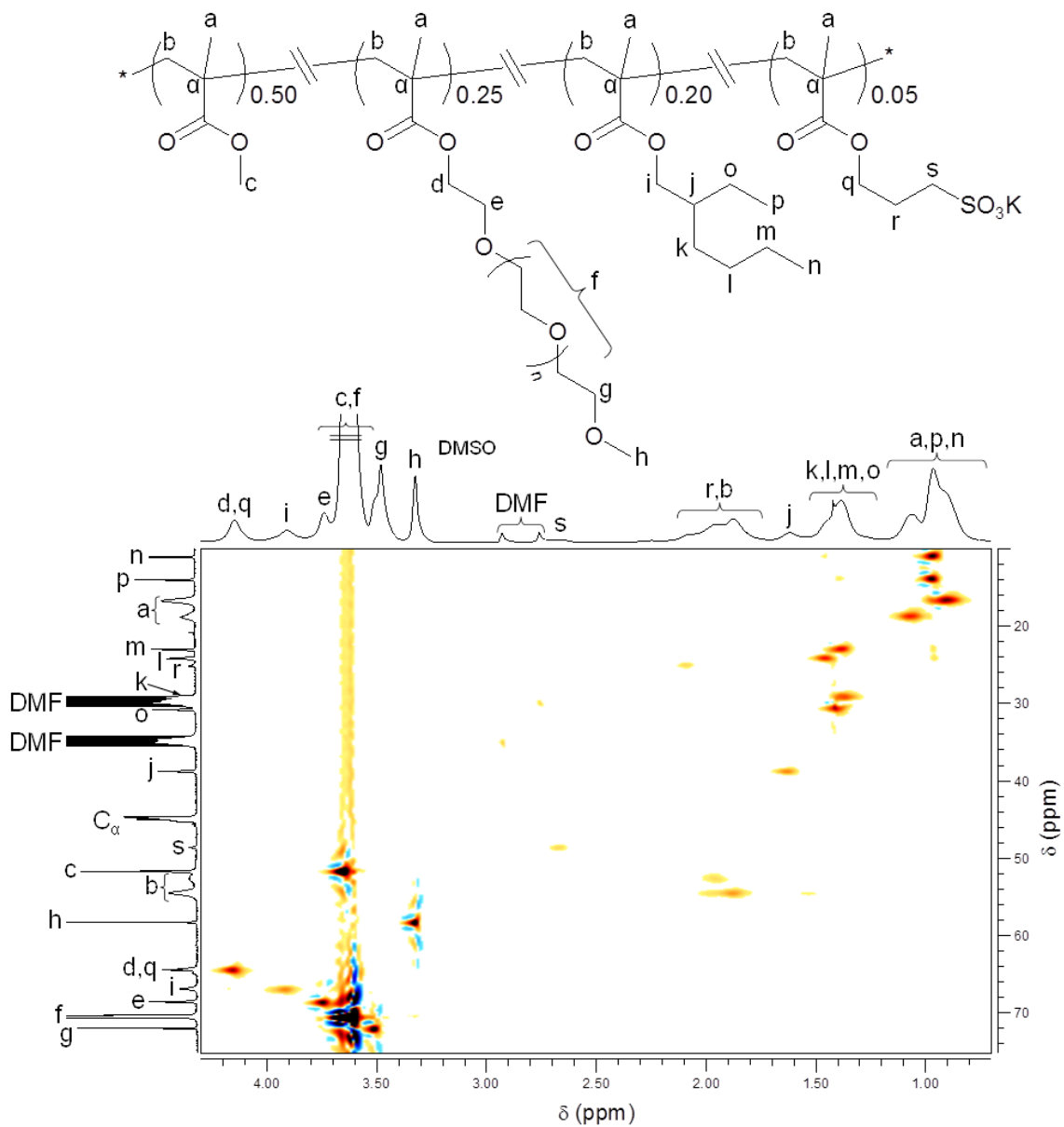
A.3.5. ^{1}H-^{13}C HSQC 2D NMR (DMF-d$_7$, 100 MHz) of SRHP-4.
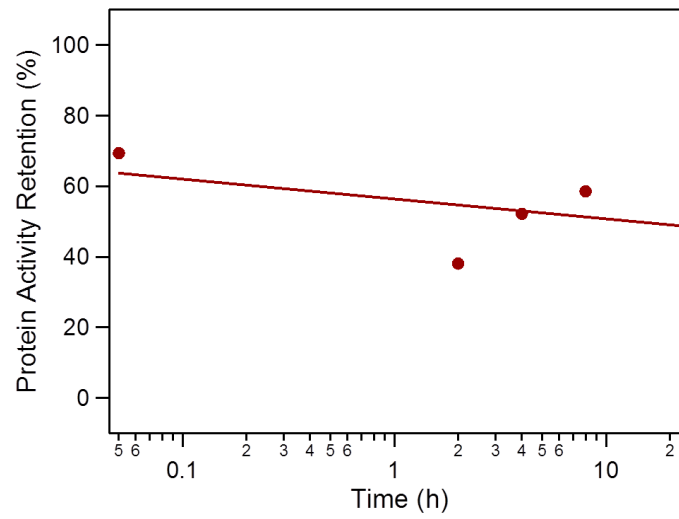
A.3.1. Activity of GOx after storage in organic solvent using SRHP-4 reverse micelles and dispersed in aqueous buffer.
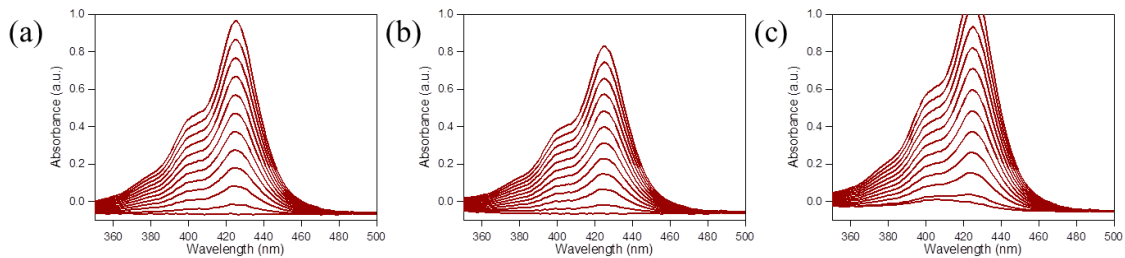
A.3.2. UV-visible absorbance spectra of benzoyl peroxide/3,3',5,5'-tetramethylbenzidine assay. Monitoring (a) toluene, (b) SRHP-4, and (c) SRHP-4/HRP lyophilized complex over 5 min. Each spectrum is collected every 30 s.
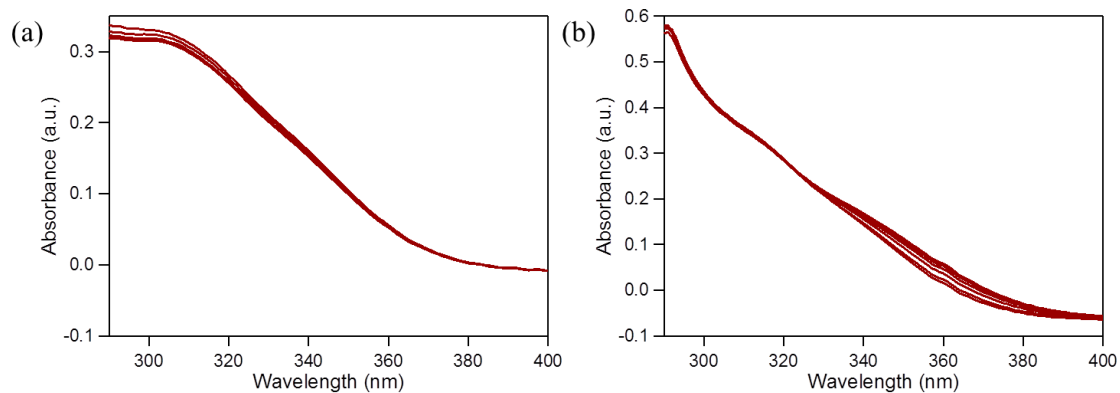
A.3.3. UV-visible absorbance spectra of n-succinyl-Ala-Ala-Pro-Phe p-nitroanilide assay. Monitoring (a) SRHP-4 and (b) SRHP-4/CT lyophilized complex over 30 min. Each spectrum is collected every 1 min.
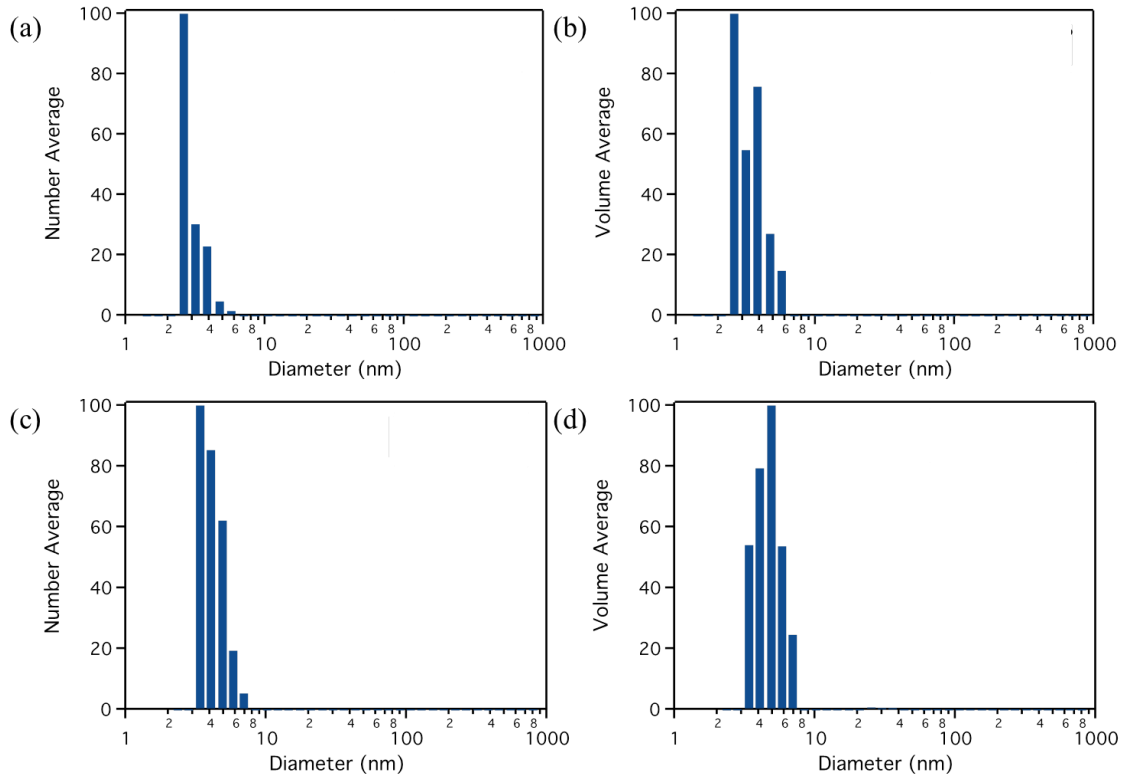
A.4.1. Dynamic light scattering histograms. (a) and (b) are number and volume average distributions of HRP in water after 4 h at 70°C respectively. (c) and (d) are number and volume average distributions of SRHP-4 and HRP in water after 4 h at 70°C respectively.
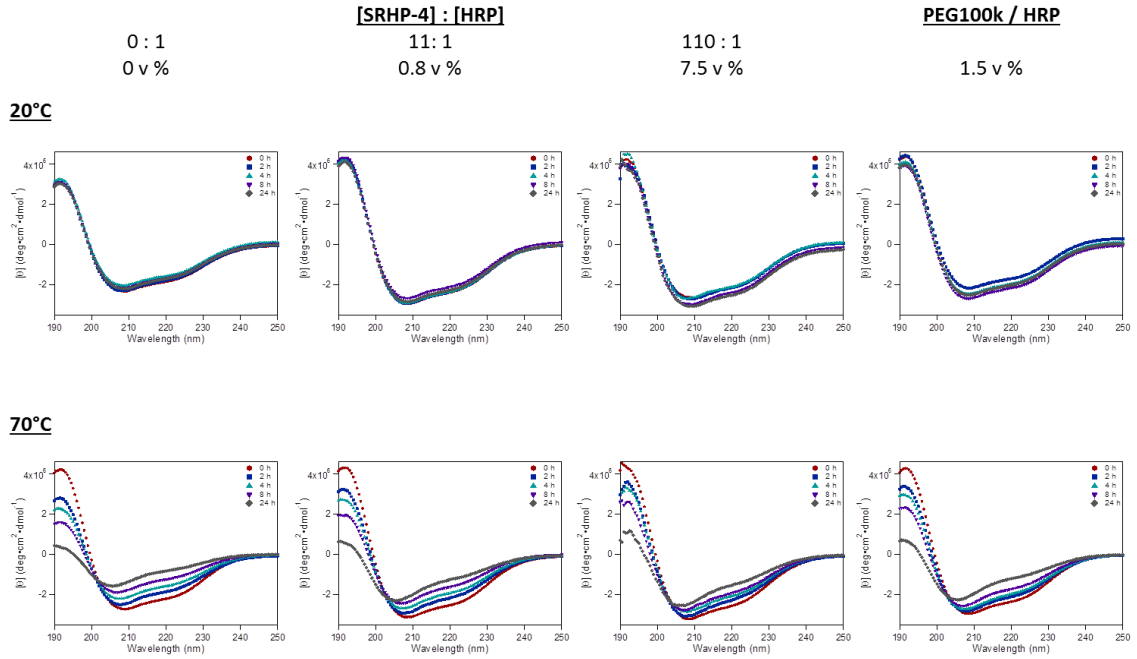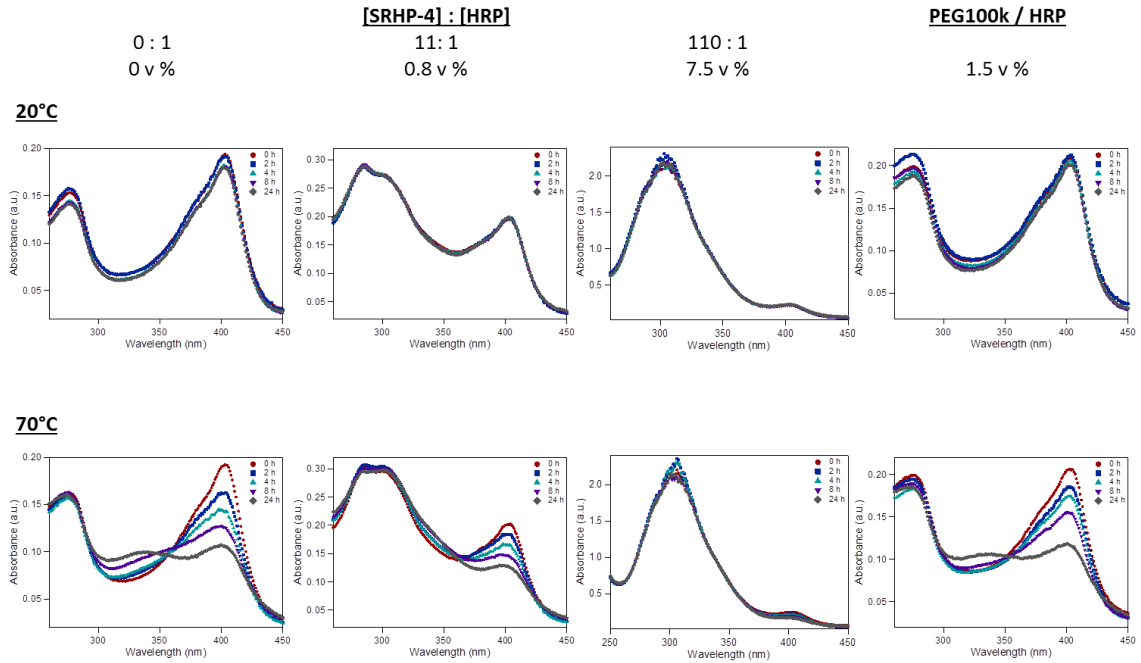
A.4.2. Circular dichroism spectra at 20°C and 70°C of SRHP-4 or PEG and HRP in water.
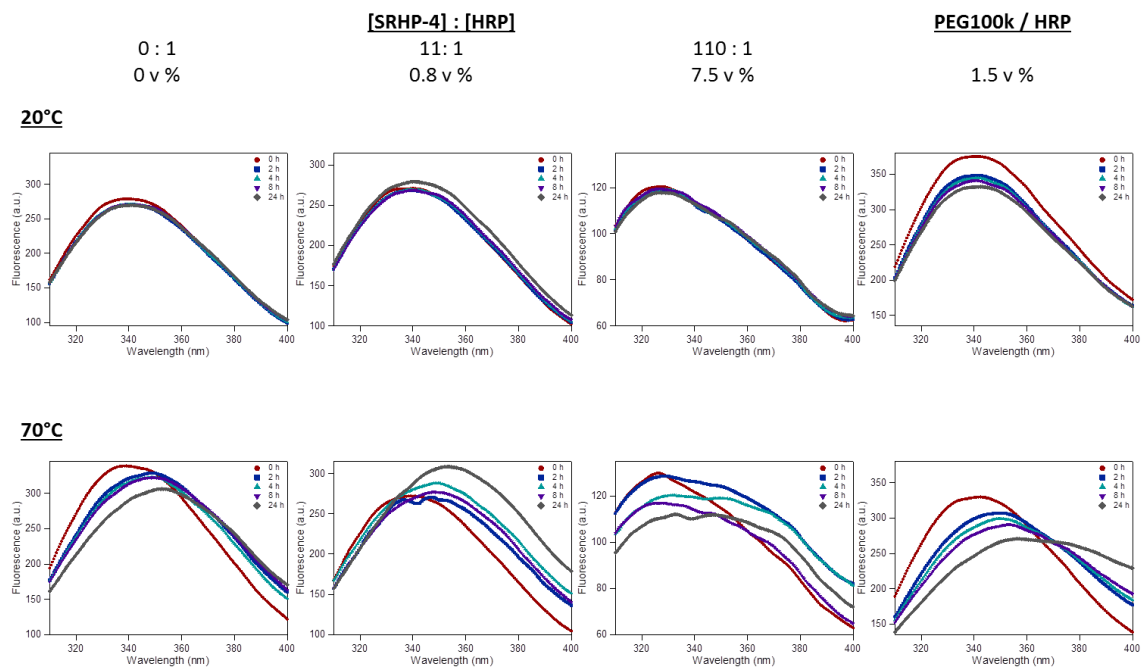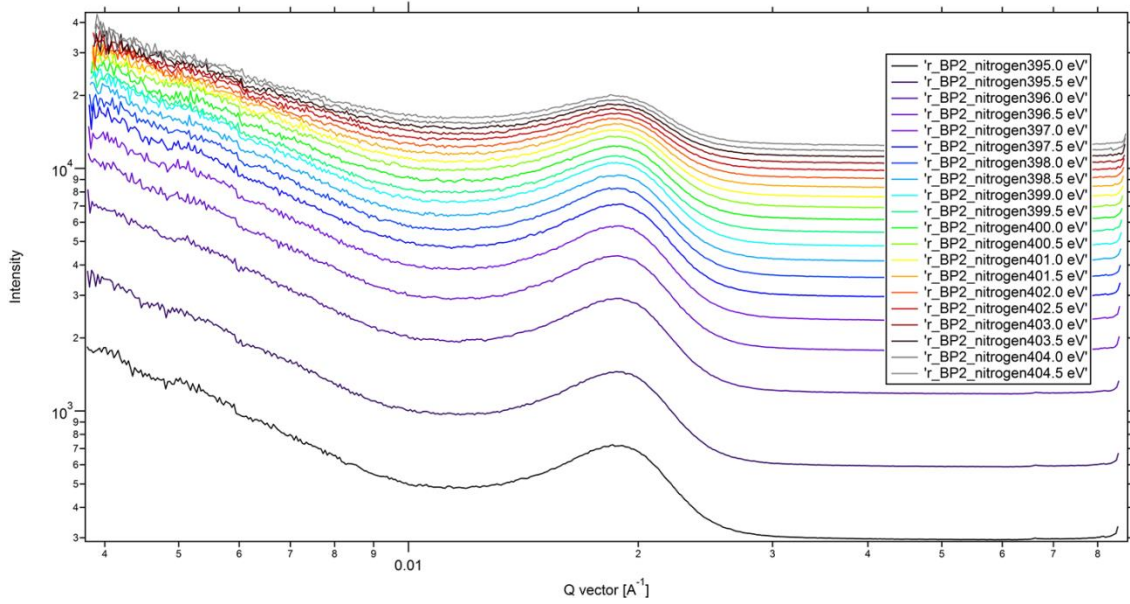
A.4.3. Fluorescence spectra at 20°C and 70°C of SRHP-4 or PEG and HRP in water.

A.4.4. UV-visible absorbance spectra at 20°C and 70°C of SRHP-4 or PEG and HRP in water.

A.5.1. Resonant soft x-ray scattering profiles as a function of energy of hybrid thin films composed of SRHP-4/HRP reverse micelles and poly(styrene)-*block*-poly(ethylene oxide). Increasing the x-ray energy allows us to target the nitrogen edge, which allows us to highlight protein periodicity. HRP has nitrogen whereas the block copolymer and SRHP-4 do not.
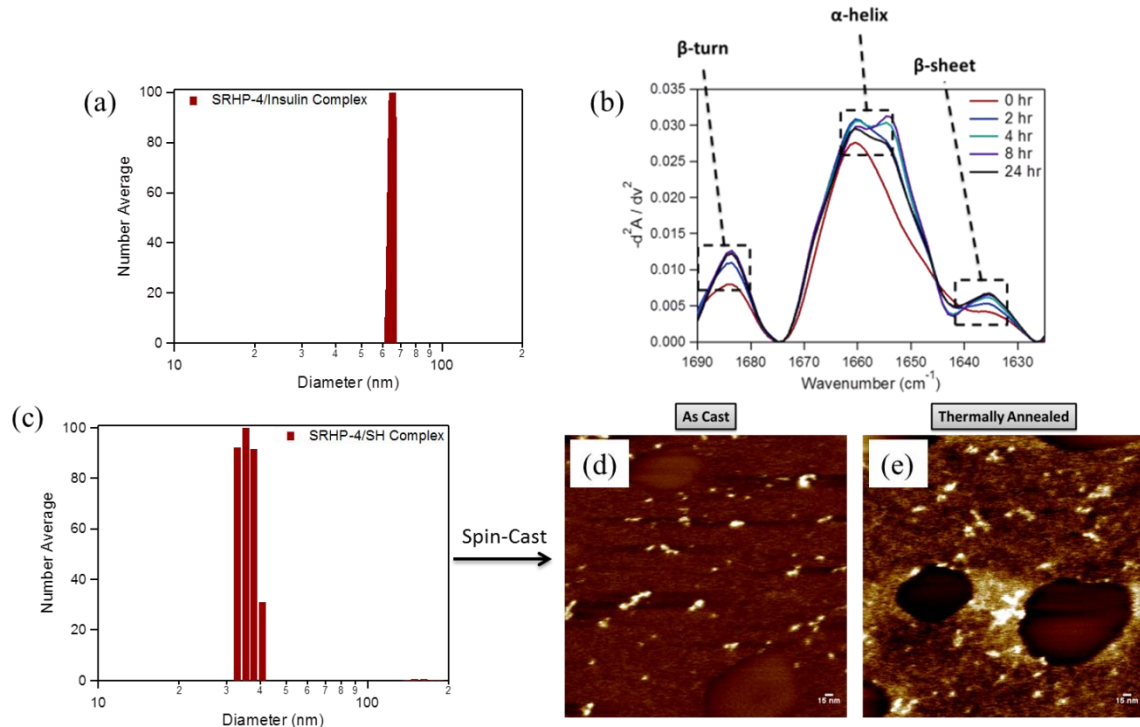
A.5.2. Encapsulation of other proteins using SRHP-4. (a) Number average DLS histogram of lyophilization-assisted encapsulation of insulin into SRHP-4 complexes. Prior to resuspension in solution, insulin was in a phosphate buffer at pH 2. (b) Negative second derivative of insulin FT-IR spectra over 24 h. Secondary structure remained relatively intact after solubilization in toluene (c) Number average DLS hisogram of lyophilization-assisted encapsulation of a computationally designed three helix bundle into SRHP-4 complexes. AFM images of spin-cast SRHP-4/computationally designed three helix bundle complexes onto a silicon wafer (d) before and (e) after thermal annealing at 70°C. Bundling of the helix was observed after thermal annealing.